THESIS

HYDROTHERMAL FLUID AND ORE PARAGENESIS OF THE

GOLD-BEARING RATTLESNAKE HILLS ALKALINE COMPLEX,

WYOMING

Submitted by

Ashley Ripple

Department of Geosciences

In partial fulfillment of the requirements

For the Degree of Master of Science

Colorado State University

Fort Collins, Colorado

Summer 2012

Master's Committee:

    Advisor: John Ridley

    Judy Hannah
    Tom Sale

ABSTRACT

HYDROTHERMAL FLUID AND ORE PARAGENESIS OF THE

GOLD-BEARING RATTLESNAKE HILLS ALKALINE COMPLEX,

WYOMING

Rattlesnake Hills is a recently discovered alkaline rock gold system located in
central Wyoming. Rattlesnake Hills is currently being explored by Agnico Eagle Ltd.
Alkaline igneous complex hosted gold deposits are a rare, but potentially substantial type
of gold deposit. Cripple Creek, Colorado is one of the best known world class alkaline
rock gold deposits. While Cripple Creek is one of the largest gold alkaline systems in the
world, gold enrichment in these systems is still not well understood. Both complexes lie
along a trend of Tertiary alkaline complexes that extend from Mexico to Canada.

The project area is part of the larger Rattlesnake Hills Alkaline Igneous Complex
(RHAC). The local geology of the project area consists of Archean mica-rich schist
basement rocks and 15 Tertiary intrusive bodies with varying lithologies of phonolite to
quartz monzodiorite. The age of Rattlesnake Hills alkaline complex is dated as 43-44 Ma.
The three largest and most extensively drilled bodies of the alkaline complex: North
Stock, South Stock, and Antelope Basin; however, South Stock is not currently being
explored.

North Stock is dominated by explosive diatreme breccias and porphyritic bodies, both containing gold mineralization. Antelope Basin is a large quartz monzodiorite body that intruded schist basement and remains a target for gold mineralization. Gold mineralization aligns with the wall of the collapse cone of the diatreme breccia and the schist wall rock which are parallel to local faulting. These structures provide structural controls for the gold mineralization. Gold mineralization occurs in at least two styles: high grade gold+carbonate veins and low grade disseminated gold in altered rocks.

Mineralized and barren samples were analyzed to determine the form and setting of gold mineralization. Ore microscopy of thin sections shows the main ore minerals are gold, pyrite, marcasite, chalcopyrite, sphalerite, and other trace sulfides. Gold grains are found in marcasite grains and rarely as free gold in carbonate veins. The gold grains analyzed with scanning electron microscopy (SEM) have similar contents of gold and silver. Gold and silver are also found in marcasite and pyrite grains either in the lattice structure and/or nanonuggets. Laser ablation inductively couple plasma mass spectrometry (LA-ICP-MS) of pyrite grains show there is an increased concentration of arsenic and gold in the rims while the cores are depleted. In general, there are two trends of arsenic and gold in pyrite grains: 1) high gold and arsenic values and 2) low arsenic and low gold values. Additionally, lattice bound and/or nanonuggets of silver are found in marcasite grains.

Quantitative evaluation of minerals by scanning electron microscopy (QEMSCAN) analysis of 11 thin sections samples using back scatter imaging produces false-colored images taken across a 20-micron resolution. QEMSCAN images show several additional features that were not recognizable with ore microscopy: 1. Strong K-

feldspar alteration in all samples, by percent volume ~40-84%, 2. Pyrite or marcasite with arsenian rims is associated with muscovite-sericite zones, 3. There are generally two generations of carbonate in veins (in calcite-rich veins early calcite is rimmed by Mg and Fe-bearing calcite, and dolomite-rich veins show early dolomite with late Mg and Fe-bearing dolomite), 4. Pyrite associated with gold mineralization is at the vein contacts with wallrock or is associated with early carbonate generations, 5. Most gold, silver, and electrum grains range from 10-25 μm.

Fluid inclusion studies show the fluid at Rattlesnake Hills is low temperature of 180-210°C with a low to moderate salinity. The inclusions measured show no evidence of boiling; however, there are inclusions that are vapor-rich but do not yield any microthermometric data. There are rare solids, daughters and/or accidental solids, in complex three-phase inclusions. Some inclusions have low, but detectable CO_2 present. LA-ICP-MS of inclusions show there is up to 2-9ppm of gold and silver in solution.

The stable oxygen and carbon isotopic compositions show two distinct isotopic trends: 1) large cluster with positive covariation of oxygen and carbon and 2) a scatter to strongly negative $\delta^{13}C_{PDB}$ values. The covariation signature is most likely caused by magmatic degassing at depth within the magma chamber causing the progressive release of CO_2 rich fluids which then resulted in the precipitation of carbonate. The signature implies that Rattlesnake Hills is dominated by a mantle-derived magma.

Rattlesnake Hills is comparable to world class alkaline gold deposits throughout the world, but has most similarities with both high and low sulfidation epithermal style

deposits. The fluid at Rattlesnake Hills was low temperature, low to moderate salinity, magmatic, and contains trace gold and silver in solution.

ACKNOWLEDGEMENTS

TABLE OF CONTENTS

LIST OF TABLES

LIST OF FIGURES

1. INTRODUCTION

Rattlesnake Hills is a 125km^2 alkaline igneous complex that is part of a larger volcanic field (325km^2) known as Rattlesnake Hills Alkaline Igneous Complex (RHAC) (Shive et al., 1977). Within the Rattlesnake Hills, there is gold mineralization hosted by alkaline igneous rocks and diatreme breccias. Rattlesnake Hills is a part of the Wyoming Craton (Figure 1.1). The volcanic field (RHAC) consists of over 50 individual igneous stocks or plugs (Shive et al., 1977). The K-Ar age of rhyolite and phonolite are respectively, 44.0±2.6 and 43.6±1.0 million years old, indicating magmatism occurred during the Eocene (Pekarek et al., 1974). Overall, the igneous bodies are oval in map view and are topographic highs (Evolving Gold Corp, 2009).

The volcanic field (RHAC) can be divided into three different packages: central alkali group (CAG), western felsic group (WFG), and the eastern felsic group (EFG) (Hoch, 1991; Hoch and Frost, 1993) (Figure 1.2). The intrusive complexes consist of phonolites, quartz-monzodiorites, and feldspar porphyries (Evolving Gold Corp, 2009). The volcanic centers show significant variations based on silica content, and calcium vs. sodium rich phonolites and porphyries (Hoch, 1991; Pekarek, 1977). The alkali-rich centers tend to be smaller than the silica saturated centers, but overall the sizes range from 250 to 2000 feet in diameter, with North Stock being one of the largest centers (Pekarek et al., 1974). Additionally, Rattlesnake Hills has an explosive history, and that history is represented by extensive diatreme breccias (Evolving Gold Corp, 2009).

1

The igneous centers intruded into a remnant of an Archean greenstone belt, which is mostly biotitic schist, gneiss, and granite (Hausel, 1996). The granite (2.6 Ga) and gneiss (3.2 Ga) have similarities to the sequence seen in the South Pass District of Wyoming (Hausel, 1998; Hausel, 1996). Yet, Rattlesnake Hills is dominated by metavolcanic rocks and metagraywackes, while South Pass has a more mafic influence than Rattlesnake Hills (Frost et al., 2006).

Rattlesnake Hills can be characterized as an alkaline gold-bearing deposit, where gold mineralization occurs within and along the margins of large igneous bodies. The host complex is partially silica undersaturated, shallowly intruded (0-3000'), and the ores share similarities with epithermal and porphyry-style alkaline hosted precious metal deposits throughout the world (Jensen and Barton, 2000). While the area was initially investigated for precious metals associated with banded iron formation and metachert that is located in the area of the WFG, the main gold mineralization is associated with the igneous bodies of the CAG (Hausel, 1998; Evolving Gold Corp, 2009). Hausel (1998) first noted potential for gold mineralization in 1982, but American Copper and Nickel (ACNC) had already acquired Rattlesnake Hills and started a gold exploration program in the early 1970s (Evolving Gold Corp, 2009). Evolving Gold acquired the property in 2008 and at that time began an extensive exploration drill program (Evolving Gold Corp, 2009). At the time of writing this thesis, Evolving Gold and Agnico-Eagle Mines Ltd formed a joint-venture for the 2011 drill program. In depth mineralization descriptions are in the following chapter.

Alkaline hosted gold deposits have been studied in great detail, but there are still many unknown factors. Important papers that discuss gold in alkaline complexes are:

Davies et al., 2008; Jensen, 2003; Jensen and Barton, 2000; Jensen and Barton, 2007; Jinzhong and Li, 2000; Kelley et al., 1998; Kelley and Ludington, 2002; Mutschler et al., 1985; Mutschler et al., 1991; Ronacher et al., 2000; Ronacher et al., 2004; Scherbarth and Spry, 2006; Sillitoe, 2008. Gold enrichment in alkaline systems is not well understood (Jensen and Barton, 2000). Gold bearing alkaline magmatic centers range significantly in age, size, composition, metal content and the grade of metal content (Mutschler et al., 1991; Jensen and Barton, 2000). Alkaline magmatic centers are located predominately in North America and in southwestern Pacific arcs (Jensen and Barton, 2000).

One of the most important belts of alkaline magmatic centers in North America is the Colorado Mineral Belt (CMB) (Figure 1.3). The CMB includes Boulder County, and Central City, Colorado (Kelley and Ludington, 2002). The CMB formed during two periods: 1) SW-NE trend 70-40 Ma during the Laramide Orogeny and (2) N-S trend at 35-27 Ma along the Rocky Mountains (Kelley et al., 1998). All these deposits of the CMB formed in the same geographical area (inboard North American Cordilleran) or distant from the subduction zone, during a specific time and environment (ages previously mentioned, the second of which corresponds to the transition between subduction related compression and post-subduction extension), with similar magma chemistry (alkalic) that indicated these are spatially related and potentially genetically related (Kelley and Ludington, 2002). While these centers have many similarities, there are also many differences (see further discussions in Chapter 2).

However, alkaline complexes do occur globally (Jensen and Barton, 2000) (Figure 1.4). World class gold deposits like Porgera, Ladolam, and Emperor are island-

3

arc alkaline hosted gold deposits that have produced million tonnes of gold with significant reserves (Jensen and Barton, 2000). The compositions of world class alkaline-hosted gold deposits vary notably: mafic, intermediate, felsic and silica-saturated or silica-undersaturated (Jensen and Barton, 2000). The complexity of the compositions implies the range of rock types in the systems were formed by more than crystal fractionation (Jensen and Barton, 2000). Some of the compositional variations can be caused by potassic alteration, which occurs at all alkaline deposits but with differing degrees (Jensen and Barton, 2000).

Additionally, questions concerning the differences between calc-alkaline and alkaline-type epithermal gold deposits have arisen. Ronacher et al. (2000) suggested that the relative abundance of CO_2 (~1.5 to 4 mol%) present in fluid inclusions can separate the two types of deposits. Cripple Creek and Porgera are alkali-type deposits, with similar CO_2 content of fluid inclusions (Ronacher et al., 2000). Other questions concerning alkaline hosted gold deposits relative to Rattlesnake Hills are/include:

- What distinguishes world-class gold deposits from sparsely mineralized or barren alkaline centers?

- How do compositional characteristics discriminate alkaline-hosted gold deposits from other deposit types?

- What are the characteristics of the hydrothermal fluids? What is the origin of gold bearing fluids? Is the hydrothermal fluid responsible for gold mineralization at Rattlesnake Hills related to fluids controlling gold mineralization in other alkaline-hosted gold deposits?

- What controls gold deposition in alkaline complexes?

- Does geologic environment impact size or grade of deposit?

- Does lattice bound or free gold influence grade?

- Is Rattlesnake Hills an extension of the CMB?

- Is Rattlesnake Hills genetically related to the CMB and/or the large alkaline igneous belt that extends from Mexico to Canada?

- Does Rattlesnake Hills follow similar geochemical trends as in the CMB or Cripple Creek? Do Rare Earth Elements (REEs) spider diagrams resemble those of volcanic rocks from rifts zones? Do the REEs indicate fractional crystallization? And is the geochemical composition similar to the bulk earth or primitive mantle?

Not all of these questions will be addressed and/or answered in this thesis.

In order to better understand alkaline hosted gold mineralization, this study focuses on North Stock mineralization. North Stock is ~2000' in diameter, and is roughly oval in plan-view (Evolving Gold Corp, 2009) (Figure 1.5). North Stock is within Archean basement that has been intruded by and is composed of three phases of the CAG: dominantly feldspar-porphyry with lesser phonolite and dikes of quartz monzodiorite (Evolving Gold Corp, 2009). North Stock has pyroclastic rocks on the western side with included organic carbon xenoliths, and has diatreme breccias throuhout (Evolving Gold Corp, 2009). North Stock is a late stock in the CAG (Evolving Gold Corp, 2009). There are no evident surficial structural controls for gold deposition; however, there are defined zones of high grade mineralization (Ch.3).

To better understand what controlled gold mineralization at North Stock, this study focuses on ore microscopy, fluid inclusion microthermometry, stable isotope

geochemistry (O and C), scanning electron microscopy (SEM) for trace element content of ore minerals, and laser ablation inductively coupled mass spectrometry (LA-ICP-MS) studies of major ore minerals. Samples of schist, porphyry, phonolite, quartz-monzodiorite, and a variety of breccias were collected and analyzed. All samples were collected from drill core at a variety of depths. Detailed ore microscopy descriptions were made from the samples in order to determine ore paragenesis. Microthermometry measurements on fluid inclusions were made and analyzed from carbonates, primarily calcite with minor dolomite and rare quartz, from veins in porphyry, schist, schist breccias, and heterolithic igneous breccias. Samples of veins and altered rock of porphyry, schist, phonolite, and heterolithic igneous and metamorphic breccias were selected for LA-ICP-MS multi-element analysis of generations of pyrite and marcasite to determine gold and related trace element controls.

The geochemistry of the fluids will be compared to those known to have impacted by ore-bearing rocks in similar alkaline hosted gold deposits throughout the world. The most closely analogous alkaline hosted gold complex to RHAC is Cripple Creek, Colorado (Jensen and Barton, 2000). Hence this deposit is summarized in this thesis. This comparison coupled with geochemical information creates a history of gold mineralization and crystallization of the different source materials for the stocks. The fluid chemistry, pressure-temperature, and conditions of mineralization will better define proposed source(s) of the fluids and environmental factors that control gold deposition at Rattlesnake Hills.
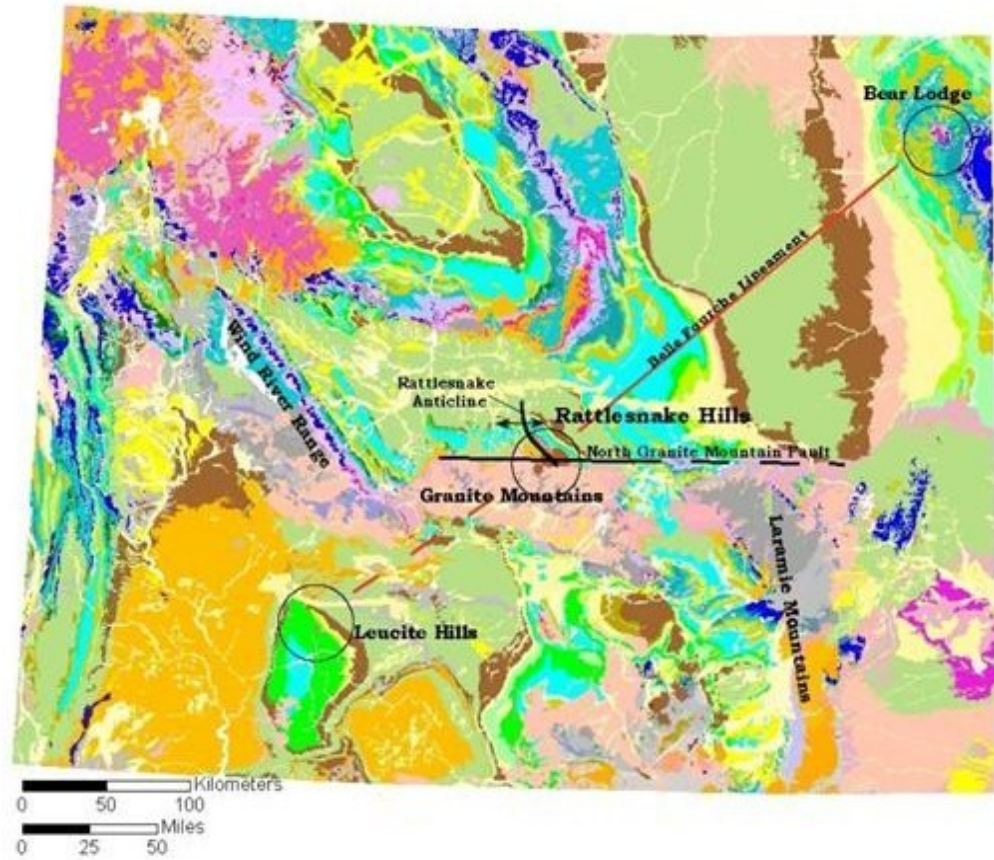
Figure 1.1 Geologic map of Wyoming showing the Rattlesnake anticline, North Granite

Mountain fault (NGM), Belle Fourche Lineament connecting Rattlesnake Hills to Bear

Lodge and Leucite Hills, which are other Tertiary alkaline complexes (from Evolving

Gold Corp, 2009).
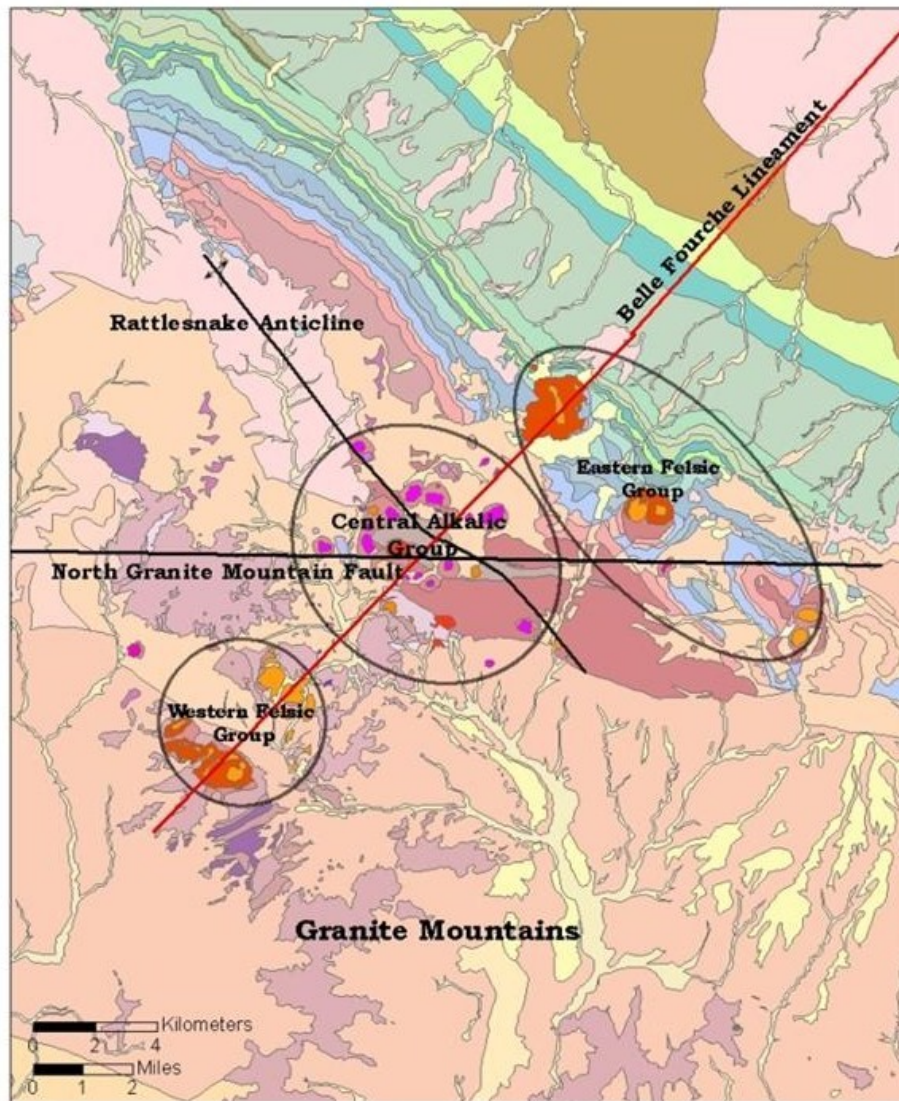
Figure 1.2 Rattlesnake Hills alkaline complex separated into three distinct groups: western felsic group (WFG), central alkalic group (CAG), and eastern felsic group (EFG). Red, orange, bright pinks located within the three groups represent Tertiary intrusive phases. Blues and greens represent Cretaceous continental type deposits (i.e. Wagon Bed or Split Rock Formations) and the muted pinks are Precambrian metamorphic rocks (from Evolving Gold Corp, 2009). For discussion of structures (Rattlesnake anticline, North Granite Mountain Fault, and Belle Fourche Lineament) see text in Chapter 2.
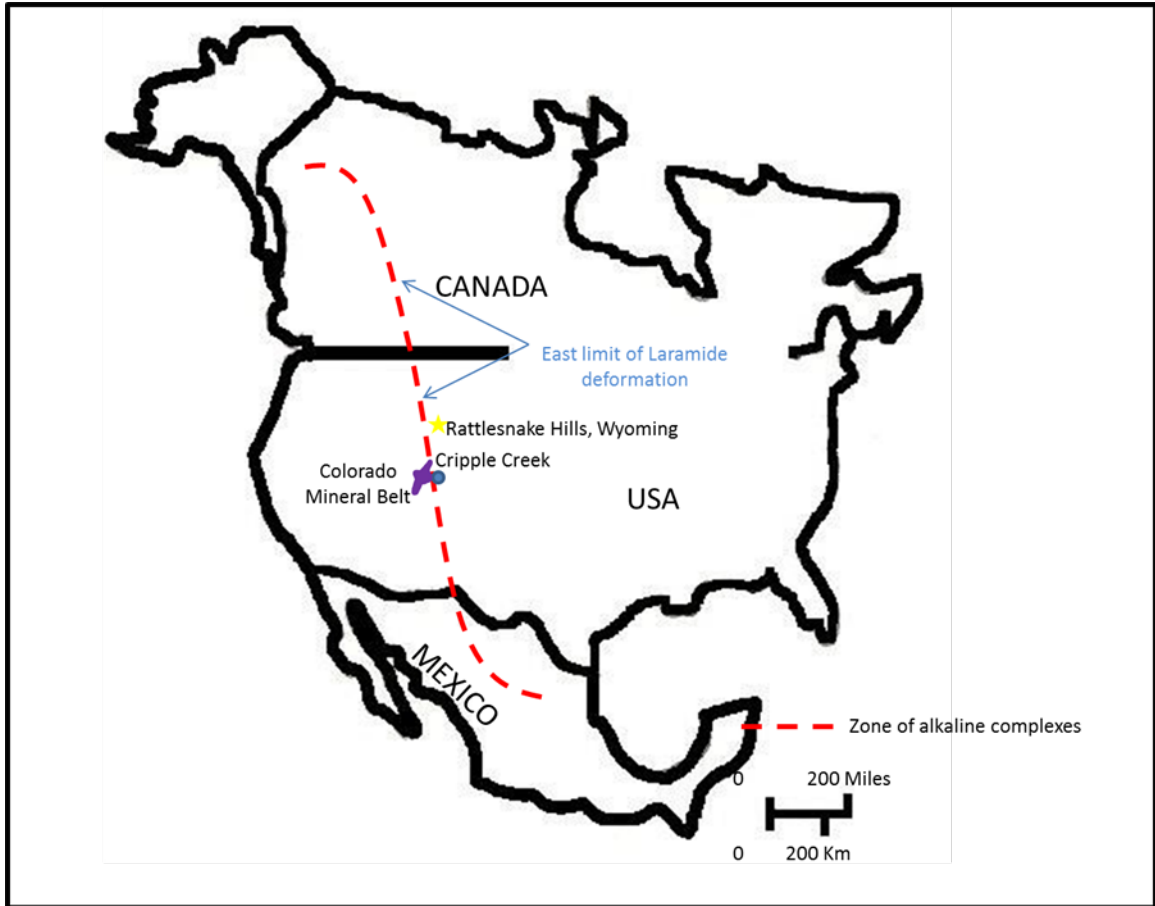
Figure 1.3 Map of North America outlining alkaline igneous complexes, Cripple Creek, the Colorado Mineral Belt, and Rattlesnake Hills alkaline complex (adapted from Kelley and Ludington, 2002).
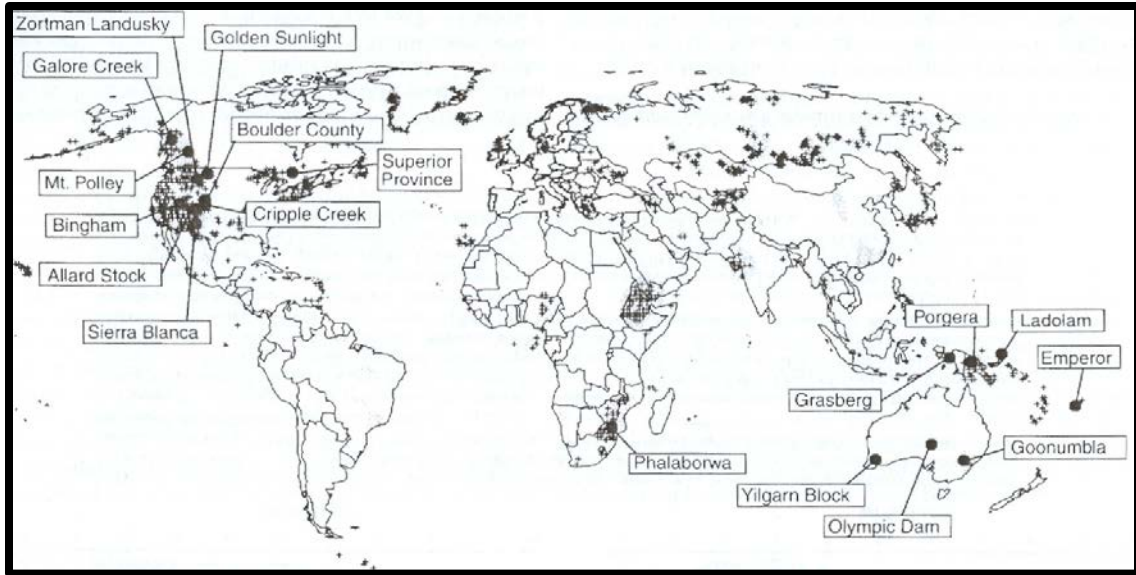
Figure 1.4 Map of alkaline igneous complexes throughout the world. World class

deposits are outlined and the labeled deposits are gold producing locations (from Jensen

and Barton, 2000).
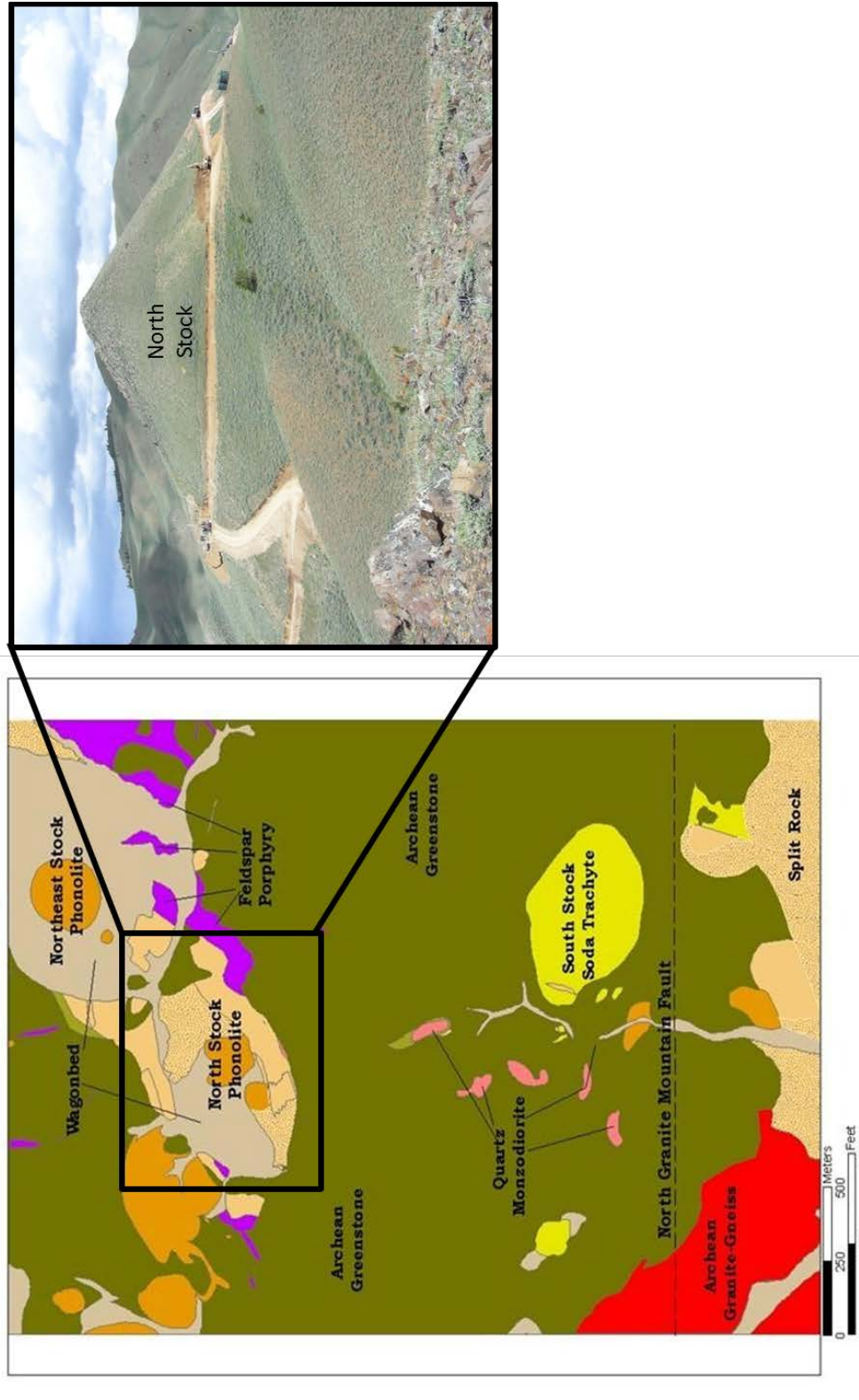
Figure 1.5 Detailed map of CAG of the Rattlesnake Hills; photograph of North Stock from Antelope Basin showing the type of style of outcrop of rocks of the complex (adapted from Evolving Gold Corp., 2009).

2. REGIONAL GEOLOGY

2.1 GEOLOGICAL SETTING

Rattlesnake Hills is a part of a much larger volcanic field known as the Rattlesnake Hills Alkaline Complex (RHAC). RHAC is located approximately 15 miles south of the geographic center of Wyoming (Figure 1.1). The complex is in Natrona County, and is directly west of the Gas Hills Uranium district, bordered to the north by the Wind River Basin, and is on the northern edge of the Granite Mountains (Figure 2.1) (Hausel 1998; Shive et al. 1977).

2.2 BRIEF GEOLOGIC HISTORY OF WYOMING

The Wyoming Craton is 500,000km^2 in size and represents ~10% of all surface exposure in the state (Grace et al., 2006; Houston, 1969). Of those Precambrian surface exposures, granites and granitic gneisses are the most common and provide much of the history (Houston, 1969) (Figure 2.1). These rocks mainly preserve amphibolite grade metamorphism (Grace et al., 2006).

The overlying Paleozoic units become progressively thinner toward the East (Houston, 1969). The Paleozoic represents multiple sequences of land emergence and uplift, shown by deposition of sandstone, shales, and dolomites transitioning into limestones (Houston, 1969). This transition occurred during the Mississippian, a period

of the Paleozoic. From the early Paleozoic transition into the Mississippian, Wyoming was close to the western margin of the North American Craton. For the duration of the Pennsylvanian, there was an orogeny in an ancient sea forming the ancestral Rocky Mountains (Houston, 1969).

Mesozoic rock units are generally thicker than Paleozoic units. The Triassic units are red beds that indicate a period when Wyoming was a shallow marine shelf and adjacent desert (Houston, 1969). The Jurassic was a period of erosion followed by the invasion a sea shown by deposition of shales, siltstones, and sandstones (Houston, 1969). The Cretaceous was a time of marine transgressions and regressions (Houston, 1969). During the early Tertiary, there was a period of deformation, uplift, and retreat of the Cretaceous sea. This deformation and uplift is the Laramide Orogeny. There are Tertiary clastic deposits from erosion from the uplift, which created topography similar to the modern day Rocky Mountains (Houston, 1969). The Eocene experienced volcanism (Houston, 1969). Lastly, during the Oligocene the area has undergone another climate change to similar to modern climates (Houston, 1969). Deposition of terrestrial sediments occurred in the basins between the uplifts, which are comprised of Precambrian cores.

2.3 EVOLUTION OF THE BASEMENT ROCKS OF RATTLESNAKE HILLS

Rattlesnake Hills exposes a fragment of the Archean rocks of the Wyoming Craton and is located on the northern edge of the Granite Mountains (Figures 2.1 and 2.2). The oldest rocks in the Granite Mountains are gneiss, which are characterized by calc-alkaline granitic gneiss or the Sacawee gneiss, and date to ~3.3 to 3.6 Ga (Grace et al., 2006). The younger intrusive rocks in the Granite Mountains are ~2.62 plutons of the

Granite Mountain Batholith, which have intruded into the older units (Frost et al., 2006). The Sacawee gneiss is widely distributed unit throughout the Granite Mountains (Grace et al., 2006). This gneiss represents a block of Paleo- and Mesoarchean crust, named the Sacawee Block (Grace et al., 2006). The Sacawee Block records two periods of deformation: 1) contractional deformation, ~2.83 Ga, but this might only be a metamorphic age; 2) the formation of the Oregon Trail structural belt (OTSB) an east-west, high strain shear zones (Grace et al., 2006). The multiple shear zones are related tectonically (Grace et al., 2006). The age of the shear zone is poorly constrained from different ages at different locations from ~2.65 Ga at West Sage Hen Rocks to ~2.86 Ga at the Beulah Belle Lake area but an age of ~2.62 Ga is the age Grace et al. gave for the entire structure (Grace et al., 2006).

McDougal Gulch is a small northwest-southeast shear zone that is part of the larger OTSB shear zone (Grace et al., 2006). The McDougal shear zone is represented by the McDougal Gulch metavolcanic unit (Grace et al., 2006). The deformation of the OTSB is dated ~2.62 Ga (Grace et al., 2006) (Figure 2.3). The foliations imply the shear zone is dipping steeply to the south and lineations plunge down-dip (Frost et al., 2006). While the McDougal Gulch shear zone is ~2.62 Ga, the adjacent supracrustal rocks are ~2.72 Ga (Grace et al., 2006).

The nature of the Sacawee Block has major implication for the style of plate tectonics and deformation for Wyoming (Figure 2.4). According to Grace et al. (2006) there are two models for the formation of the Sacawee Block: 1) it was originally a fragment of crust of the Wyoming Craton that existed before Neoarchean magmatism or

2) it was an accreted exotic terrene. However, based on U-Pb zircon dates and Nd

isotopic compositions implies that the Sacawee Block most likely fits model one (Grace

et al., 2006). Overall the Sacawee Block is "evidence for plate-tectonics style horizontal

convergence and crustal modification along the southern margin of the Wyoming craton"

(Grace et al., 2006).

RHAC is hosted in supracrustal rocks to the north of the Sacawee Block. Nd

isotopic compositions of these supracrustal rocks, specifically greywackes of the Archean

UT Creek formation, imply that they formed from a juvenile source (Frost et al., 2006).

The magmatic phases also indicate a juvenile source or depleted mantle source (Frost et

al., 2006). According to Frost et al. (2006) juvenile and sedimentary rocks were

deposited, deformed, and intruded by plutons. The age of the juvenile supracrustal rocks

range from 2.73-2.72 Ga to 2.68-2.67 Ga (Frost et al., 2006). This precise sequence "is

interpreted to record episodes of juvenile crust formation and amalgamation, a process

that appears analogous to modern plate-tectonics processes of lateral accretion" (Frost et

al., 2006).

In summary the Paleo- and Mesoarachean Crustal Evolution of the Rattlesnake

Hills area is interpreted to as:

1. Deposition of precursors to orthogneiss in a back-arc basin sea approximately
   3.6 to 3.3 Ga (Hausel, 1996),
2. The tectonically calm period was ended by a release of volcanic gases and
   fluids followed by the creation of an island arc (Hausel, 1996),

3. Precursor of the current day orthogneiss was intruded into an island arc (Frost et al., 2006),

4. The island arc-rocks were thrust onto the margin of the Wyoming Province ~2.65Ga (Frost et al. 2006) ,

5. The area experienced extreme crustal shortening causing a deformation and folding (Hausel, 1996), which may be related to deformation in the OTSB (Grace et al., 2006; Frost et al., 2006), and lastly

6. Emplacement of Granite Mountain Batholith ~2.62 Ga (Frost et al., 2006).

2.4 RATTLESNAKE HILLS LARAMIDE AND POST LARAMIDE STRUCTUAL GEOLOGY

Rattlesnake Hills is in the core of a northwest-trending anticline, known as the Rattlesnake anticline, which has experienced a significant amount of erosion to expose the Precambrian core (Hausel, 1996) (Figure 1.1 and 1.2). Even though the area has undergone intense deformation and folding during the Laramide, there is only one Laramide fold phase related to the formation of the northwest-southeast trending Rattlesnake anticline (Pekarek, 1977).

There are minor normal faults and numerous reverse faults, which are most commonly, control the locations of alkalic centers in the RHAC (Pekarek, 1977). This faulting is post-Laramide (Pekarek, 1977). The largest fault in Rattlesnake Hills is the North Granite Mountain (NGM) fault (Evolving Gold Corp, 2009) (Figure 1.1 and 1.2). The NGM fault is east-west trending, and intersects the Rattlesnake anticline and Belle Fourche Lineament (Evolving Gold Corp, 2009). The NGM fault has experienced

multiple episodes of movement that has created approximately 1500 meters of dip slip displacement across the fault zone (Evolving Gold Corp, 2009; Love, 1970) (Figure 1.1 and 1.2). The NGM fault is interpreted as a reactivated Proterozoic zone of weakness (Evolving Gold Corp., 2009).

The Archean McDougal Gulch shear zone has been described previously, but there is one other structure related to shear zones: Belle Fourche Lineament. This is the only manifestation of the northeast-trending lineament that is potentially a Precambrian reactivated shear zone linking Rattlesnake Hills to Leucite Hills and Bear Lodge Mountain, which are other Tertiary alkalic complexes in Wyoming (Evolving Gold Corp., 2009; Slack, 1981).

In summary the Laramide and subsequent Evolution of Rattlesnake Hills (Pekarek, 1977) is:

1. Thrust of Granite Mountains southwest-ward, proceeded by the uplift, folding, and faulting of the Granite Mountains during the Eocene at the same time as subsidence of the Wind River Basin,

2. Start of Rattlesnake Hills volcanic activity followed by 20 million years of stability, and followed by

3. Subsidence of Granite Mountains during the Miocene.

2.5 GOLD MINERALIZATION AT RATTLESNAKE HILLS

2.5.1 Overview of Exploration History

Most of the exploration of Rattlesnake Hills has been completed by private companies, and therefore, not all the information is readily available to the public. Hausel (1996) reported that there had been no past production in the area. However, 20 to 30 prospect pits from the early 1900s with an additional couple of shallow long shafts were discovered in 2003 (Evolving Gold Corp, 2009). In 1982, Hausel was searching the area for disseminated gold and found an outcrop of pyritiferous metachert (Hausel, 1996).

In the early 1970s American Copper and Nickel Company (ACNC) began a reconnaissance exploration program on the property. During the early 1980s, ACNC's presence in Rattlesnake Hills grew from mapping, geophysical surveys, and surface geochemistry sampling in 1983 and 1984 to drilling 32 reverse circulation drill holes with a total footage of 9,815 feet (Evolving Gold Corp, 2009). ACNC were testing both the Archean metacherts and Eocene mineralization, but this exploration was slightly south of the current study area (Evolving Gold Corp, 2009).

In 1992 Canyon Resources started mapping and a rock chip sampling survey of the area before striking a joint venture with Newmont Exploration. Newmont Exploration identified North Stock as a potential target for mineralization. From 1993 to 1995, Newmont drilled 14 reverse circulation and core holes with a total combined footage of 10, 705'. Assay results are more complete and there is some preserved core and rock chip samples from the drill program. However, all 14 holes were shallow and while there were minor intersections of gold mineralization, Newmont's drill program did not penetrate the

extensive gold mineralization in Rattlesnake Hills. Canyon Resources and Newmont relinquished interest in the property in 1997 (Evolving Gold Corp, 2009).

The assay results from previous exploration companies were not made available until Bald Mountain Mining Company leased claims in 2003 and provided copies of ACNC and Newmont assay results (Evolving Gold Corp, 2009). From 1997 to 2008, the property experienced limited exploration. Evolving Gold Corp (EGC) acquired Rattlesnake Hills in 2008 and began an extensive drill program. The 2008 and 2009 drill seasons, EGC completed 93 drill holes with a total footage of 118,585 feet, a geophysical survey, extensive surface-outcrop sampling and surface mapping (Evolving Gold Corp, 2009). The 2010 drill season continued on the same trend with 62 core holes, 42 which focused on the North Stock mineralized target, with 79,442.5' drilled and additional mapping and surface sampling (Evolving Gold Corp, 2009). The three drill seasons expanded the known zones of mineralization with numerous anomalous intersections of gold. At the time of writing this thesis, EGC had formed a joint venture with Agnico-Eagle Mines Ltd and is currently preparing for the 2012 drill season which will focus on continuing to expand known gold mineralization (Evolving Gold Corp, 2012).

While it is premature to state gold resources at Rattlesnake Hills, some metallurgical tests have been completed to determine the recovery and milling feasibility of the ore minerals (Evolving Gold Corp, 2009). Gravity, leach, and flotation tests were done on a sample from Antelope Basin; however, the test did not specify rock type, style of mineralization, or gold assay results of the sample (Evolving Gold Corp., 2009). The tests determined the ore is favorable to leaching and milling (Evolving Gold Corp, 2009).

2.5.2 Alkaline Complexes Genetic Models

The conceptual deposit model EGC has utilized for exploration is outlined by Jensen and Barton (2000) for alkaline hosted gold deposit similar to Cripple Creek, Colorado. However, EGC doesn't make a distinction between epithermal and porphyry-style mineralization that was made by Jensen and Barton (2000).

The similarities and differences of alkaline hosted gold deposits are more pronounced when comparing alkaline complexes throughout the world (Figure 1.4). Alkaline hosted gold deposits are broken into 2 groups: epithermal-style and porphyry-style deposits (Jensen and Barton 2000) (Figure 2.5). Epithermal deposits are characterized by low temperatures (<300°C), low salinity (<10wt %NaCl), shallow (<1-2km) formation, Au-rich veins with high Au:Ag ratios, with more tellurides than native gold (Jensen and Barton, 2000). Gold mineralization can be hosted by calderas, diatremes, and hypabyssal stocks depending on the type of environment: island arcs or areas of thickened continental crust (Jensen and Barton, 2000). The mineralizing phase is late stage and controlled by structures such as reactivated or radial emplacement structures (Jensen and Barton, 2000). Epithermal fluid sources are magmatic with variable meteoric fluid interaction (Jensen and Barton, 2000). Epithermal deposits include: Porgera, Emperor, Ladolam, Golden Sunlight, Ortiz, Cripple Creek, Boulder County in Colorado, and Montana telluride belt (Jensen and Barton, 2000).

Porphyry style deposits are formed in arc environments, the host intrusive range from silica-saturated to silica-undersaturated, and mineralization is generally associated with early intrusive phases but there are multiple stages of alteration and mineralization

(Jensen and Barton, 2000). The ore-bearing hydrothermal systems are hot (400-700°C) and involve saline fluids (range to 65 wt %NaCl) (Jensen and Barton, 2000). The fluids responsible for mineralization are similar to epithermal systems: magmatic with meteoric influences (Jensen and Barton, 2000). Porphyry style deposits include: Sierra Blanca in New Mexico, Galore Creek, Allard Stock, Goonumbla, Copper Mountain and Mt. Polley in British Columbia (Jensen and Barton, 2000). Porphyry-type and epithermal alkaline deposits overlap and it is possible that they grade into the other deposit type for instance at Emperor and Porgera.

2.6 COMPARISON TO GOLD ENRICHED ALKALINE DEPOSITS

2.6.1 Comparison to Cripple Creek, Colorado

From Canada to Mexico, the Rocky Mountains are scattered with Laramide and post-Laramide alkaline igneous complexes (Figure 1.3). While a few are gold bearing, the most economically important is Cripple Creek. Cripple Creek is a large explosive volcanic diatreme complex, and is the largest diatreme complex in the alkaline trend of the Rocky Mountains (Kelley et al. 1998). Cripple Creek was discovered in 1891, and has since produced over 22 million ounces of gold (Kelley et al., 1998; Jensen and Barton, 2007). Cripple Creek is one of the top gold producers in the United States (Kelley et al., 1998). Cripple Creek is analogous to other alkaline complex hosted gold deposits throughout the world, and within a local context Rattlesnake Hills. Even though Cripple Creek is a world class gold deposit, there are still many unanswered questions concerning the genetic relationships of the alkaline complex to the ore deposit (Kelley et al., 1998).

21

Cripple Creek is described and documented in this thesis due to the similarities between it and Rattlesnake Hills.

Cripple Creek formed between 32 and 27 Ma and is a partially silica undersaturated system (Kelley et al., 1998). Major lithologies range from phonolite to tephriphonolite to phonotephrite. There are lamprophyric dikes, and hostrocks of granites, and schists throughout the region (Kelley et al., 1998). Additionally, geologic mapping of the Cripple Creek area shows multiple, small intrusive phases outside the primary ore zones (Reinhard et al., 1976; Kelley et al., 1998) (Figure 2.6). While the relationship of these units is not well understood, they are genetically related (Kelley et al., 1998). It is thought that the felsic phases are generally later in the whole field, but at Cripple Creek there is evidence that the mafic phases are the latest events (Kelly et al., 1998). Field observations verify that phonolites are more abundant than the mafic phases; therefore, the mafic phases cannot be the parent material of the phonolites (Kelley et al., 1998). Jensen and Barton (2007) suggest that mineralization is associated with late mafic magmatic events. It is probable that mineralizing fluids are the result of a combination of eruptive and diatreme complex histories, which as will be shown in this work is similar to Rattlesnake Hills.

The Cripple Creek system has multiple generations of hydrothermal events (Jensen and Barton, 2007). Gold mineralization is associated with the later stages of magmatism, but it is uncertain which magmatic events are responsible for the hydrothermal alteration, early or late (Jensen and Barton, 2007). At Cripple Creek, there are two primary styles of mineralization present. The first type, narrow, high-grade veins

22

bearing gold, gold-tellurides, and gold-silver-tellurides are extensive throughout the system (Pontius and Butts, 1991; Kelley et al., 1998). The second type is low-grade disseminated gold in hydrothermally altered rocks (Pontius and Butts, 1991; Kelley et al., 1998). From these two styles of mineralization, gold occurs in three ways. Gold can be adsorbed as a fine growth onto edges of pyrite grains and as intergrowths with pyrite (CC&V, 2005). Gold also occurs as free gold after telluride mineralization with oxides and in the high-grade quartz-fluorite veins as gold-silver tellurides (CC&V, 2005). The average size of mined gold grains is less than 20 microns (CC&V 2005).

Ore controls at the Cresson deposit at Cripple Creek, Colorado are related to the pre-mineralization structural fabric. Fractures are the primary mineralization control (Pontius and Butts, 1991). For the high-grade narrow zones, westerly dipping fractures control gold mineralization, but for low-grade disseminated gold fluids used an existing fracture pattern developed during the emplacement of the diatreme (Pontius and Butts, 1991). Pontius and Butts (1991) provide a conceptual model for ore deposition in the Cresson Deposit:

> 1) Development of the primary structural fabric and fracture systems prior, during and following the Cresson diatreme emplacement. 2) Initial relatively high temperature hydrothermal alteration along structural permeable conduits, which created broad zones of increased permability by dissolution of potassium feldspars and carbonate matrix material. 3) Gold was deposited from an alkaline, CO_2 dominated, low salinity fluid with high meteoric water content. The mixing of hypogene fluids with meteoric water and the abundant

23

open space reduced pressure and temperature causing the gold and gangue

minerals to deposit. As porous areas were filled, the hydrothermal fluids

migrated along more permeable areas with the highest gold grades located

near the margins. 4) Following the main gold depositional event, supergene

oxidation occurred within most of the mineralized zones to an average depth

of approximately 600 feet. The depth of the oxidizing event was primarily

controlled by the existing structural fabric.

By comparing regional geochemical trends, it is evident that Cripple Creek is

unique within the Rocky Mountain area and its geochemistry is not regionally controlled.

Most of the alkaline systems of the Rocky Mountains area are depleted in Ta and Nb, but

Cripple Creek is not (Jensen and Barton, 2007). In general, Cripple Creek most closely

resembles alkaline centers in the Rio Grande rift region, especially in New Mexico

(Jensen and Barton, 2007).

The magmas have an asthenospheric-mantle origin, not crustal (Jensen and

Barton, 2007). Rifting or plumes could have created this type of parental melt for the

Cripple Creek alkaline system. REE Spider Diagrams of Cripple Creek are comparable to

mantle melts in areas that have undergone rifting or affected by plumes. If Cripple Creek

can be linked to an asthenospheric-mantle source, it would be one of the earliest along the

Rio Grande Rift with an approximate age between 32 and 27 Ma (Jensen and Barton,

2007; Kelley and Ludington, 2002). Other CMB deposits range from 85 to 19 Ma with an

average of ~40Ma (Kelley and Ludington, 2002).

Oxygen isotopic compositions were analyzed from eight different samples with compositions of phonolite, trachyandesite, and tephriphonolite (Kelley et al., 1998). These samples are representative of the least altered rocks. From these eight samples, potassium feldspar, plagioclase, clinopyroxene, and magnetite were measured; however, not all samples had multiple minerals (Kelley et al., 1998). K-feldspar isotopic compositions range from 7.2 to 6.7 per mil (‰), but there were only two measurements (Kelley et al., 1998). Four grains of plagioclase were measured and ranged from 6.8 to 7.5‰ (Kelley et al., 1998). Clinopyroxenes vary in composition from 5.3 to 6.0‰ of the four measured samples (Kelley et al., 1998). Lastly, six separate magnetite grains were analyzed with compositions of 2.8 to 6.0‰ (Kelley et al., 1998).

The uniformity of the $\delta^{18}O$ values indicates that fractional crystallization rather than assimilation is the dominant process in the magmatic evolution (Kelley et al., 1998). The felsic minerals are more enriched in $\delta^{18}O$ than the mafic minerals, implying the magma was fractionating. Additionally, the $\delta^{18}O$ values infer the source material is derived from upper mantle or lower crust (Kelley et al., 1998). Lastly, there is little upper crustal interaction with the system due to the limited amount of crustal contamination.

2.6.2 Other Alkaline Magmatic Centers in the Rocky Mountain Region

Cripple Creek is part of a regional trend of Tertiary-age alkaline complexes that extends from Mexico to Canada (Kelley and Ludington, 2002) (Figure 2.7). Kelley and Ludington (2002) summarized these characteristic the systems share: 1) multiple episodes of alkalic igneous activity; 2) evidence of magmatically driven hydrothermal activity; 3) hydrothermal events are late events; 4) hydrothermal alteration is characterized as

potassic; 5) vein paragenesis is early sulfide followed by later gold and gold-tellurides.

The differences are: 1) mineralization styles; 2) type of alkaline lithologies; 3) not all

veins have similar ore minerals; 4) age (Kelley and Ludington, 2002).

2.7 MINERALIZATION OF RATTLESNAKE HILLS

The exploration to date has allowed for the recognition of several forms of gold

mineralization present in RHAC. They are categorized by host rock. The gold hosted in

Archean metacherts previously discussed is not a focus of current exploration. Visible

and disseminated gold within veins and host rocks of Eocene intrusive rocks and

diatreme breccias are the most common forms of gold mineralization present and these

are confined to North Stock (Figure 2.8). North Stock is formed of upward fanning

breccias with a phonolite center. There are stockworks of feldspar porphyry stocks and

dikes. The phonolite and breccias are bound by wallrock and brecciated wallrock. Lastly,

micron and disseminated gold is hosted by the quartz-monzodiorite in Antelope Basin.

This type of mineralization is limited to Antelope Basin, and not a primary focus of this

study. The aim of current exploration by EGC and Agnico Eagle is to expand the ore

zones at Rattlesnake Hills into a district scale (Evolving Gold, 2012).

The mineralization can also be categorized in terms of gold grades. Low grade

disseminated gold is not restricted to the Eocene volcanic intrusive but extends into

surrounding countryrock, Archean schist, forming halos of mineralization. High grade,

narrow zones of gold are located throughout North Stock and Antelope Basin. Some

zones form well-defined trends while others are patchy. All of these zones are potentially

defined by fracture zones in the intrusives and schist. The style with narrow bands of high

grade gold veins with halos of low grade disseminated gold is similar to the

mineralization styles at Cripple Creek, Colorado (Jensen and Barton, 2000).

North Stock gold mineralization is spatially associated with explosive diatreme

breccias bodies, which tend to be vertically-plunging and sub-circular (Evolving Gold

Corp, 2009) (Figure 2.8). However, gold mineralization is hosted by diatreme breccias,

feldspar porphyry, and schist wallrock. Gold is concentrated in the wall of the diatreme

breccias and in the footwall Archean schist country rock (Evolving Gold Corp, 2009).

Gold mineralization at Rattlesnake Hills can be categorized by two zones. According to

EGC, zone one "mineralization at North Stock consists of a northeast-southwest-trending,

structurally controlled, tabular body extending from surface to over 300m depth"

(Evolving Gold Corp, 2009). This zone of mineralization is high grade, with grades ~7

grams per ton (g/t) (Evolving Gold Corp, 2009). The second zone is related to a

subparallel northeast-trending fault (Evolving Gold Corp, 2009). This fault is steeply

dipping and is proposed as the southeast wall of the diatreme (Evolving Gold Corp,

2009). Overall, the North Stock mineralization is approximately 1300 feet by 650 feet

wide and extends at least 500 feet below the surface (Evolving Gold Corp., 2009).

There are several distinctive facies of alteration associated with gold

mineralization. Four main types of alteration are recognized: potassium feldspar,

carbonate, FeOH, and clay (Evolving Gold Corp, 2009). FeOH can be categorized as

jarosite, Fe-oxyhydroxides, and Mn oxyhydroxides (Evolving Gold Corp, 2009).

Potassium feldspar and carbonate alteration are most closely associated spatially to

mineralization. Alteration is described in more detail in Chapter 3.

2.8 OTHER CURRENT RESEARCH

Currently, additional work is underway at Rattlesnake Hills. A Masters of Science student at Idaho State University is working on several aspects of the project to answer questions related to gold mineralization and history of the complex. The study focuses on analyzing a possible carbonatite, and determining its geochemical and petrographic relationship to gold mineralization (Durk, 2011). Additional geological mapping, alteration mapping, and detailed petrographic analysis of rock units will be used to better constrain the emplacement history of the alkaline complex (Durk, 2011). Previous studies have only defined magmatism as Eocene, however, there is been no attempt as yet to determine the timing relationships of the various intrusive bodies.
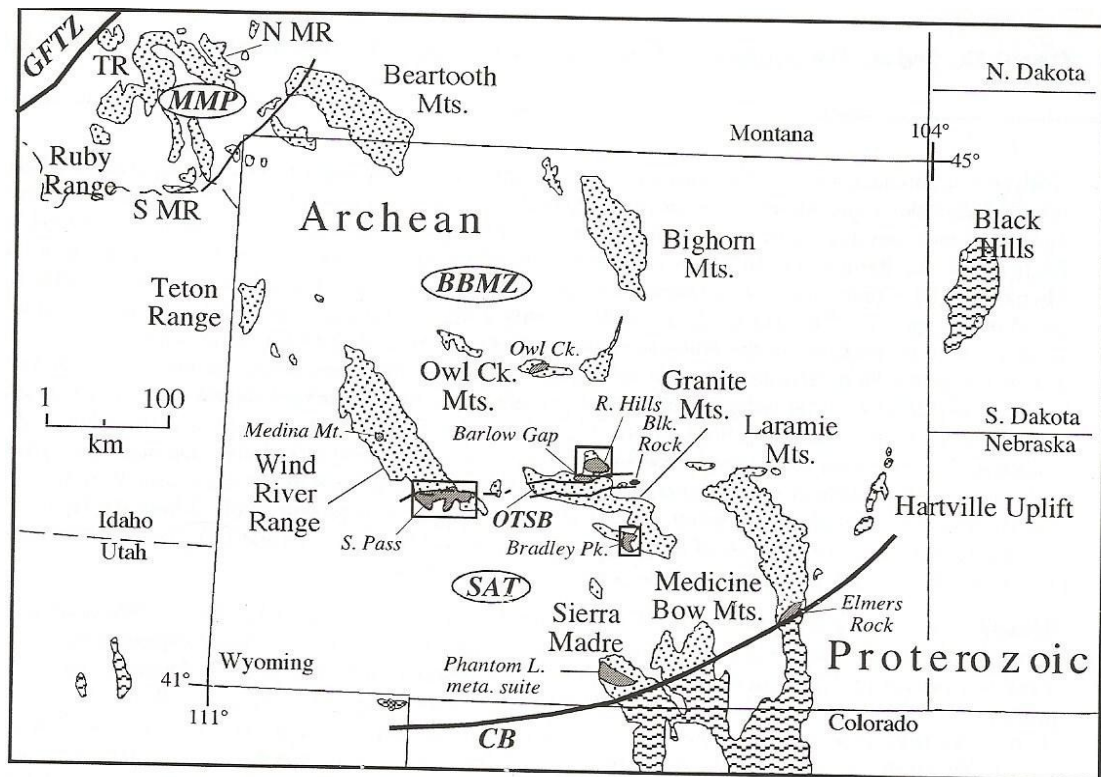
Figure 2.1 Map of Wyoming showing Laramide uplifts that have Precambrian cores and the distribution of Archean relative to Proterozoic basement. R. Hills is Rattlesnake Hills Alkaline Complex, CB Cheyenne Belt, GFTZ Great Falls Tectonic Zone, OTSB Oregon Trail Structural Belt, BBMZ Beartooth-Bighorn magmatic zone, MMP Montana metasedimentary province, SAT southern accreted terranes (From Grace et al., 2006).
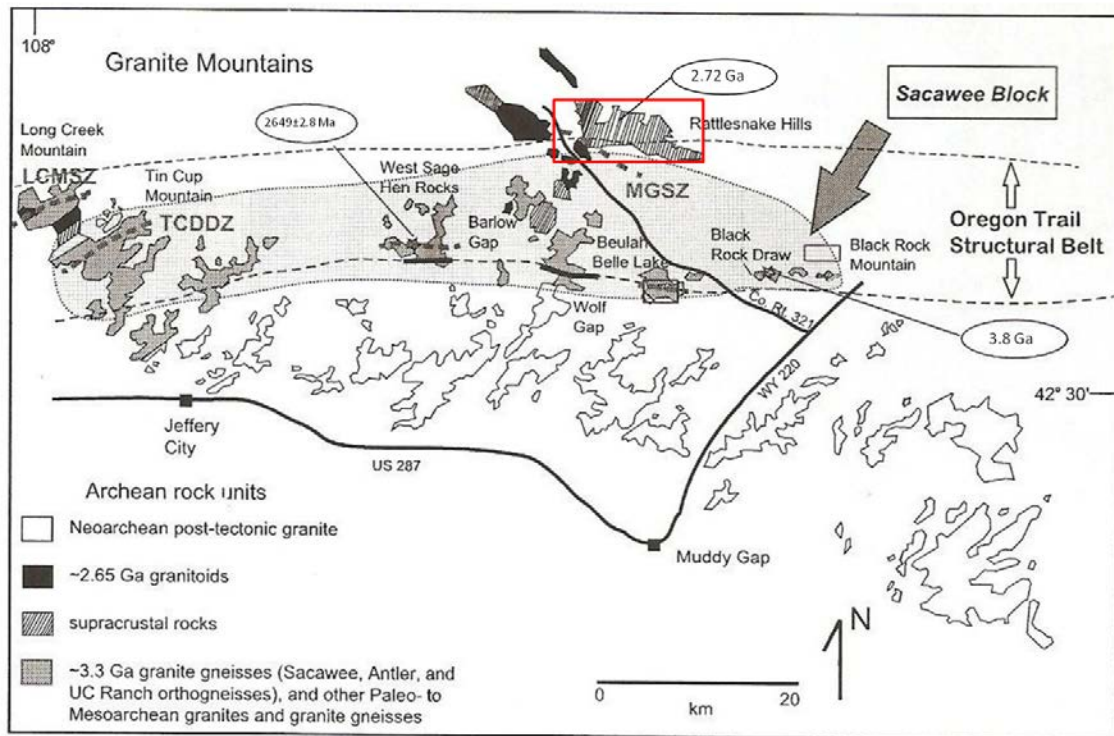
Figure 2.2 Map of Granite Mountains showing Neo and Meso-Archean rocks and
structural zones. The red outlined area is the map area of Figure 2.3. Long Creek
Mountain shear zone (LCMSZ), Tin Cup ductile deformation zone (TCDDZ), McDougal
Gulch shear zone (MGSZ). The dates are U-Pb age. Note the juxtaposition of the
Rattlesnake Hills supracrustal rocks (2.72 Ga) against the MGSZ (2.62 Ga) (adapted from
Grace et al., 2006).
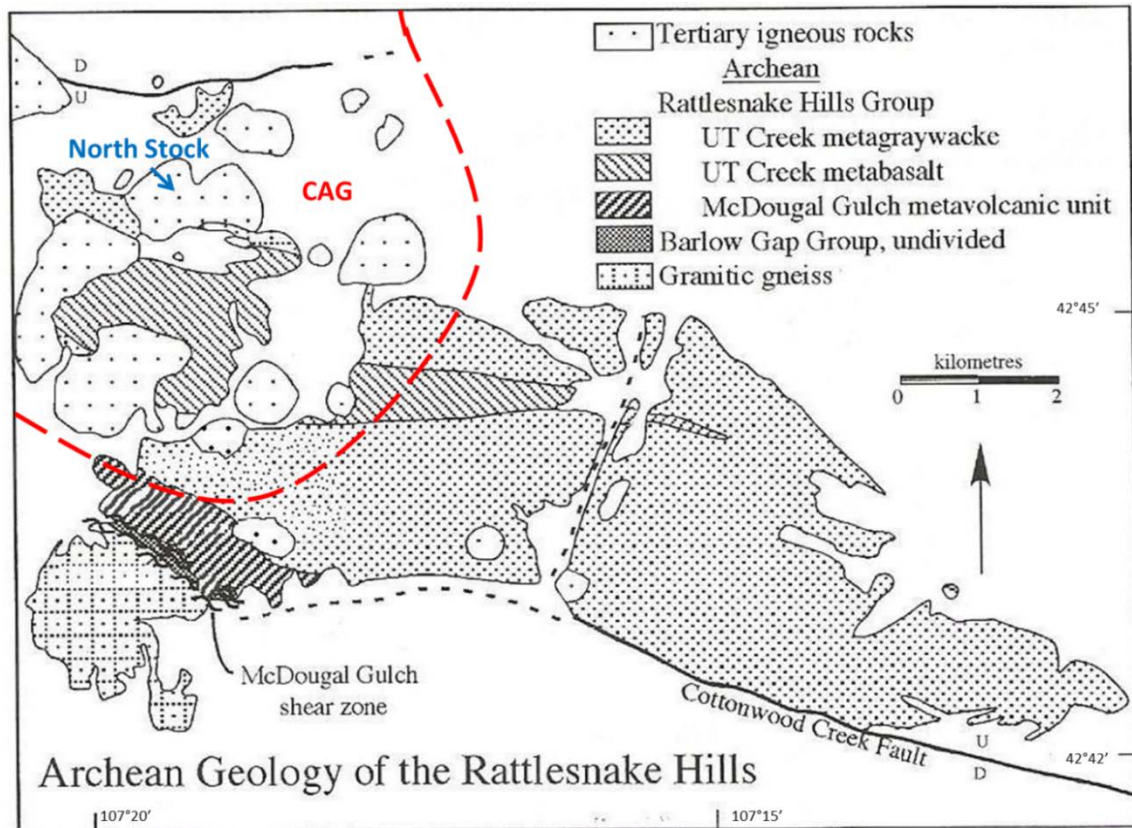
Figure 2.3 Archean geology of the Rattlesnake Hills and the Tertiary Central alkalic
group (CAG) outlined with a red dashed line (adapted from Frost et al., 2006). The
Cottonwood Creek Fault is a local name for the North Granite Mountain Fault.
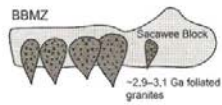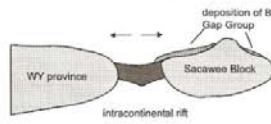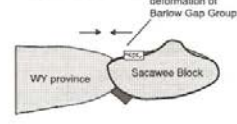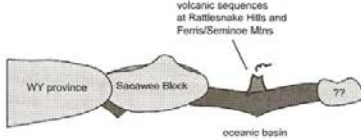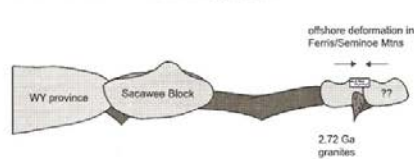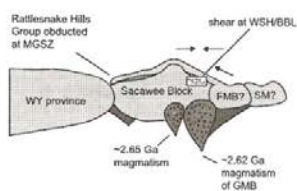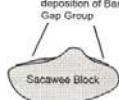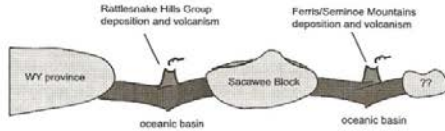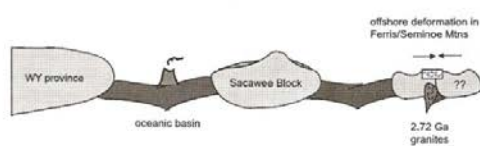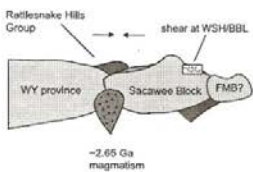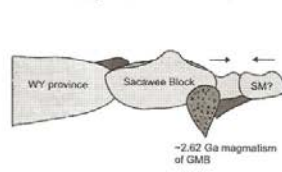
Figure 2.4 Schematic diagrams showing the two models for the formation of the Sacawee Block. Beartooth-Bighorn magmatic zone (BBMZ), McDougal Gulch shear zone (MGSZ), West Sage Hen (WSH), Granite Mountain batholiths (GMB), Ferris Mountains block (FMB), Sierra Madre block (SM). See text for further discussions (From Grace et al., 2006).
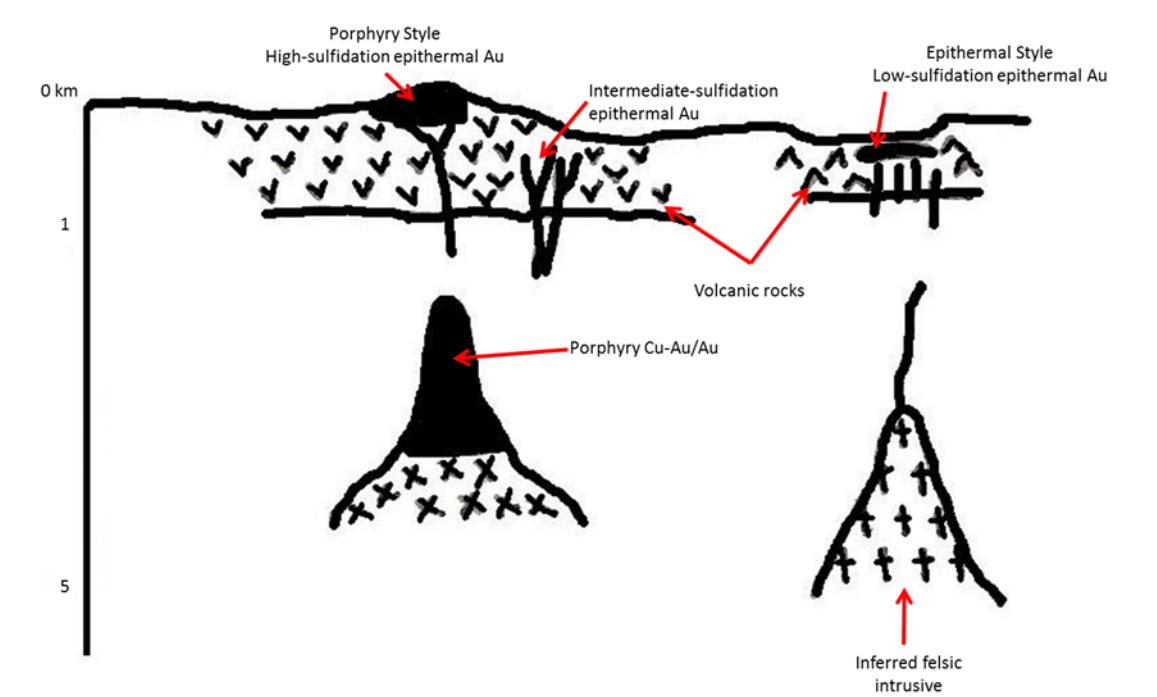
Figure 2.5 Schematic diagram of epithermal gold systems and porphyry gold systems.

Note the depth scale is log-based (adapted from Sillitoe, 2008).
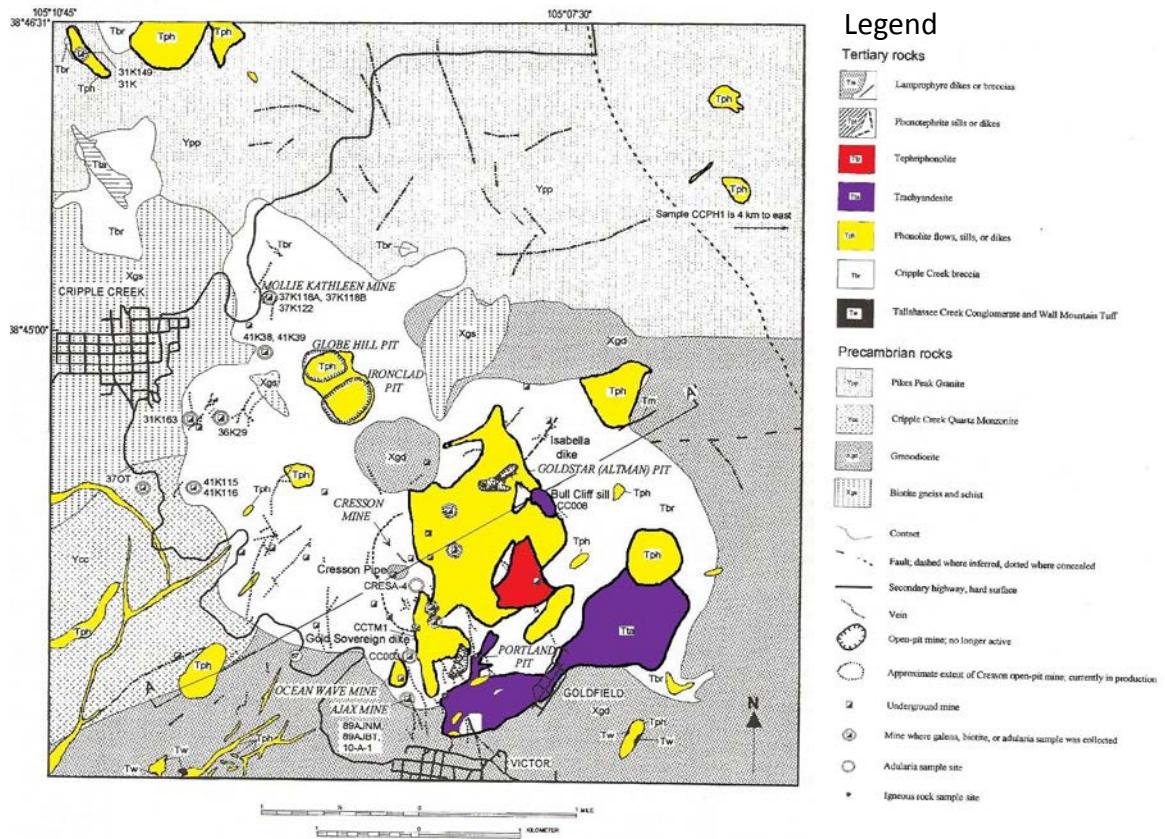
Figure 2.6 Geologic map of Cripple Creek, Colorado highlighting Tertiary intrusive

centers (adapted from Kelley et al., 2006).
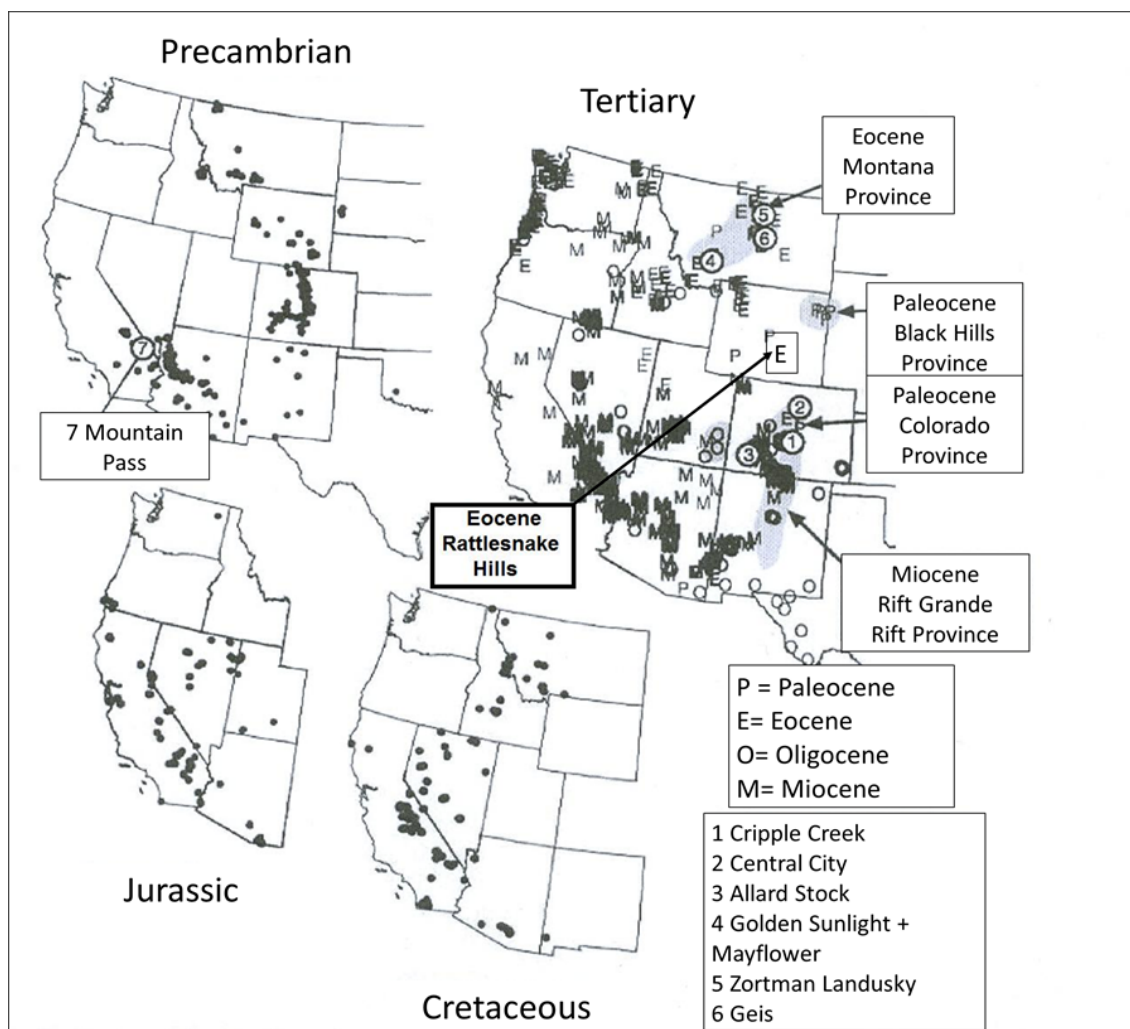
Figure 2.7 Distribution of alkaline complexes in North America, separated by age (Jensen and Barton, 2000) with the addition of Rattlesnake Hills.
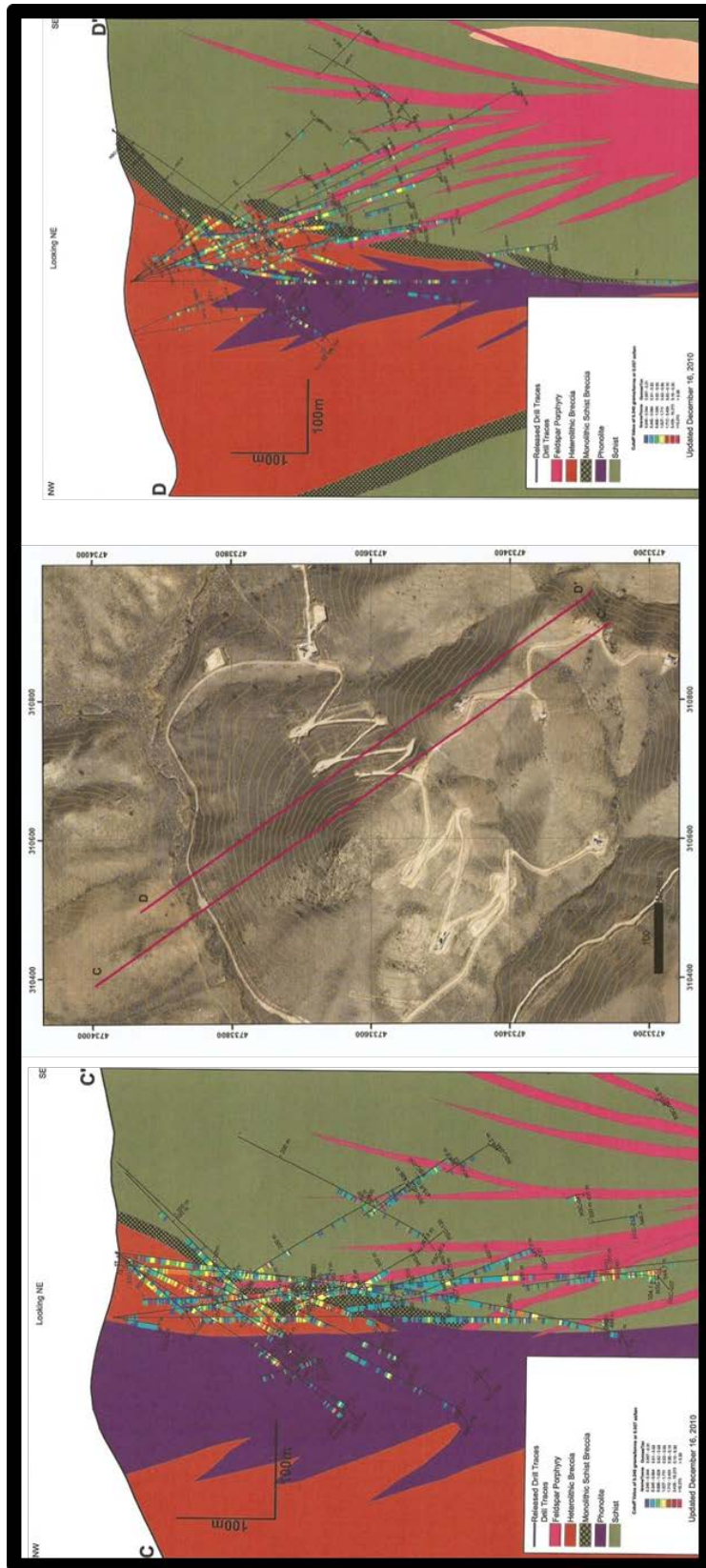
Figure 2.8 Geologic cross-section of North Stock with the grade of gold mineralization from drill holes. High grade zones are represented by pink, red, and orange colors. Higher intensity of mineralization associated with the contact of heterolithic breccias, which are diatreme breccias, and schist country rock (adapted from Evolving Gold Corp, 2011).

3. ROCK UNIT DESCRIPTIONS

North Stock has an inner cone-shaped phonolite intrusive in the core, with heterolithic or diatreme breccias on both sides of the phonolite, and late intruded fingers of feldspar porphyry (Figure 2.8). The porphyry intrusives are immediately adjacent to the schist wallrock, with minor wallrock brecciation in the form of monolithic schist breccias. These main rock units present in the North Stock study area were analyzed with QEMSCAN® at the Advanced Mineralogy Research Center at Colorado School of Mines, Colorado. QEMSCAN® is a quantitative electron microscopy-scanning electron microscopy system (Gottlieb et al., 2000). Individual minerals are identified by using chemical compositions from X-ray spectra (Gottlieb et al., 2000).

QEMSCAN® was primarily used to extend characterization of rock units based on mineral modal percentages. Additionally, an aim of the analysis was to determine where gold is located within samples of known gold mineralization (i.e. vein center, edges, or strongly associated with sulfides). Mineralized samples are samples with gold grade> 1.5ppm in 5' composite assay results, and thin sections were chosen based on sparsely visible gold in a high grade zone. Other samples were analyzed to characterize the rock units and alteration. These samples were chosen based on the criteria that 1) each sample represented a different rock unit present at Rattlesnake Hills and 2) unaltered and altered samples were selected for comparison. However, the QEMSCAN® results indicate that

samples which appear unaltered in hand specimen have undergone substantial potassic alteration.

Thirteen samples were carbon coated and analyzed at a variety of resolutions ranging from 20μm to 2μm depending on precious metal content, specifically gold. All samples are from drill core and have a range of depths. Two types of images were created from QEMSCAN analysis: backscatter images at specific resolution and false-colored image of mineral compositions. A detailed description of mineral modes is included in Table 1 and detailed explanation of analytical techniques in Appendix 2. All rock unit names are from Evolving Gold's criteria and do not all correlate with previous works by Hausel, 1996; Hausel, 1998; Hoch, 1991; and Hoch and Frost, 1996.

There are four main facies of alteration, with seven less common types of alteration present at Rattlesnake Hills. The main alteration facies recognized in hand specimen examination are: carbonate, potassic, clay, and FeOH (Evolving Gold Corp., 2009). Potassic alteration is characterized as green alteration halos around carbonate and lesser adularia veinlets or discrete veinlets of other potassic alteration minerals (Evolving Gold Corp., 2009). Carbonate alteration is widespread and can occur as: veinlet or breccia cement and mineral site replacement (Evolving Gold Corp., 2009). Clay alteration is characterized by color and softness and is occasionally associated with gold mineralization. FeOH alteration, which is supergene, has variably: jarosite and Fe- and Mn- oxy-hydroxides (Evolving Gold Corp., 2009).

There are also less important alteration types described by Evolving Gold Corp. that are not all widespread. These alteration types have been recognized as multiphase

with the following sequence listed from oldest the youngest including the main alteration facies previously discussed: 1) epidote-hematite; 2) actinolite-riebeckite-magnetite and roscoelite; 3) early potassic; 4) later potassic; 5) silica, carbonate, latest potassic, anhydrite, clay, and talc; 6) browning; and 7) FeOH, clay, and gypsum or the oxidized zone (Evolving Gold Corp., 2009). This thesis does not discuss the minor alteration types due to the limited development within the available sample suite. At the time of writing this thesis, there has been no study to link gold grade to different facies of alteration. Gold mineralization is spatially associated with multiple facies of alteration including potassic and FeOH. However, determining the genetic relationship between gold and alteration facies is difficult because it is still unclear if gold mineralization was deposited by the same fluids responsible for the potassic alteration, or if the mineralizing fluid event occurred before, during or after the potassic alteration. There is a lack of cross-cutting relationships and clear paragenetic relationship between alteration and mineralization; however, as a provisional interpretation, it is postulated that gold mineralization is related to potassic alteration spatially and genetically.

3.1 QUARTZ-MONZODIORITE

Quartz-monzodiorite, a name designated by Evolving Gold Corp., is mostly confined to Antelope Basin, but there are smaller outcrops and dikes in the North Stock area (Figure 2.8). Generally, most quartz-monzodiorite is grey-blue color in hand sample and drill core (Figure 3.1). Most samples appear silica undersaturated in hand sample because of the lack of quartz phenocrysts; however, QEMSCAN analysis quartz modal percent ranges from 5.8 to 8.1 mass% in the matrix. Carbonate veins consisting of calcite

and dolomite range in thickness from millimeters to several centimeters. Occasionally, carbonate veins have small grains of purple fluorite. There are few open-space/vuggy filling textures in carbonate veins hosted in this unit. Most quartz-monzodiorite has blue clay alteration of mineral sites and veins. Within the upper limits of Antelope Basin, the unit is oxidized.

One potassically altered sample was analyzed. The sample has a plagioclase-quartz-rich groundmass with a calcite vein that is ~1000μm thick and a halo of potassium feldspar that is ~2000μm. Most quartz-monzodiorite has significant potassium feldspar; this sample is approximately 23.4% potassium feldspar (Figure 3.2). The sample has disseminated sulfides throughout; however, QEMSCAN cannot differentiate between pyrite and marcasite. This sample has abundant mineralization, but the mineralization varies throughout Antelope Basin from barren to >10ppm. Small (5-10μm) individual grains of gold, silver or silver sulfide and electrum are hosted in pyrite and less frequently in potassium feldspar (Figure 3.3). There are 2 grains of lead-bearing mineral phase associated with the pyrite and silver.

3.2 SCHIST

Evolving Gold Corp has described the schist on the property as Archean meta-pelites, sandstones, tuffaceous sediments, and intrusive rocks (Evolving Gold Corp., 2009). Schist is the most abundant Archean greenstone basement rock in the study area (Figure 2.3). Most of the basement rocks are amphibolite metamorphic facies. Unaltered samples of schist are dark gray to black. While potassically altered schist is green and those that have undergone secondary biotite alteration are brown (Figure 3.4). Secondary

biotite at Rattlesnake Hills is considered brown biotite that is typically spatially

associated with carbonate veins. In general, primary biotite is black and not associated

with any other type of hydrothermal activity. Schist is variably oxidized at the surface

and along fractures at depth.

Schist has centimeter-sized zones of quartz+pyrite, but this is the only occurrence

of quartz vein within this unit. This is interpreted as mesothermal quartz that formed in

association with greenschist-metamorphism (Evolving Gold Corp, 2009). Typically the

mesothermal quartz, possibly Archean, is bull white quartz with minor pyrite. Carbonate

veins range from millimeters to centimeters in size, with preserved open-space filling

textures. Infrequently, there are small, purple fluorite grains in the carbonate veins.

Mineralization is concentrated along contacts with diatreme breccias and

porphyritic intrusive phases. Six samples were analyzed due to promising assay results

showing high grade gold and of sulfide mineralization in these samples; however, one

sample was only analyzed using backscatter imagery because of the lack of precious

metals as grains. All samples have veins, and the mineralogy of the samples vary

significantly depending on vein type, calcite or dolomite, and type of alteration. Some

samples have veins entirely comprised of dolomite, some of calcite, and some a mixture

of both. However, dolomite is the most abundant carbonate mineral present in these

samples. The carbonate veins tend to have FeOx, unidentified iron-oxide minerals,

present in lower concentrations. There is zonation in carbonate veins based on increasing

iron and decreasing abundances of magnesium towards the rims (Figure 3.6).

Additionally, a fair amount of carbonate vein minerals are zoned with euhedral dolomite

cores with calcite overgrowths. Samples with potassium flooding have >50% potassium feldspar (Figure 3.5). Samples with chlorite alteration, have modal compositions >1% chlorite. Likewise, secondary biotite is indicative of samples with modal composition >1% biotite.

Schist hosts disseminated sulfides with low gold grades (1-10ppm); however, not all samples analyzed have mineralization. A variety of ore minerals identified with QEMSAM were; gold, electrum, silver, pyrite, chalcopyrite, sphalerite, galena, bismuthinite, cobaltite, gersdorffite, molybdenite, cassiterite and arsenopyrite (Figure 3.7). Most ore grains are between 5-30μm in size but there are some grains >60μm. Other mineralized schist samples analyzed with ore microscopy only show gold, pyrite, chalcopyrite and sphalerite. Mineralization is discussed further in Chapter 6.

3.3 FELDSPAR PORPHYRY

There are two distinct feldspar porphyries: a fine to medium grained and a coarse grained. Evolving Gold Corp describes the fine to medium grained porphyry as occurring as dikes, hypabyssal intrusives and lesser extrusives; while the coarser grained porphyry occurs as dikes, and may include xenoliths of other intrusive bodies (Evolving Gold Corp., 2009). In hand and core samples, the porphyries are light grey in color (Figure 3.8). There is no quartz veining in this unit. Carbonate veins range in size from millimeters to several centimeters with preserved open space textures. There is minor oxidation and potassic alteration manifested in the hardness of the sample, not the color.

The sample analyzed has large plagioclase feldspar crystals and fewer calcite crystals. Similar to most samples there is a significant amount of potassium feldspar,

some primary crystals and some secondary fine grained groundmass from alteration (Figure 3.9). The sample shows no mineralization, but feldspar porphyries typically host high grade narrow zones of mineralization and low grade disseminated mineralization.

3.4 PHONOLITE

Phonolites occur at North Stock and the surrounding areas. The majority of phonolites are intrusive and most phonolites have the typical "ring" but have a variety of colors depending on type of alteration (Figure 3.10). Phonolites have small, millimeter scale barren carbonate veinlets.

The two samples analyzed have both undergone significant potassic alteration. One sample is a nepheline-rich phonolite while the other has no nepheline phenocrysts. Both samples have ~4% modal plagioclase feldspar (Figure 3.11). One sample has pyrite, but the other sample has no ore minerals. Mineralization is not indicated in most phonolites in Rattlesnake Hills. Rarely, phonolites host low grade disseminated gold mineralization.

3.5 PYROCLASTIC ROCKS

Pyroclastic rocks are confined to the easternmost part of North Stock. It is not a major unit, but is important in the interpretation of the diatreme complex. The sample consists of a fine grained potassium feldspar groundmass. While most other rock units have a significant potassium feldspar alteration, most of the potassium feldspar in the pyroclastic rock is likely primary. Plagioclase feldspar, quartz, pyrite, biotite, chlorite,

43

and calcite are smaller grains (Figure 3.12). There is a trace amount of kaolinite indicating some of the phenocrysts have been altered. There is no gold mineralization.

3.6 BRECCIAS

There are a variety of breccias in Rattlesnake Hills: diatreme, monolithic, and heterolithic. Two breccias samples were analyzed: monolithic schist breccia and heterolthic porphyry schist breccias (Figure 3.13). Mineralization is dependent on the type of breccias. Breccias that have predominately schist clasts do not have high grade ore (1-10ppm). However, igneous+ metamorphic (heterolithic) clast breccias are more enriched with gold mineralization (>10ppm). Both samples have undergone significant fine grained potassic alteration with carbonate cement and other minor minerals in the matrix and in individual clasts (Figure 3.14). One sample has gold, silver, and bismuthinite (Figure 3.15).

Figure 3.1 Core sample of RSC-001 436.5' is a quartz-monzodiorite used for QEMSCAN® analysis. There are two phases of hydrothermal activity: calcite vein and potassic alteration of the groundmass.

K-Feldspar	24.3
Plagioclase Feldspar	21.6
Fe-Mg Silicate	8.5
Quartz	8.1
Calcite (Fe,Mg-bearing)	7.2
Amphibole (Hornblende)	6.8
FeOx/Hydrox-silicate trap	4.1
Biotite/Phlogopite	4.1
Ti-minerals	4.0
Others	3.6
Pyrite	3.2
Apatite	1.5
Limonite	1.4
K,Mg,Fe Silicate?	1.0
Muscovite/Sericite	0.4
Ag-Find	0.0

K-Feldspar	23.4
Fe-Mg Silicate	18.7
Calcite (Fe,Mg-bearing)	17.9
Plagioclase Feldspar	10.9
Pyrite	9.1
Quartz	5.8
Others	3.3
Amphibole (Hornblende)	2.5
Limonite	2.1
Biotite/Phlogopite	1.9
FeOx/Hydrox-silicate trap	1.4
K,Mg,Fe Silicate?	1.3
Ti-minerals	1.2
Apatite	0.4
Muscovite/Sericite	0.3
Ag-Find	0.0

Figure 3.2 False-color images from QEMSCAN® of RSC-001 436.5'; large image at 20μm resolution and detailed vein rim image at 2μm resolution. The vein is calcite with alteration halo of fine grained silicates, euhedral to subhedral pyrite grains, and fine grained potassium feldspar.
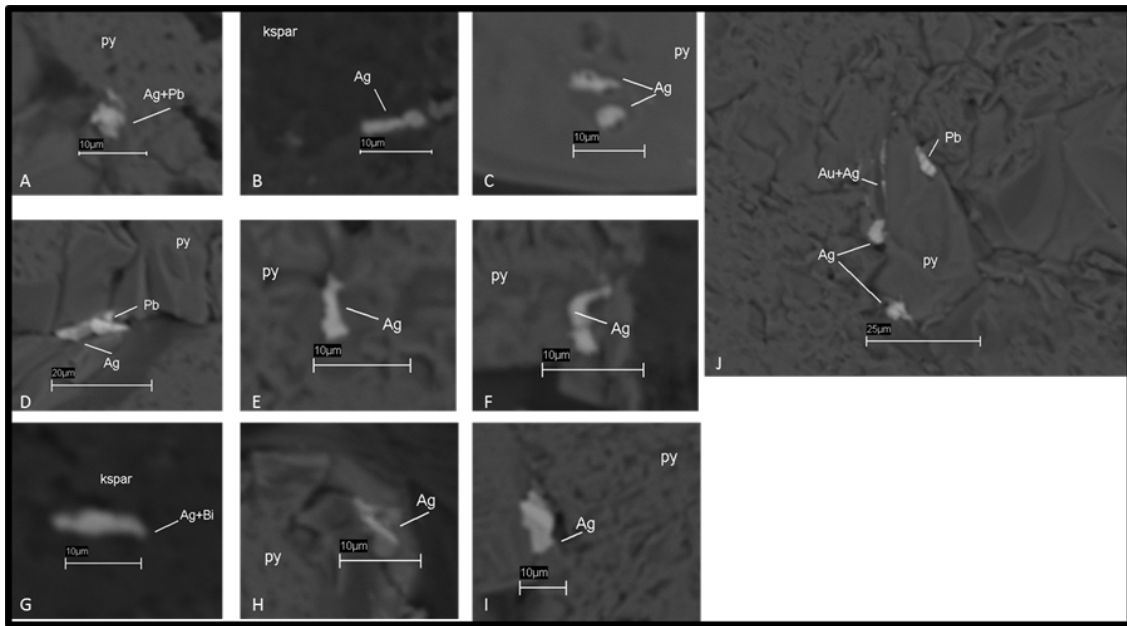
Figure 3.3 Back-scatter images from QEMSCAN® analysis of RSC-001 436.5' showing precious metals grains hosted in and on the rim of pyrite (images A, C, D, E, F, H, J, and I) and potassium feldspar (images B and H). It is not possible to differentiate between AgS and Ag. Lead minerals associated with precious metals are shown in images A and I.
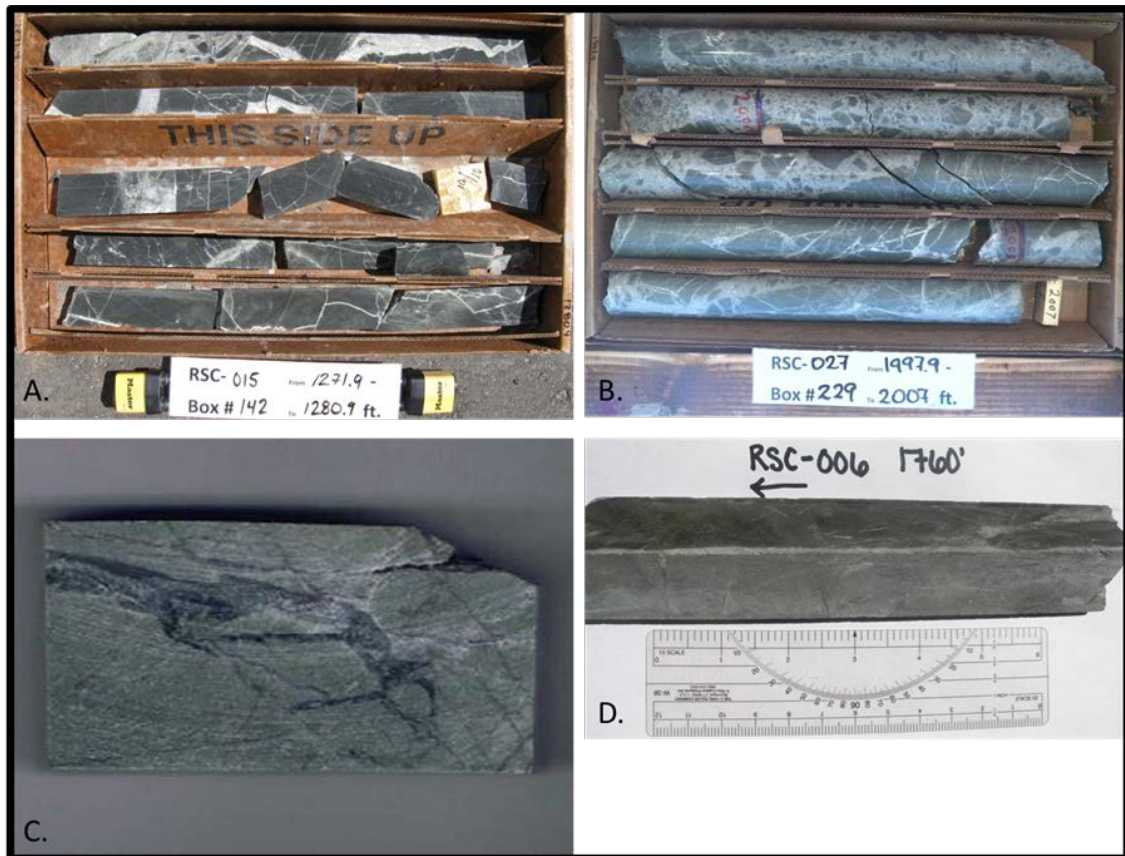
Figure 3.4 Photographs of unaltered schist (A), unaltered monolithic schist breccia (B),

and potassically altered schist (C and D). A is a core box photograph from RSC-015

1271.9-1280.9' of an unaltered black schist from North Stock. B is a core box photograph

of a relatively unaltered monolithic schist breccia from RSC-027 1997.9-2007' from

North Stock. C and D are examples of potassically altered schist from North Stock. C is a

hand sample at RSC-006 1786' with a green coloration. D is a quartered core sample

from RSC-006 1760' with a dark grey to black color. Drill hole RSC-006 is located at

North Stock.

Mineral Name	mass %
FeOx/Hydrox	32.6
K-Feldspar	26.7
Dolomite	22.4
Dolomite-FeOx Interface	7.9
Pyrite	4.7
Others	3.1
Biotite/Phlogopite	0.8
Silver	0.5
Ti-Minerals	0.3
Albite	0.3
Apatite	0.2
Chlorite	0.2
Muscovite	0.2
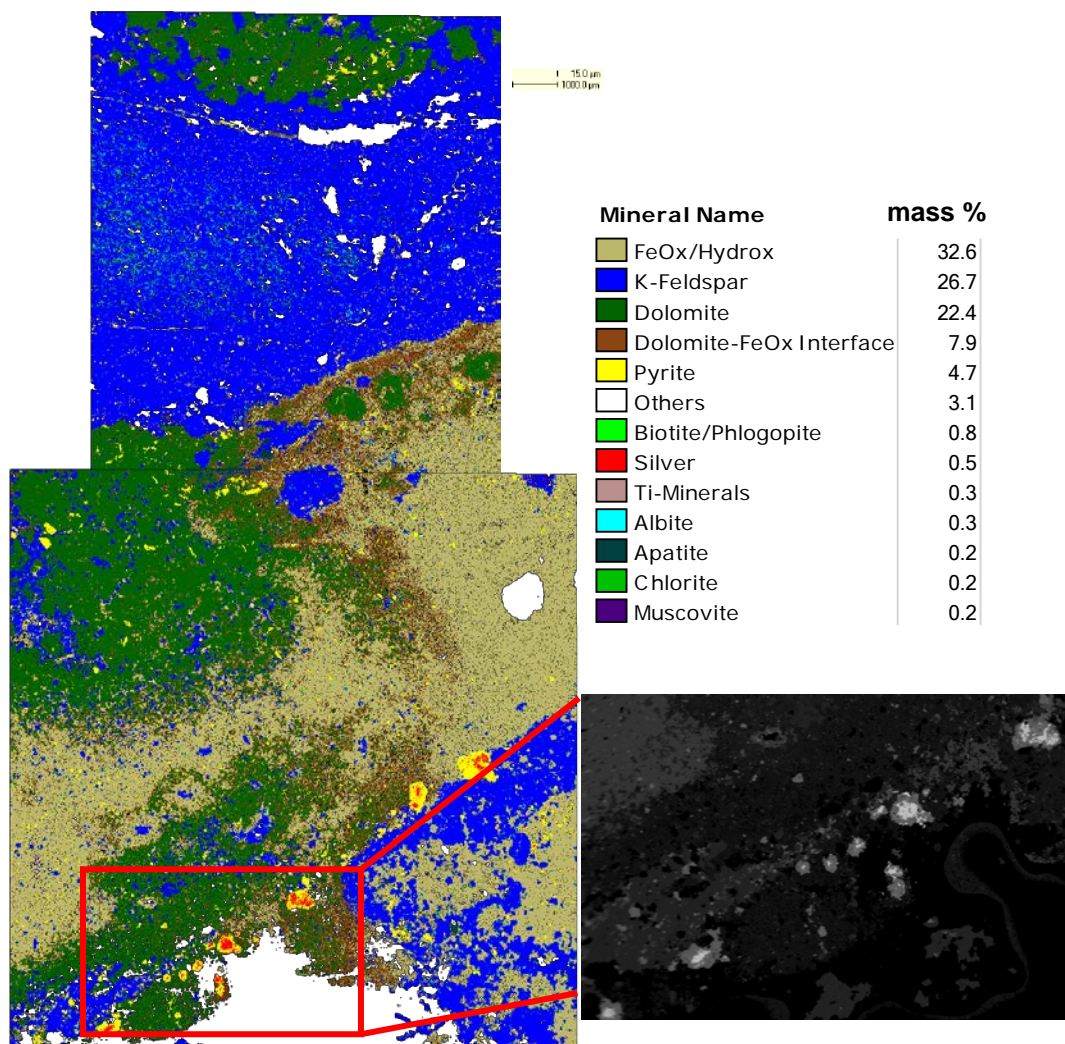
Figure 3.5 False-colored image QEMSCAN® analysis of potassically altered schist from RSC-007 540' (left) at 15μm resolution and back scatter image from QEMSCAN® of silver or silver sulfide grains in pyrite (right). The silver sulfides are the cores of subhedral pyrite grains. The breccia cement is FeOx and dolomite while the breccia clasts are potassium feldspar.
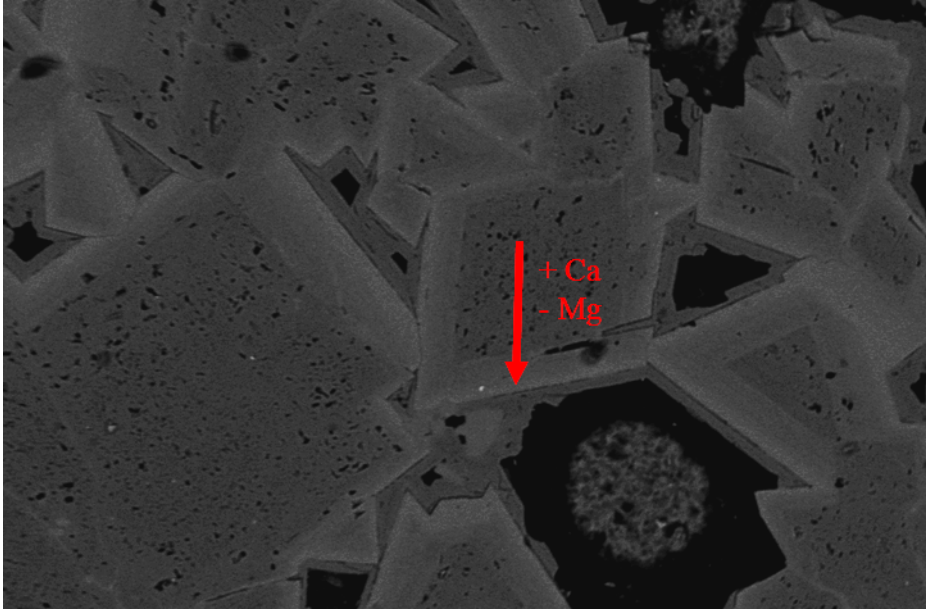
Figure 3.6 Backscatter image of carbonate showing composition growth variations of dolomite grains in the vein from sample RSC-003 968'. The center of the vein is middle to lower right of the photomicrograph with the edges of the vein not in the picture to the upper left.
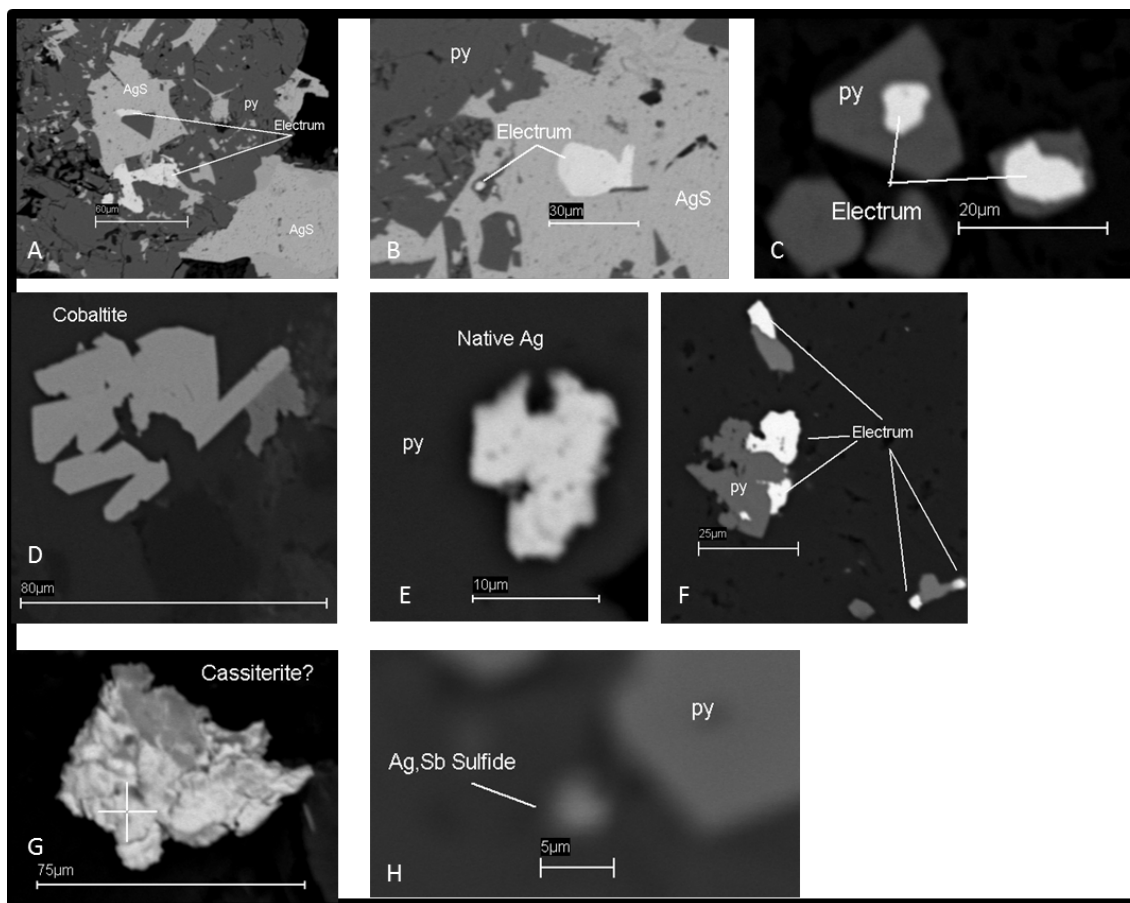
Figure 3.7 Backscatter QEMSCAN® images showing various settings of precious metal and other ore minerals. A) RSC-007 540' electrum and silver sulfide hosted in a pyrite grain; B) RSC-007 540' electrum in silver sulfide hosted within pyrite; C) RSC-007 540' electrum cores in euhedral pyrite grains; D) RSC-002 772.5'bladed grain of cobaltite; E) RSC-003 702.7' native silver grain hosted in pyrite; F) RSC-003 702.7' small electrum grains along the edges of pyrite grains; G) RSC-003 702.7' possible cassiterite grain; H) RSC-003 968' small, less than 5μm silver antimony sulfide.
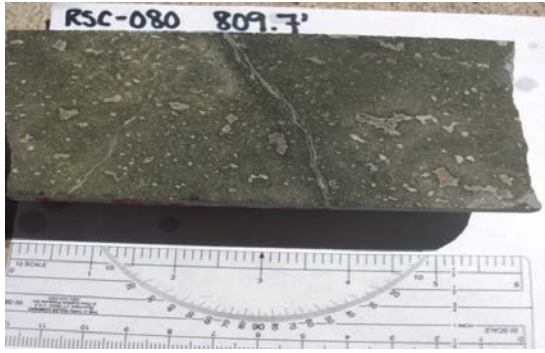
Figure 3.8 Photograph of feldspar porphyry from RSC-080 809.7'. This piece is light to medium gray with fine grained (1-2mm) white feldspars with larger, irregular shaped amygdules filled by carbonate+sulfides, this last feature is atypical of porphyries at Rattlesnake Hills.

Mineral Name	
K-Feldspar	60.7
Plagioclase Feldspar	15.8
Calcite	5.9
Biotite/Phlogopite	4.4
Quartz	3.8
Others	3.1
FeOx/Hydrox	2.5
Ankerite?	1.4
Chlorite	1.0
Ti-minerals	0.6
Apatite	0.5
Muscovite	0.3
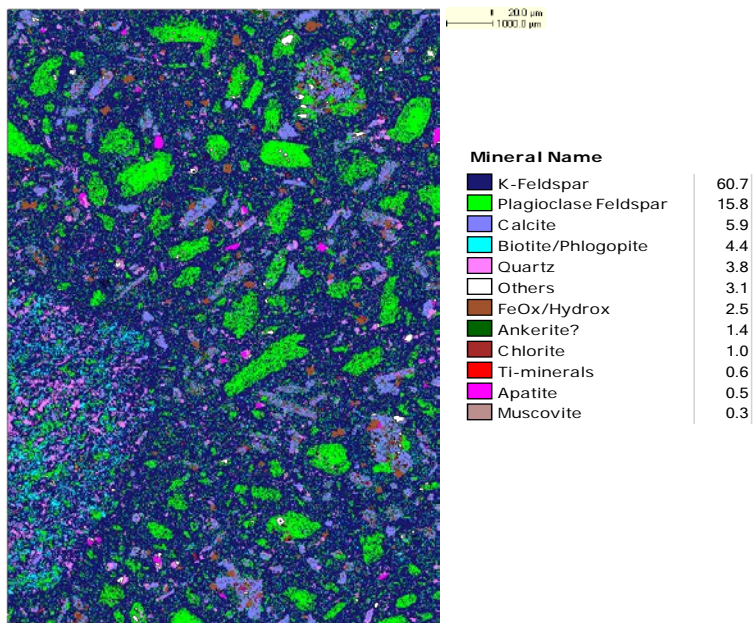
Figure 3.9 False color QEMSCAN® image at 20μm resolution of feldspar porphyry sample from drill hole RSC-005 1663'. The groundmass of the feldspar porphyry has been potassically altered. Some of the feldspars are altered to calcite while some are unaltered plagioclase.

51

Figure 3.10 Photograph of phonolite showing potassic alteration (green color halo to calcite veins) from RSC-105 1870.2'.
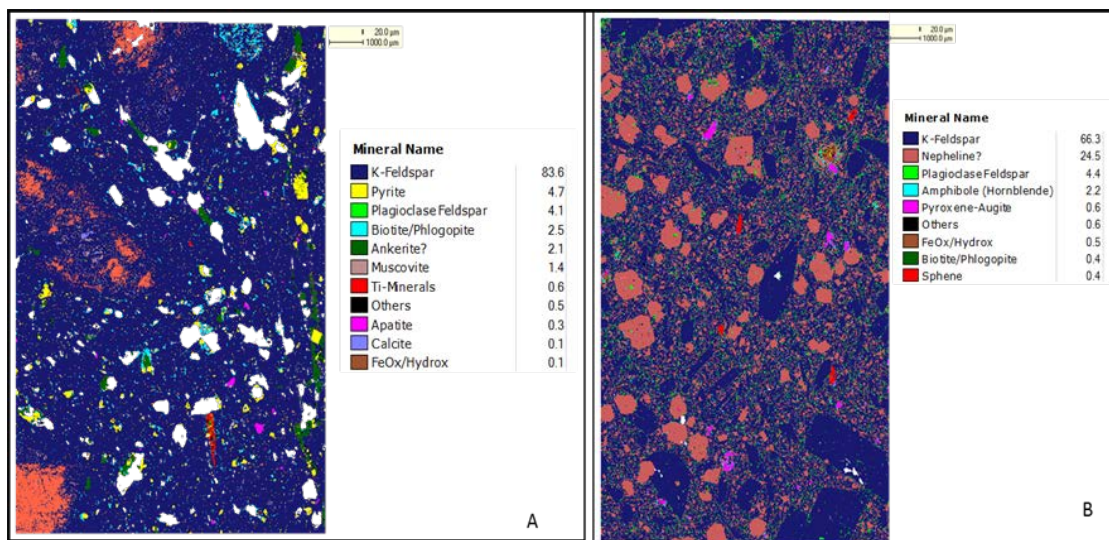
Figure 3.11 False color QEMSCAN® images of two phonolite samples at 20μm resolution. Sample A is a plagioclase phonolite from RSC-012 1769'. Sample B is a nepheline-rich phonolite surface sample from North Stock. The white, empty spots on image 1 are void spaces in the core thought to be nepheline grains plucked out by polishing.

Mineral Name	
K-Feldspar	47.8
Plagioclase Feldspar	19.7
Quartz	14.2
Others	4.3
Pyrite	3.3
Biotite/Phlogopite	3.2
Chlorite	2.9
Calcite	1.5
Ti-minerals	1.1
Muscovite	0.6
'Kaolinite' (clay)	0.5
Apatite	0.4
Amphibole (Hornblende)	0.4
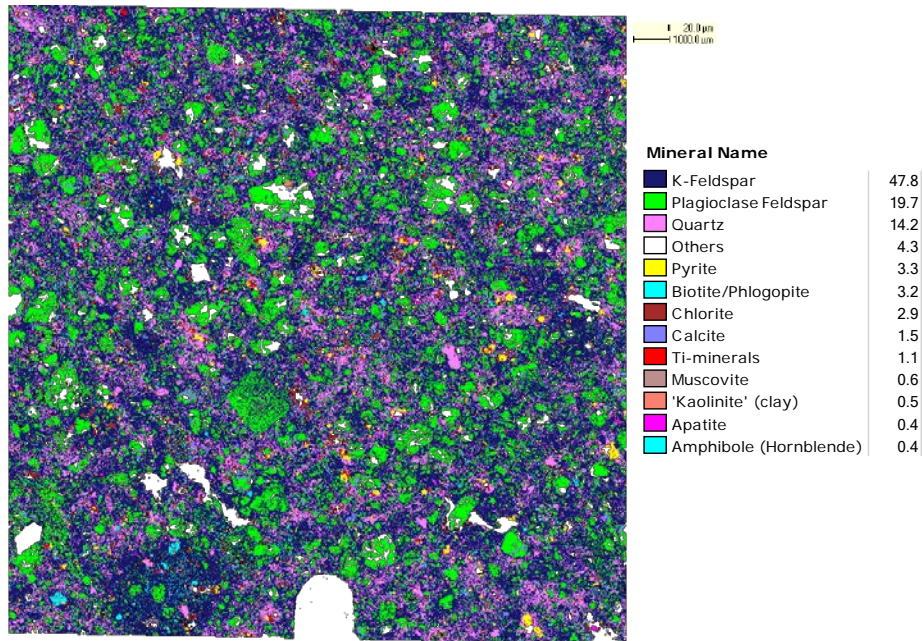
Figure 3.12 False color QEMSCAN® image at 20μm resolution of a pyroclastic rock from RSC-013 124.3'. The plagioclase feldspars are larger than the fine grained potassium feldspar-quartz groundmass.

Figure 3.13 Handsample of porphyry+schist breccias with carbonate matrix from RSC-003 504.5'. The schist clasts have potassic alteration rims.

K-Feldspar	55.8
Altered Ca-Carbonate	22.9
Pyrite	7.4
Biotite/Phlogopite	6.4
Muscovite/Sericite	4.3
Others	1.4
Ti Minerals	1.0
Chlorite	0.4
Apatite	0.2
Quartz	0.2
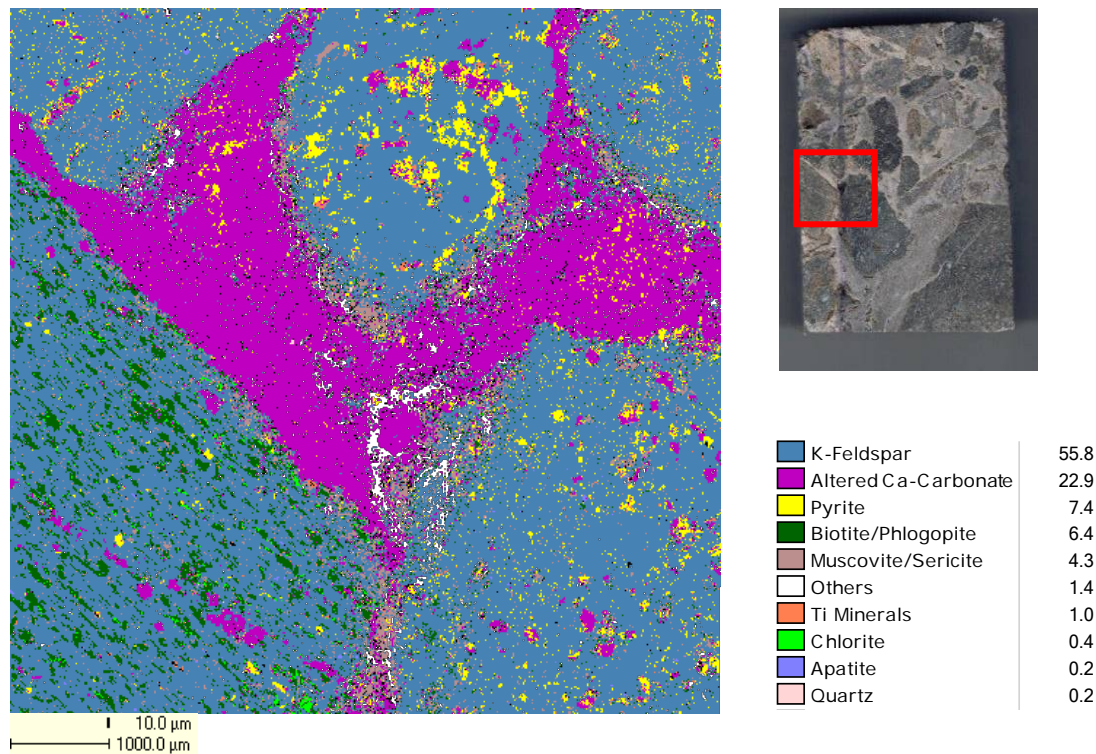
Figure 3.14 False color QEMSCAN® image at 10μm resolution (left) and photograph of sample with outlined area for QEMSCAN® analysis (right) of sample RSC-003 504.5'. The schist (lower left clast with biotite/phlogopite) and porphyry clasts are altered to potassium feldspar with altered Ca-carbonate matrix. The gold occurs as with the pyrite grains in the porphyry clasts.
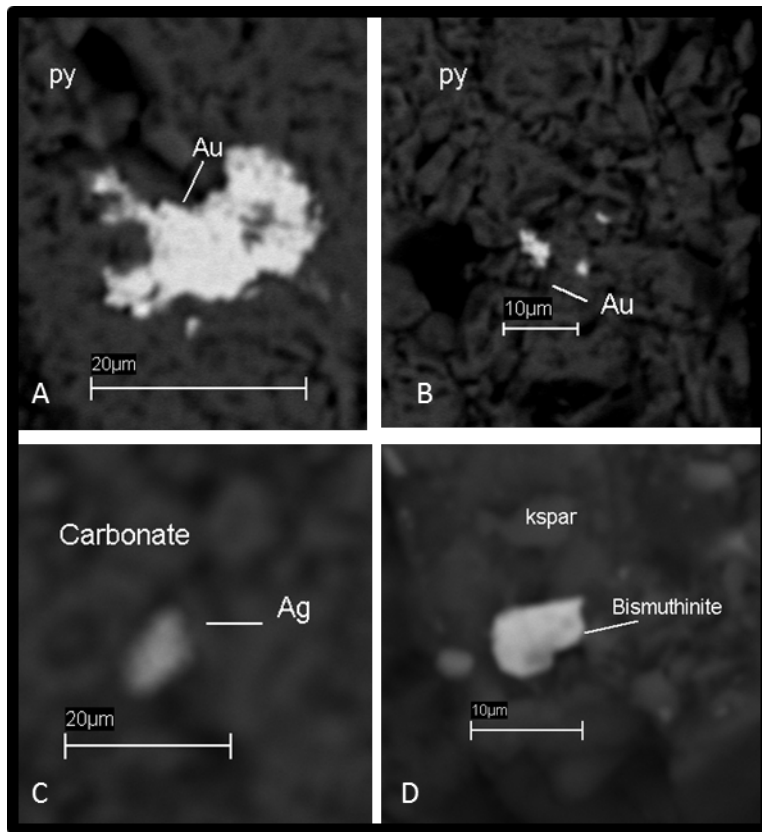
Figure 3.15 Back scatter QEMSCAN® image of precious metal minerals in RSC-003 504.5'. Images A and B show gold hosted in pyrite. Image C is silver or silver sulfides in carbonate and image D is bismuthinite in potassium feldspar. Precious metal mineralization is hosted in clasts from Figure 3.14.

4. FLUID INCLUSION PETROGRAPHY AND CHEMISTRY

4.1 VEIN TEXTURES

The carbonate veins and breccia cement/matrix range from a few millimeters to several centimeters in width. The color of the carbonate veins is dependent on the vein composition. Veins with disseminated sulfides are grey and veins with Fe or Mg-carbonate have an oxidized appearance. For sulfide rich veins, the sulfides, which range in size from <10μm to 1000μm, are concentrated along vein edges. Dolomite and calcite can occur as intergrowths, bands (occasionally with sulfide-rich bands), and/or zones enriched with respect to Mg or Fe content (Figure 3.6). An abundance of open space filling textures or vugs are preserved. At shallow depths and mainly concentrated within the oxidized zone, there are late stage gypsum veins that cross-cut all other veins. Since the hydrothermal/ magmatic system is a silica undersaturated system, there is a very limited amount of quartz veining or quartz in carbonate veins at Rattlesnake Hills. The LA-ICP-MS sample is patches of euhedrally grown quartz intergrown with carbonate. Infrequently, late stage silica forms millimeter lining of carbonate vugs and/or nondescript individual millimeter sized grains. There is no evidence that the late silica and gypsum are genetically related to ore deposition. These late stages are not spatially associated with mineralization and cross-cut carbonate veins hosting mineralization.

4.2 OVERVIEW OF FLUID INCLUSIONS

Since the formation of the alkaline and diatreme complex, Rattlesnake Hills has undergone little deformation and lacks a thermal overprint. Fluid inclusions selected for microthermometry are all hosted in carbonate. The carbonate is a mixture of calcite and dolomite, which generally occur as discrete intergrowths that are zoned with respect to Ca and Mg content (Figure 3.6). Inclusions were mostly measured in white or clear carbonate veins. Fluid inclusions in veins with higher sulfide content were not measured due to the obscured nature of the inclusions. The host carbonate veins are in a variety of rock types: schist, porphyry, monolithic schist breccias, and heterolithic igneous and metamorphic breccia. Carbonate phases were chosen because of the potential stronger relationship to alkaline magmatism and diatreme activity. It is evident from oxygen and carbon isotopic compositions that carbonate precipitation is from a magmatic fluid that is likely related to ore deposition (Chapter 5).

Fluid inclusions samples range in depth from 646.5' to 1272.7'. Since each sample was collected from drill core, it is noteworthy that the holes were drilled at various angles, and the reported depth is not true depth from surface. All samples were taken from North Stock drill holes, and represent the system at a variety of positions (Figure 4.1 A and B). Fluid inclusions were measured in eight samples (Table 4.1); however, there were some problems associated with measurements. First, since almost all the fluid inclusions were hosted in carbonate, a significant number of inclusions leaked or did not homogenize by 250°C (n= 57) (Appendix 2). The maximum temperature the fluid inclusions in carbonate can be heated to without a strong likelihood of stretching or

destruction of the inclusion is 250°C, even with homogenization (Bodnar, 2003). There were inclusions in all samples that did not homogenize by the maximum temperature. The fluid inclusions might represent a higher temperature of entrapment but vapor bubbles were not larger in these inclusions at room temperature and hence it is possible that they stretched slowly during heating. Stretching can occur experimentally or geologically due to re-equlibration of the fluid inclusions (see discussion below). Second, some inclusions stretched on heating. Inclusions that clearly experienced leakage or stress during heating were not used again. Lastly, some inclusions were small and dark, making it difficult to determine accurate ice melt temperatures.

Measurements for inclusion were made using an Olympus BX51 microscope with a Linkham THMS 600 stage. Microthermometry results of first ice melt, last ice melt, additional solid melts, clathrate melt, solid dissolution, and vapor homogenization can be found in Appendix 2. Inclusions were cooled to -75°C and slowly heated at 1°C per minute to 15°C to obtained first ice melt temperatures, last ice melt temperatures, clathrate movement, and dissolution of solids. However, a trial cooling run to -100°C to was used to check for CO_2 rich gas phase of which none were found. Freezing measurements for each chip was completed before any heating measurements. Inclusions were then heated at a moderate rate of 5 to 10°C until the vapor homogenized. If leaking occurred before homogenization, the chip from the sample was discontinued from use. Heating of inclusions was completed in multiple batches for each chip. Histograms of fluid inclusion measurements show a single modal distribution (Figure 4.4). Using Bakker's FLUIDS software package, salinities and isochores were calculated (Bakker,

2003). Molar volumes for all simple inclusions were calculated using FLUIDS (Bakker, 2003). Complex fluid inclusion salinities were determined using the CLATHRATE or AqSo computer programs. There might be some variation due to the limitations of the equations for expansion of the host mineral, calculated using pure calcite instead of a mixture of calcite and dolomite. Laser ablation ICP-MS and laser Raman were completed on one sample, RSC-015 1272.7' with large two-phase inclusions hosted in euhedrally terminated quartz crystals in a carbonate vein breccia in schist.

There are primary, secondary, and pseudosecondary inclusions present. The criteria for primary, secondary, and pseudosecondary fluid inclusions are determined by the characteristics outlined by Goldstein and Reynolds (1994). Primary inclusions represent inclusions that have a clear relationship within growth zonation of calcite and dolomite, secondary inclusions are entrapped after the initial grain growth and follow planar arrays or curved surfaces, and pseudosecondary inclusions are entrapped before grain growth is complete and arrays end at growth zones (Goldstein and Reynolds, 1994). Inclusions that occur in 3D clusters or isolated inclusions contained within growth zonation are interpreted to be primary inclusions (Figure 4.2). Since there are intergrowths of dolomite and calcite, care was taken to avoid secondary inclusions trapped along obvious cleavage planes; this is problematic because cleavage planes can mimic growth zonation. It is possible that primary and secondary inclusions closely resemble each other, and some inclusions may thus be incorrectly classified. Only inclusions that are clearly primary or pseudosecondary were measured. All types of inclusions have a wide range of sizes (2.7μm to 57μm), and have irregular shapes, which is common in calcite hosted fluid inclusions (Goldstein and Reynolds, 1994) (Figure 4.2).

The shapes of fluid inclusions can be correlated to occurrence and mechanism of textural re-equilibration of inclusions (Vityk and Bodnar, 1995). However, carbonates are susceptible to re-equilibration. Fluid inclusions typically stretch and/or decrepitate after undergoing re-equilibration (Ujiie et al., 2008); both experimental and geological effects are common with Rattlesnake Hills fluid inclusions. Stretching is defined as "deformation of an inclusion without any change in the fluid composition leading to a density decrease" (Bourdet and Pironon, 2008). Fluid inclusions in carbonates that have stretched after they have been heated increase in volume causing the density of the fluid and the homogenization temperature to change (Ujiie et al., 2008). The Rattlesnake Hills fluid inclusions that leaked typically leaked on the first heating run between 100-250°C. In general, most inclusions did not appear to have undergone stretching. It is important to make sure fluid inclusions measured have not stretched after multiple heating runs to ensure the entrapment temperature was measured. Fluid inclusions can experience leakage through the crystal structure and fractures (Bourdet and Pironon, 2008).

There are four possible pressure-temperature pathways after inclusion entrapment: nearly isothermal decompression (ITD), isobaric heating (IBH), isobaric cooling (IBC), and nearly isothermal compression (ITC) (Vityk and Bodnar, 1995). The general shape of the fluid inclusions are irregular, annular, arc to hook-like (Figure 4.3). However, there are some inclusions with a more regular, spherical shape. At Rattlesnake Hills, there has been minor re-equilibration. It is most likely the fluid inclusion shapes represent IBC, but there are shapes that fit ITD and ITC. IBC best fits the environment: implacement of magma in continental crust (Vityk and Bodnar, 1995). The concern in this interpretation is that Vityk and Bodnar used synthetic inclusions hosted in quartz, while almost all the

inclusions at Rattlesnake Hills are hosted in carbonate (Vityk and Bodnar, 1995). Rattlesnake Hills fluid inclusions might have different shapes for each path and are more likely affected by post-trapping history (Vityk and Bodnar, 1995; Bourdet and Pironon., 2008). However, the primary concern with IBC pathway is that fluid inclusion densities might be higher than original and this could provide an underestimate of temperatures.

4.3 PETROGRAPHY AND MICROTHERMOMETRY OF FLUID INCLUSIONS

The hydrothermal system at Rattlesnake Hills was dominated by low to moderate salinity aqueous fluids. However, there is evidence of discrete amounts of CO_2 that are undetectable by normal fluid inclusion microthermometry methods since it is insufficient to nucleate a CO_2 phase at room temperature. The fluid inclusions in individual samples are mostly homogeneous two-phase with similar homogenization temperatures and ice melting temperatures; however, clathrate melting temperatures are recorded in some inclusions. There are inclusions that do not fit these characteristics. There are some inclusions that are one phase at room temperature, two-phase, and rare inclusions with daughter minerals and hence higher salinity. Fluid inclusions are found in all samples with different abundances.

The aqueous fluid inclusions are one, two, and three phase. One phase inclusions are uncommon and infrequent, but usually vapor bubbles appear in the one phase inclusions after cooling but these were not measured due to inconsistency of vapor bubbles appearance. Most commonly, inclusions have two phases: liquid+vapor. Complex inclusions with three (or more) phases are the least common inclusion. The complex inclusions typically have clathrates and solids at room temperature. Clathrates

were indicated by bubble movement between 0 and 10°C, but clathrates were optically not visible. Solids ranges in size from 1-5μm and have a variety of shapes from cubic, roughly round, and highly irregular, but cubic is the most common shape of the solids. The solids tend to have high positive relief with respect to the fluid, but low relief contrast to the host carbonate. Most commonly there is a single isotropic cubic solid which is interpreted to be NaCl.

During freezing, there was no notable evidence of CO_2 present except where clathrate melting was observed. Salinities of simple, two phase inclusions were determined by the last ice melt temperature. All two-phase inclusions are low to moderate salinity. The minimum salinity is 0.9 wt. % eq. NaCl with a maximum salinity of 12.8 wt. % eq. NaCl (Figure 4.5). The histogram of the salinities of the simple inclusions shows dominant groupings of salinities at ~4.0, 8-9, and 13 % eq. NaCl (Figure 4.5).

The eutectic temperatures have a large range from -64.7° to -39.6°C with the peak at approximately -45.1°C. The eutectic temperatures of these fluid inclusions are much more negative than typical halite bearing fluid inclusions implying the fluid includes significant quantities of salts other than NaCl.

The eutectic temperatures of complex inclusions range from -64.3° to -42.1°C, implicate that there are more than NaCl salts. The vapor homogenization temperatures are 167.2° to 219.8°C and the clathrate dissolution 5.2 to 9.5°C. The salinities were determined using ICE computer program (Bakker, 1997). The parameters for analyzing the fluid inclusions for the salinity are: final clathrate melting temperature, final ice

62

melting temperature, assuming the gas is CO_2, and the salts are 100% NaCl. The fluid inclusions have a narrow range, 4.8 to 5.0 wt. % eq. NaCl.

The all fluid inclusions are high-density and contain small bubbles (10-15 vol. %). The vapor homogenization temperatures of aqueous rich inclusions range from 118°C to 257°C with only one population and limited variation from sample to sample (Figure 4.4). However, the peak in range of homogenization temperatures is 160-220°C (Figure 4.4). There is no evidence of homogenization to vapor.

4.4 ISOCHORES, PRESSURES, AND TEMPERATURE OF ENTRAPMENT OF FLUID INCLUSIONS

Isochores represent lines of constant volume (Goldstein and Reynolds, 1994) (Figure 4.10). The minimum and maximum isochore for each sample are plotted and all samples have a consistent narrow spread of molar volumes.

Homogenization temperatures are a minimum estimate of the trapping temperature and conditions (Shepherd et al., 1985). Trapping temperatures are a function of the composition of the fluid and the pressure-temperature-depth of the system (Shepherd et al., 1985). The major component composition of the fluid is taken to be H_2O-NaCl. There is no evidence of boiling, which would be evidenced by vapor-rich fluid inclusions coexisting with liquid rich inclusions, within the Rattlesnake Hills alkaline complex.

Rattlesnake Hills is a shallow system; however a minimum depth is inferred from the lack of boiling in fluid inclusions. The range of likely pressures given the estimates of

depth of mineralization of ~3,000 feet is 0-1,000 bars (see denoted box of likely pressures Figure 4.10). The inferred minimum temperature of entrapment is ~100°C and a maximum temperature of entrapment is 375°C (Figure 4.10).

4.5 LA-ICP-MS OF FLUID INCLUSIONS

One thin section, RSC-015 1272.7', was analyzed at the USGS Laser Ablation ICP-MS Laboratory in Denver for multielemental composition. The sample selected for LA-ICP-MS has the largest inclusions observed from all samples. All of the LA-ICP-MS analysis is in euhedral quartz synchronously intergrown with carbonate. In general quartz is rare at Rattlesnake Hills and occurs as intergrowths and/or late stage silica lining vugs. This procedure is only a qualitative look to determine metals present. RSC-015 1272.7' is a carbonate vein breccia with euhedral intergrowths of quartz hosted in schist (Figure 4.11).

LA-ICP-MS and Laser Raman were used for spot analysis of 26 inclusions hosted in euhedral quartz grains. The quartz grains were chosen based on the size and density of inclusions hosted in each grain. Grains were located in a calcite vein breccia. Most of the quartz host chipped during the initial ablation. Most of the ablated fluid inclusions that did not experience initial chipping formed roughly circular ablation craters (Figure 4.11).

In order to quantify concentrations from LA-ICP-MS five fluid inclusions from the same 3 chips used for LA-ICP-MS were analyzed using Laser Raman spectroscopy to determine the salinity percent and the salinity ranged from 1.7 to 8 wt % eq .NaCl. The Laser Raman utilizes 532nm and 785 nm solid state lasers while the laser ablation uses

193nm of a pulsed ArF last creating craters that range in size from 15-44µm (Todorov et al., 2009). Microthermometric measurements of fluid inclusions similar to those analyzed with LA-ICP-MS and Laser Raman had previously been measured for eutectic and final ice melting temperatures. The salinities of the fluid inclusions from microthermometric techniques range from 3.7 to 11.9 wt. % eq. NaCl (Figure 4.6). Four of the analyzed fluid inclusions are complex inclusions. Two inclusions had clathrates and two inclusions had hydrohalite. The salinities overlap but are higher than those calculated using Laser Raman techniques; however, these salinities are comparable to other fluid inclusions measured at Rattlesnake Hills (Figure 4.6).

The fluid inclusions have a wide range of elements. Based on the salinity measurements Na is calculated to 17,500ppm. Other major elements present in the fluid inclusions are: Mg (270-19,300ppm, 6,831 ppm average), K (420-11,200ppm, 4,782ppm average), and Fe (<50-8,050ppm, 2,701ppm average). Ca was measured in all the fluid inclusions but all measurements were under the limits of detection. The lithophile elements are: Rb (<1-1,020ppm, 118ppm average), Sr (<0.3-470ppm, 92ppm average), and Cs (<0.1-38ppm, 13ppm average). The ore forming elements are: Co (<2-11ppm, 10ppm average), As (<2-210ppm, 70ppm average), Zn (<7-1,410ppm, 524ppm average), Cu (<3-273ppm, 179 ppm average), and Pb (<0.5-43ppm, 24ppm average). Interestingly, gold was detected in three fluid inclusions (0.2-4ppm) and silver in two fluid inclusions (2-9ppm). The raw count rate data from fluid inclusions are plotted against the elements present show that the elevated values of the elements are hosted in the fluids and not in the matrix (Figure 4.12).

The LA-ICP-MS of fluid inclusions show large variations in the K/Rb, K/Cs, and Rb/Cs ratios. The K/Rb ratios range from 91.67 to 224.78 with the average of 168.87 (n=9) which have similar values to fine grained peraluminous granites (Cerny, 1991). The K/Cs ratios range from 113.57 to 1,651.85 with an average of 791.48 (n=7) which are comparable to beryl type rare element pegmatites (Cerny, 1991). The Rb/Cs ratios are a narrower range of 1 to 26.32 with an average of 6.68 (n=9) and are comparable to lepidolite sub-type rare element pegmatite (Cerny, 1991). Although each ratio is comparable to a different type of granites or pegmatites, overall they represent values similar to evolved magmatic granites and less evolved pegmatites (Cerny, 1991). These ratios are markers of magmatic fractionation, Audetat et al (2008) states that "the concentrations of Cs in the residual melt and associated fluid increases exponentially with increasing magma crystallization." The Cs concentrations in fluid inclusions range from 3.5 to 38 ppm. This implies that "the fluids with high Cs content were much less abundant than those with low Cs content" and is evidence that the fluid at Rattlesnake Hills was derived from a magma that had undergone fractionation (Audetat et al., 2008).

4.6 INTERPRETATION OF ORE FLUID CHARACTERISTICS AND COMPOSITIONS

4.6.1 Summary of major characteristics

Major characteristics of Rattlesnake Hills alkaline complex are summarized:

- No high temperature homogenization of inclusions. The average range is T_h 180 to 210°C with estimated trapping temperatures of ~100 to 375°C

66

- No higher salinity phase, only low to moderate salinities

- No evidence of boiling or a vapor-rich phase

- Little variation between the compositions or entrapment conditions of simple two-phase inclusions and complex multiple phase inclusions (Figure 4.6)

- Low but detectable CO_2 (comparable to Porgera (Ronacher et al., 2004)

- Lack of vertical or horizontal gradients, no spatial variation in temperatures and salinities

- There is no trend between gold values and equiv. wt. % NaCl (Figure 4.9)

- Provisional LA-ICP-MS points show comparable major element contents to other magmatic hydrothermal systems measured fluid inclusions, precious metals are carried in the fluids, the ratios of K/Rb, K/Cs, and Rb/Cs show an evolved magmatic signature

- Evidence of crystallization in the magmatic source of the fluid

There is no evidence of boiling in the Rattlesnake Hills alkaline complex. Boiling occurs when a "vapor phase separation from a saline, gas-rich fluid (cf. Truesdell, 1985, p. 7) resulting in the coexistence of two separate phases" (Ronacher et al., 2004). Systems that are indicative boiling have vapor-rich inclusions coexisting with hypersaline inclusions (Ronacher et al., 2000). The lack of vapor-rich and hypersaline inclusions implies there has been no boiling at Rattlesnake Hills.

There does not seem to be a correlation between any one of eutectic temperature, first ice melt temperature, homogenization temperature, and weight percent NaCl to

depth subdivided by shallow (0-1000') and deep (1000-2001') (Figure 4.7) or host rock

type (Figure 4.7 and 4.8). Since the true depth at Rattlesnake Hills is unknown, a

minimum depth is used to constrain the pure water boiling point curve using the

minimum and average homogenization temperatures of fluid inclusions (Figure 4.13).

The minimum is estimated as 200' of erosion.

4.6.2 Comparison with other Alkaline Gold Systems

The fluid inclusions at Cripple Creek, Colorado vary by the location, stage in

paragenesis, and host minerals. Four fluid inclusion studies from the Cripple Creek

region are compared to the results of the study at Rattlesnake Hills. The Ajax Vein

system, located within the Cripple Creek Mining District, was analyzed for fluid

inclusions by Dwelley (1984). Fluid inclusion microthermometry data from four types of

fluid inclusions hosted in quartz, fluorite, and sphalerite present a large range of

homogenization temperatures and salinities. Stage 1 T_h range from 206-510°C with 26-

47wt % eq. NaCl, stage 2 T_h ranges from 271-289°C with no salinity data, stage 3 T_h

ranges 123-350°C with salinity 0-8.3 wt. % eq. NaCl, and stage 4 T_h varies from 105-

159°C with salinity between 2.4-3.5 wt. % eq. NaCl (Dwelley, 1984). There is evidence

of CO_2 rich inclusions (Dwelley, 1984).

The Cresson Deposit, currently located in the open pit mine of Cripple Creek, a

fluid inclusion study shows evidence of a boiling system and CO_2 rich inclusions, but the

author did not state the amount of CO_2 (Burnett, 1995). Fluid inclusions hosted in quartz

(n=52), fluorite (n=103), and adularia (n=4) were analyzed (Burnett, 1995). Quartz-

hosted fluid inclusion homogenization temperatures are between 105-295°C and most

falling within 135-175°C with salinities ranging 5.5 to 6 wt. %NaCl; fluorite-hosted

inclusions have more T_h variation that range from 115-305°C with salinities between 3.5-

5 wt. %NaCl; adularia inclusions have a wide range for the number measured, T_h 195-

265°C and no salinity data (Burnett, 1995).

At Grassy Valley, which is located within the Cripple Creek mining district, fluid

inclusion study shows 2 and 3 phase inclusions (Rosdeutscher, 1996). All

microthermometry measurements are from quartz. Two-phase inclusions ($l+v$)

homogenization temperatures range from 228-432°C with salinities of 3.3-6.6 wt.

%NaCl; three-phase inclusions ($l+v+s$) T_h are between 407 and 467°C, and there is no

salinity data available (Rosdeutscher, 1996). Lastly, Granite Island is located along the

margin of the Cresson Deposit within the current Cripple Creek open pit mine. Granite

Island fluid inclusions are hosted in quartz, carbonate, sulfates, and potassium feldspar

(Mote, 2000). Some inclusions have multiple daughter minerals, but the majority are two-

phase inclusions (Mote, 2000). Homogenization temperatures vary significantly (T_h: 50-

650°C); however, most inclusions fall within a much narrower range, T_h 150-350°C, with

salinities of 0.1 to 25 wt. %NaCl (Mote, 2000).

The fluid inclusion studies have shown that Cripple Creek has two main

populations of fluid inclusions (Figure 4.14). There are low to moderate salinity

inclusions with lower vapor homogenization temperatures, which correlate to Rattlesnake

Hills. However, there is a higher temperature homogenization phase with more saline rich

inclusions and rare CO_2 rich inclusions. Cripple Creek fluid inclusions are hosted by

mineral phases (quartz, fluorite, and sphalerite) that are rare at Rattlesnake Hills.

Evidence for boiling implies that Cripple Creek was hotter or shallower than Rattlesnake

Hills. As both Rattlesnake Hills and Cripple Creek were shallowly emplaced intrusive

with diatreme complexes and presence of volcanic facies, therefore, it is likely Cripple

Creek was transiently hotter. Additionally, homogenization temperatures and salinities

have a larger range at Cripple Creek (Figure 4.14). However, when Rattlesnake Hills

fluid inclusion data is compared to other prominent alkaline hosted gold deposits, La

Plata Mountains, Emperor, and Porgera (stage 2 fluids) deposits have similar

homogenization temperatures and salinities (Jensen and Barton, 2000) (Figure 4.15).

At Porgera, fluid inclusions were measured in quartz veins and breccias. There are

two populations of fluid inclusions: low salinity and higher salinity (Ronacher et al.,

2004). Higher salinity inclusions range from 7.5±1.0 to 9.6±0.2 wt. %NaCl, while the

lower salinity inclusions range between 4.4 to 6.2 wt.%NaCl (Ronacher et al., 2004). The

homogenization temperatures for the lower salinity inclusions are 145±9°C, and the

higher salinity inclusions range from 127±12° to 167±25°C (Ronacher et al., 2004). There

are CO_2 enriched fluid inclusions, for the higher salinity inclusions there is up to 2 mol

percent CO_2 (Ronacher et al., 2004).

Ladolam Deposit, Lihir Island, Papua New Guinea is an epithermal deposit hosted

in alkaline type rocks in a breccia complex. Ladolam is similar to Rattlesnake Hills with

the exception Ladolam has a boiling phase that is evident in vapor-rich fluid inclusions

(Carman, 2003).

In summary, Rattlesnake Hills and Cripple Creek have low-temperature, low

salinity fluid inclusions hosted in carbonate and quartz. Both systems have inclusions that

have trace amounts of CO_2. Cripple Creek is characteristically different from Rattlesnake Hills because it has a second population of fluid inclusions: higher temperature and higher salinity. Additionally, Rattlesnake Hills has similarities to other alkaline gold systems throughout the world.
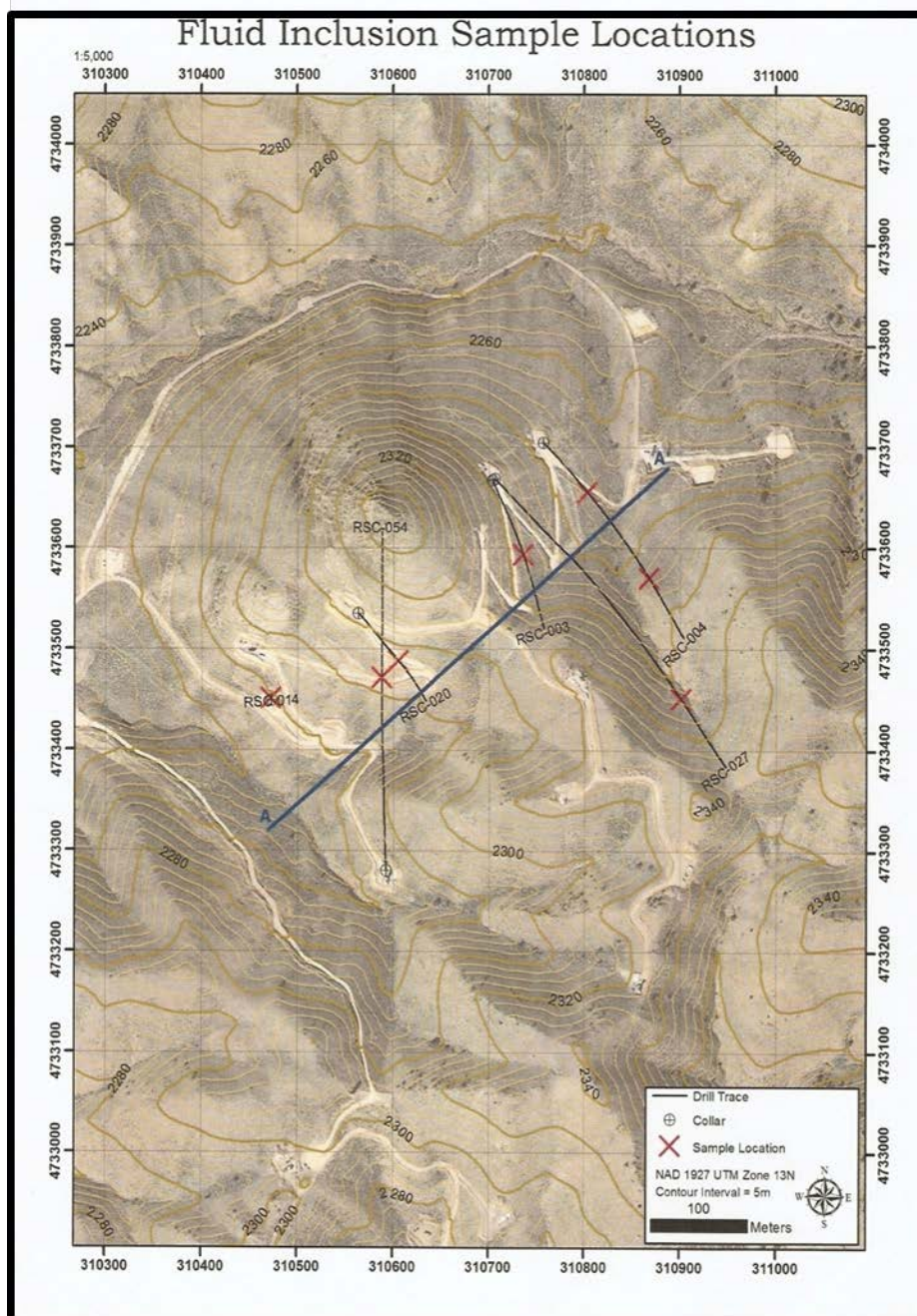
Figure 4.1A Map of North Stock showing location of samples, which are marked red X
with gold assay results in red, used for fluid inclusion microthermometry. (See Figure 1.1
and 1.2 for regional geology and ore deposit geology.)
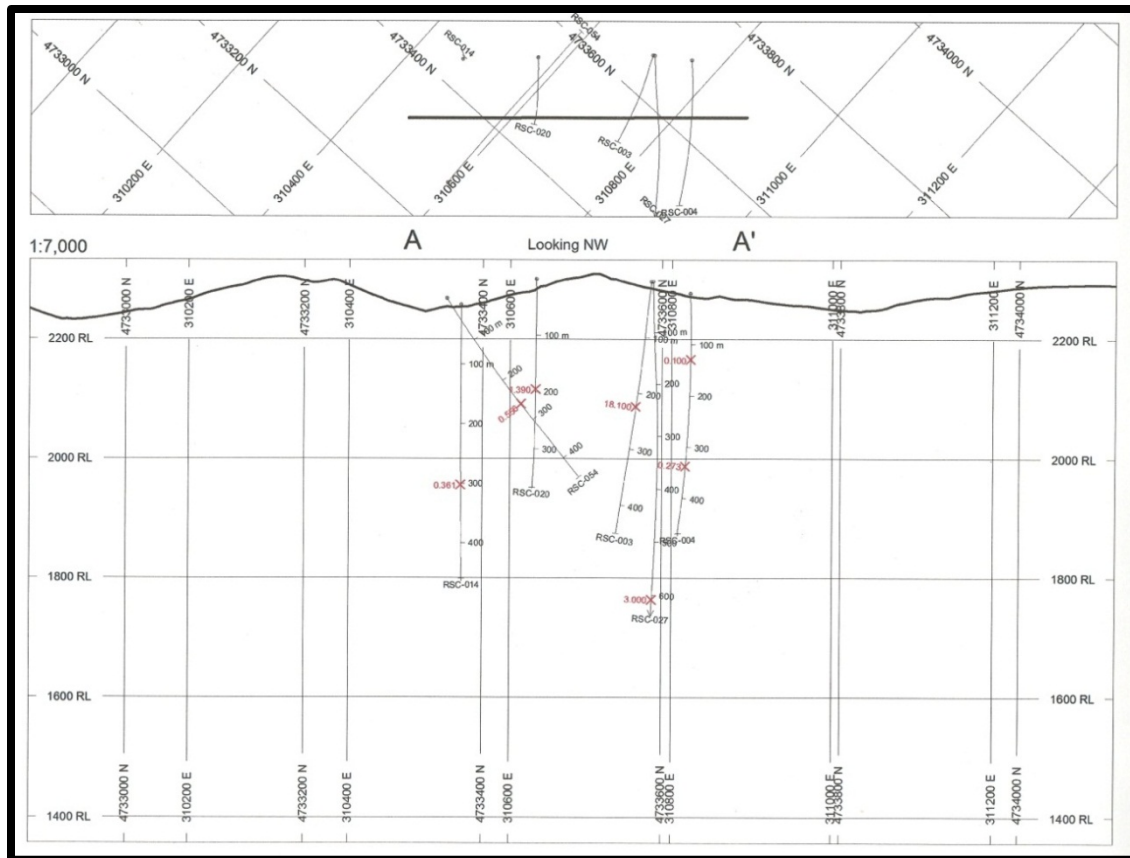
Figure 4.1B Section of North Stock showing location of samples, which are marked red X with gold assay results in red, used for fluid inclusion microthermometry. (See Figure 1.1, 1.2, and 2.8 for regional geology and ore deposit geology.)
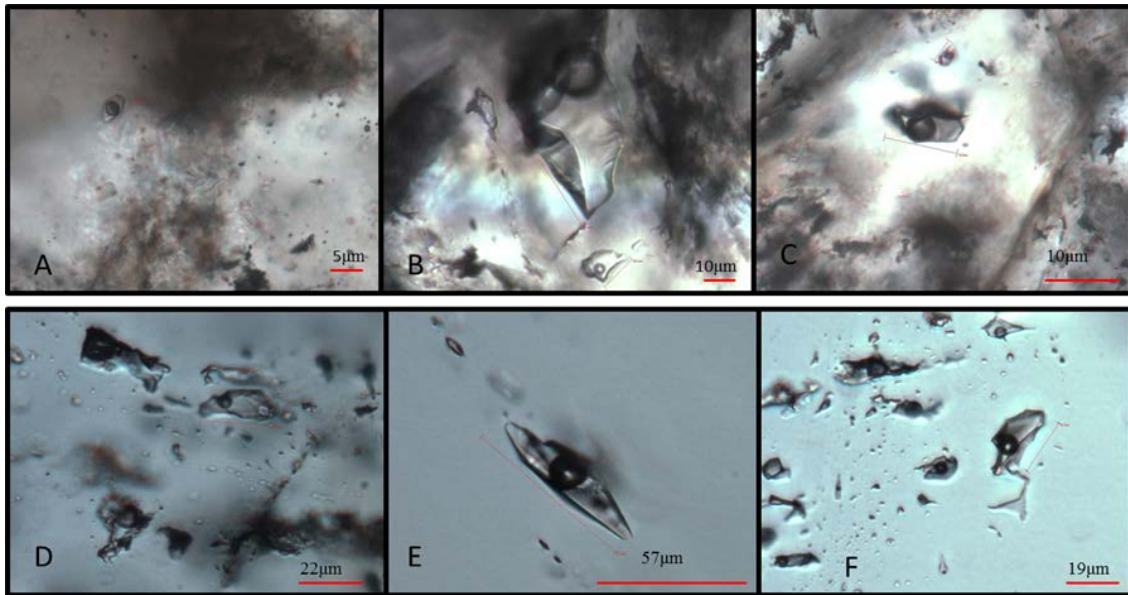
Figure 4.2 Photomicrograph of typical fluid inclusions. A) RSC-012 1557.1' has a small

5μm two-phase liquid-vapor fluid inclusion hosted in cloudy calcite vein in altered schist.

B) RSC-020 646.5' a large 40μm and small 10μm two-phase liquid-vapor fluid inclusions

hosted in vein calcite in an altered schist. C) RSC-054 859' has two small 2 and 10μm

two-phase liquid-vapor fluid inclusions hosted in a clear pocket of calcite within schist.

D) RSC-054 859' has trail of fluid inclusions in a calcite vein with the central inclusion

being a 22μm three-phase liquid-vapor-solid, which is isotropic, fluid inclusion in a

quartz vein. E) RSC-054 859' has on large 57μm three-phase liquid-vapor fluid inclusion

in calcite vein with the solid being irregular and isotropic with low relief to the host

mineral. F) RSC-015 1272.7' a trail of irregular two and three phase liquid-vapor±solid

fluid inclusions hosted in a calcite-dolomite vein where the three phase inclusions are

cubic and have high relief to fluid in the inclusion with low relief to calcite.
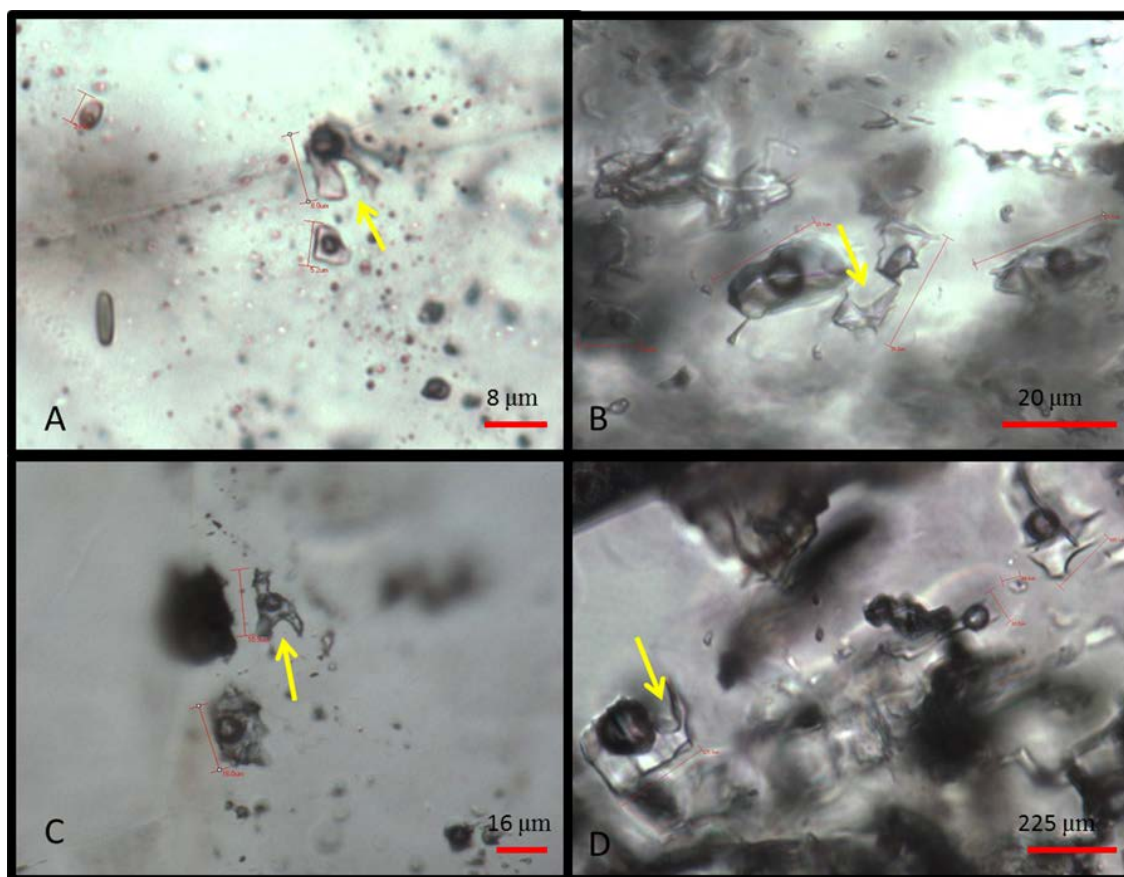
Figure 4.3 Photomicrograph of fluid inclusions showing textural re-equilibration. These inclusions have a distinct arc or hook-like shape, indicating isobaric cooling. A) RSC-012 1557.1' B and C) RSC-020 646.5' and D) RSC-027 2001'
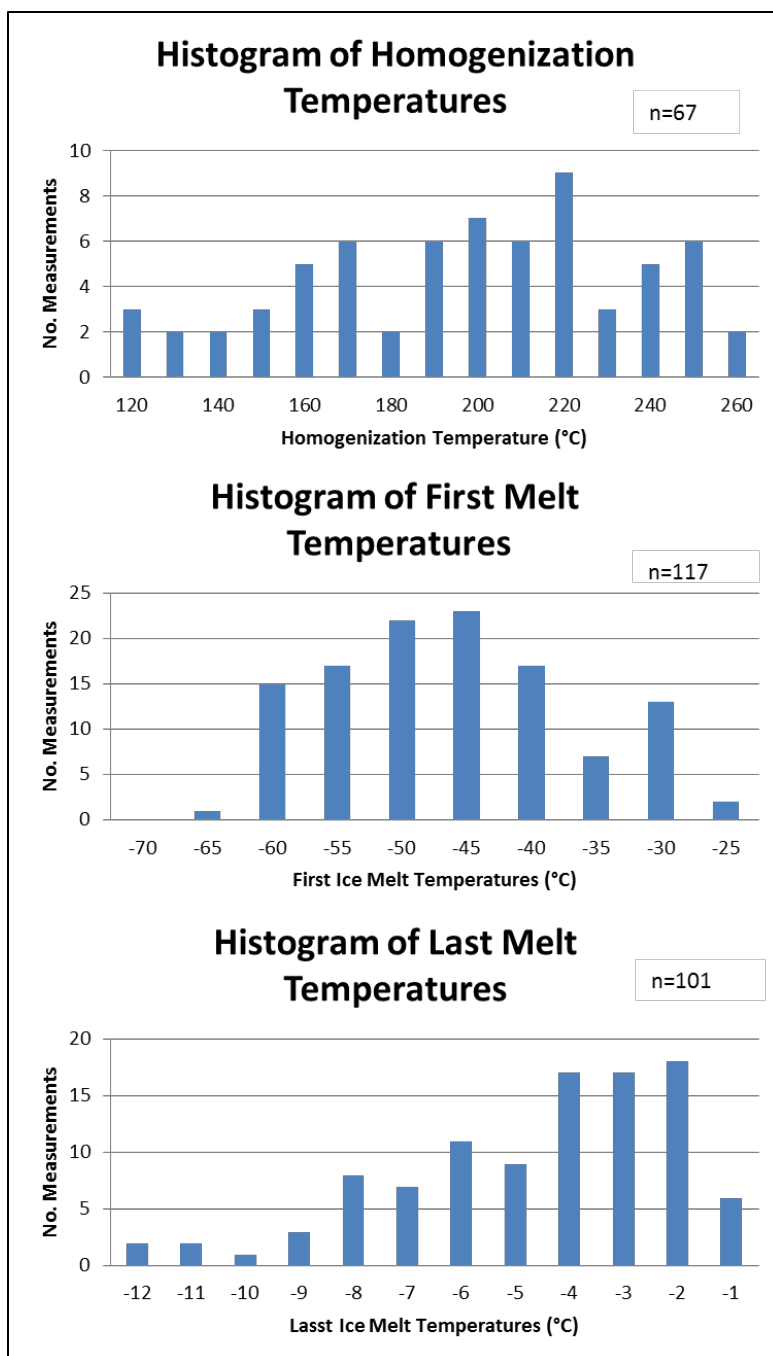
Figure 4.4 Histograms of vapor homogenization temperatures, last ice melt temperatures, and first ice melt temperatures from all samples in Table 4.1. The first ice melt temperatures peak is approximately -56 to -48°C suggesting $NaCl$-$CaCl_2$ as the most significant salt components.
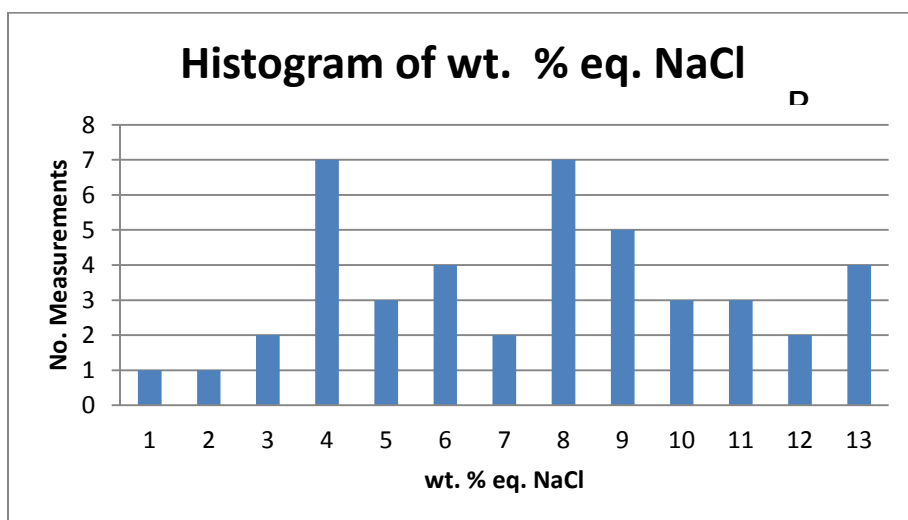
Figure 4.5 Histogram of the wt. % eq. NaCl for measured fluid inclusions calculated from

ice melting temperatures.
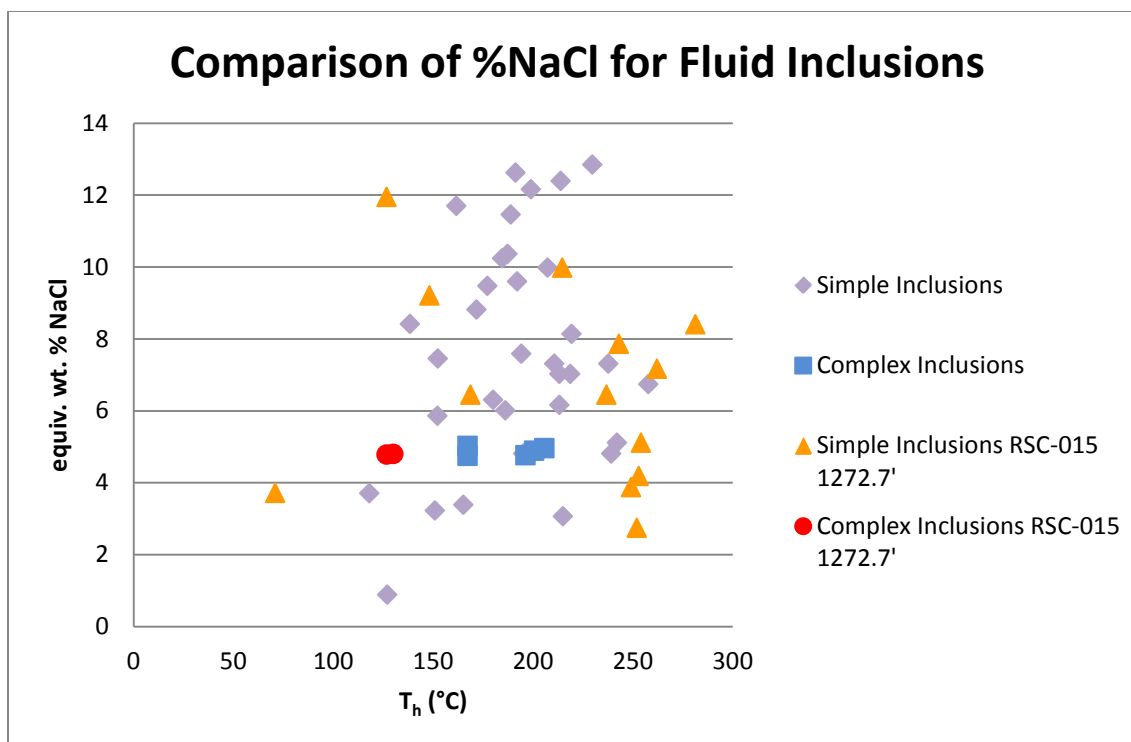
Figure 4.6 Scatterplot comparing microthermometric measurements of simple, two phase inclusions and complex, multiphase ($l+v+s$) inclusions showing the salinity and vapor homogenization temperatures from RSC-015 1272.7' (used for LA-ICP-MS) and all other inclusions measured. The salinity for complex inclusions was determined from clathrate melting temperature. No trend can be interpreted but the sample measured using LA-ICP-MS is representative of the whole population.
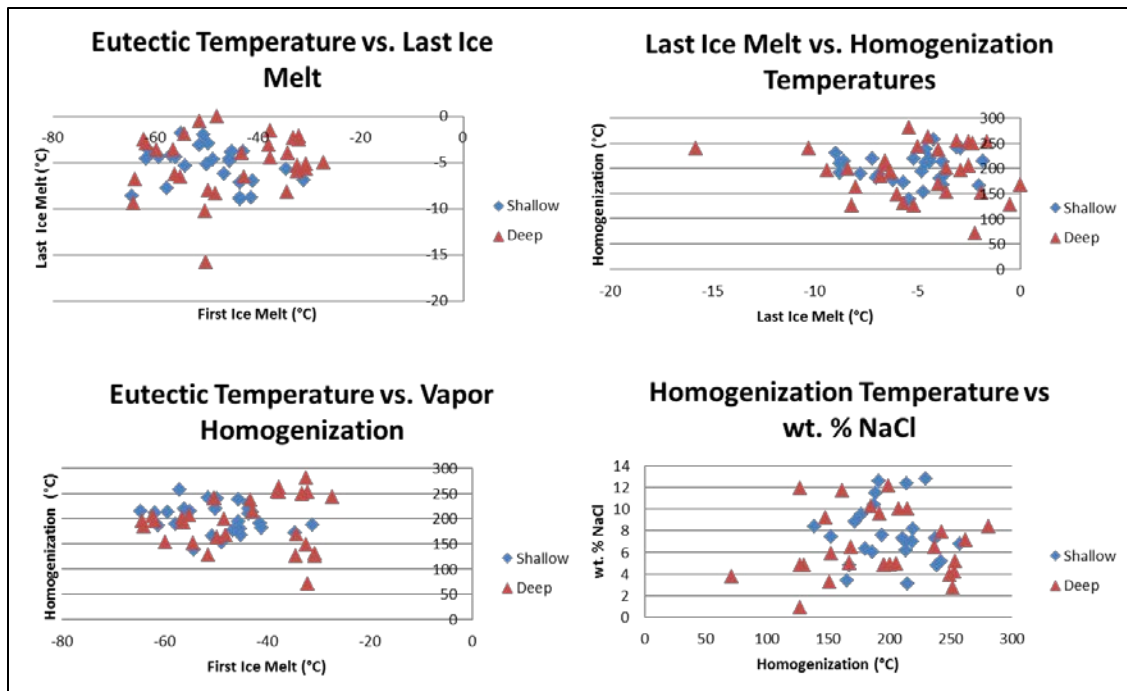
Figure 4.7 Scatterplots of various microthermometric measurements divided by depth. Shallow is 0-1000' and deep is 1000-2001'. The Eutectic Temperature vs. Last Ice Melt scatterplot of microthermometric measurements shows slight statistical differences between shallow and deep located fluid inclusions. It is probable there are slightly more complex solutions at depth.

Homogenization Temperatures vs. equiv. wt. %NaCl based on Rock Type
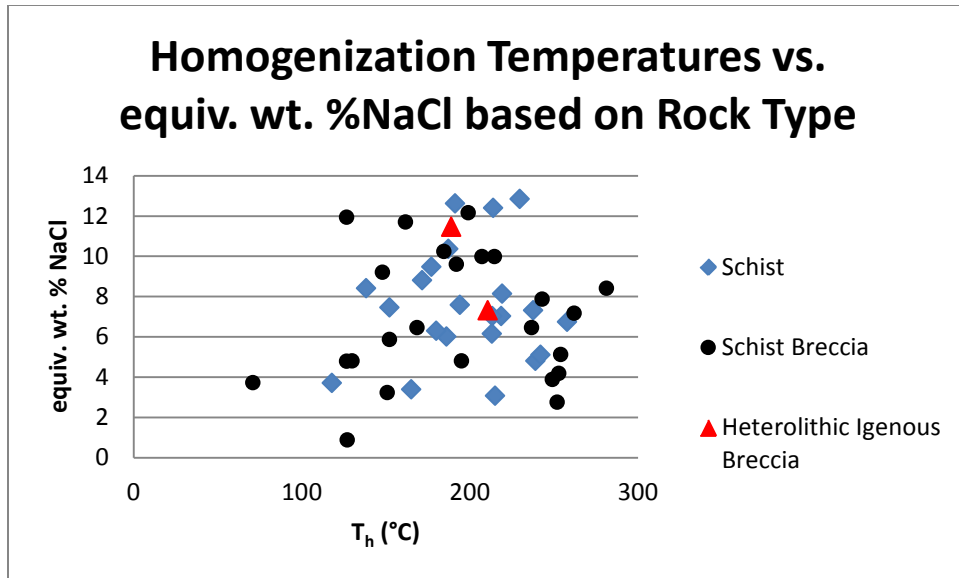
Figure 4.8 Scatterplots of microthermometric simple, two-phase fluid inclusions showing the salinity based and homogenization temperatures divided by rock types (Rock units are discussed in detail in Chapter 3).
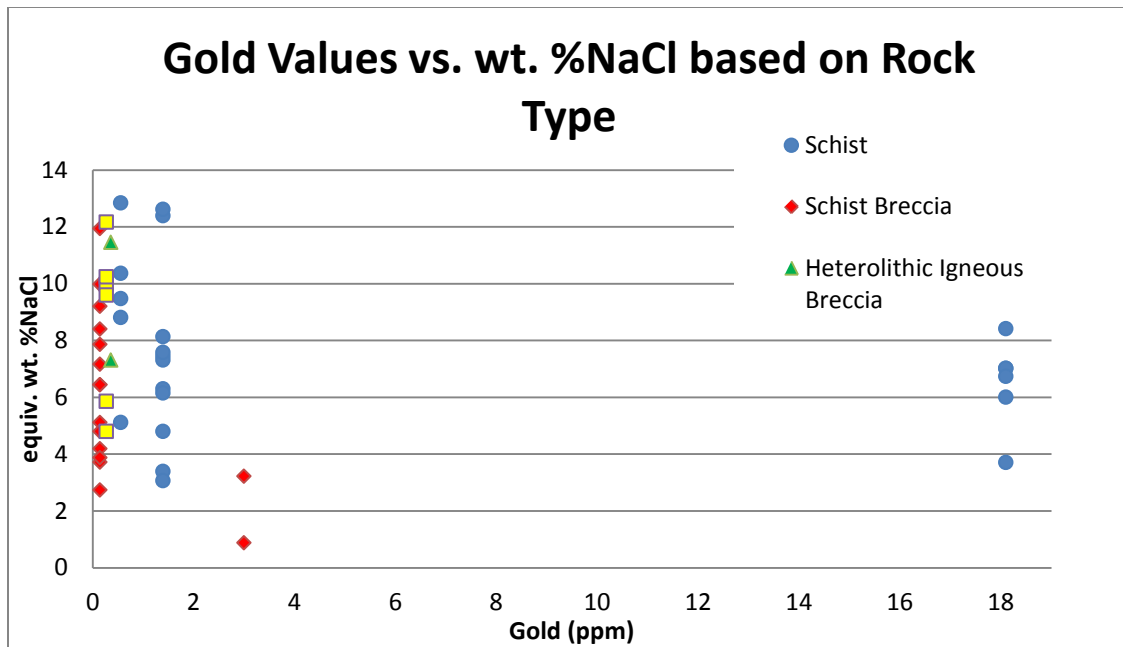
Figure 4.9 Scatterplot of gold grade and equivalent weight percent of NaCl based on rock types. There is no correlation between higher salinity inclusions and higher gold grade. Additionally, in general there is no trend between rock unit and gold grade but the scatterplot indicates a weak trend of higher gold grade in schist while the lowest grades are in porphyry.
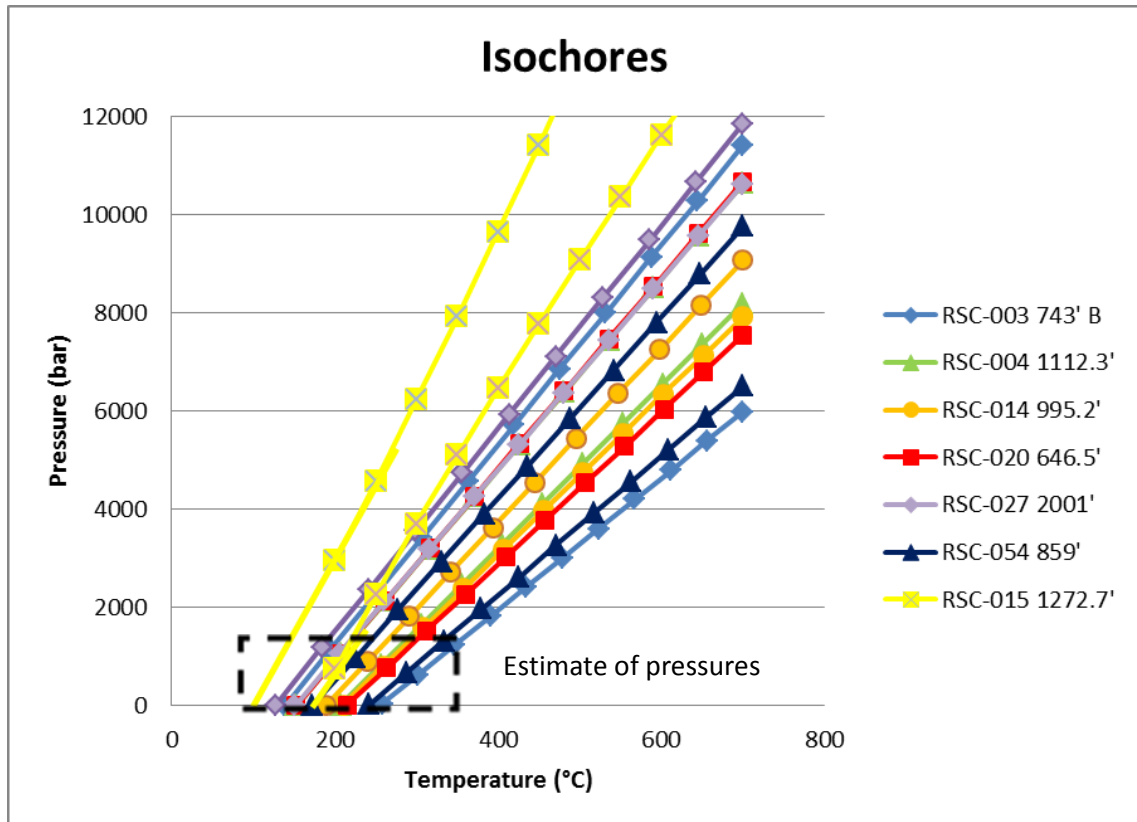
Figure 4.10 Average isochores of representative two-phase inclusions in each of the six

samples. The highest and lowest isochore for each drill hole is plotted above to show the

range of isochores. The dashed box outlines the zone of likely pressures given the

estimated depths of mineralization. The isochores from the sample used for LA-ICP-MS,

RSC-015 1272.7', has higher pressures and lower temperatures than the other samples.
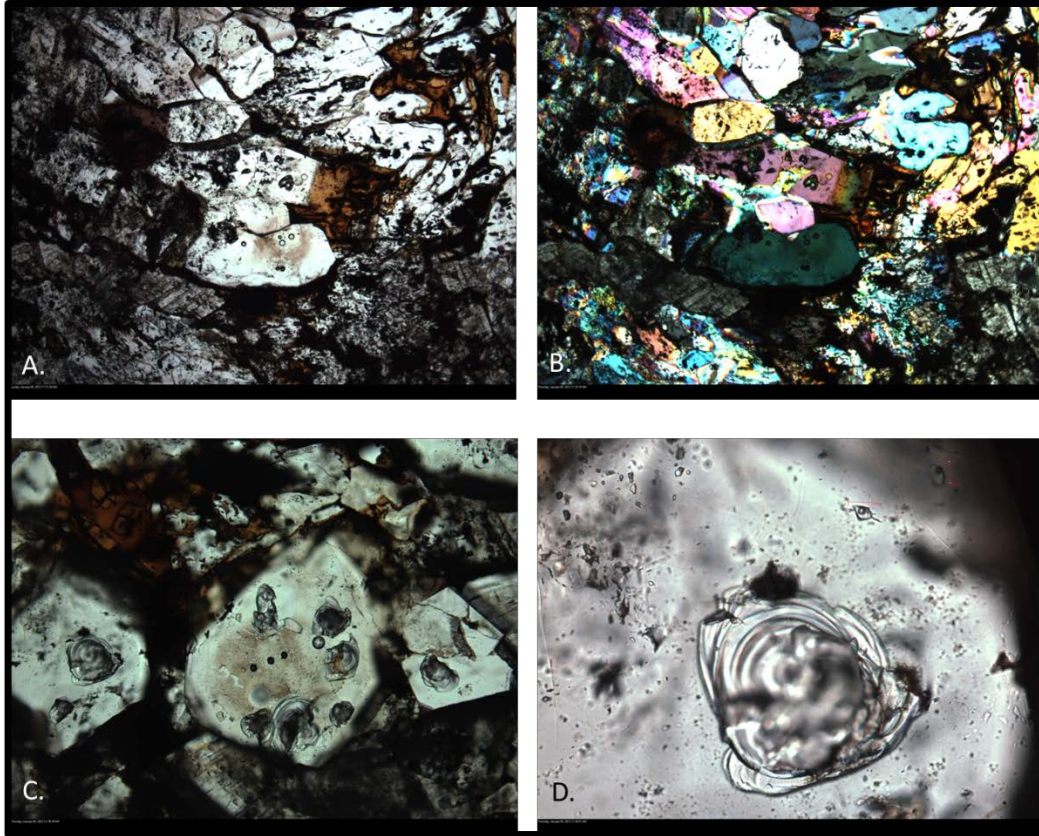
Figure 4.11 Photomicrographs of LA-ICP-MS sample RSC-015 1272.7'. A and B) Euhedral quartz intergrown with carbonate hosted in schist with small ablation pits in quartz grains. A is in plane polarized light and B is in cross-polarized light. C) Three euhedral grains of quartz with multiple ablation pits. D) Quartz grain (far left grain from photomicrograph C) with irregular ablation pit and two fluid inclusions.
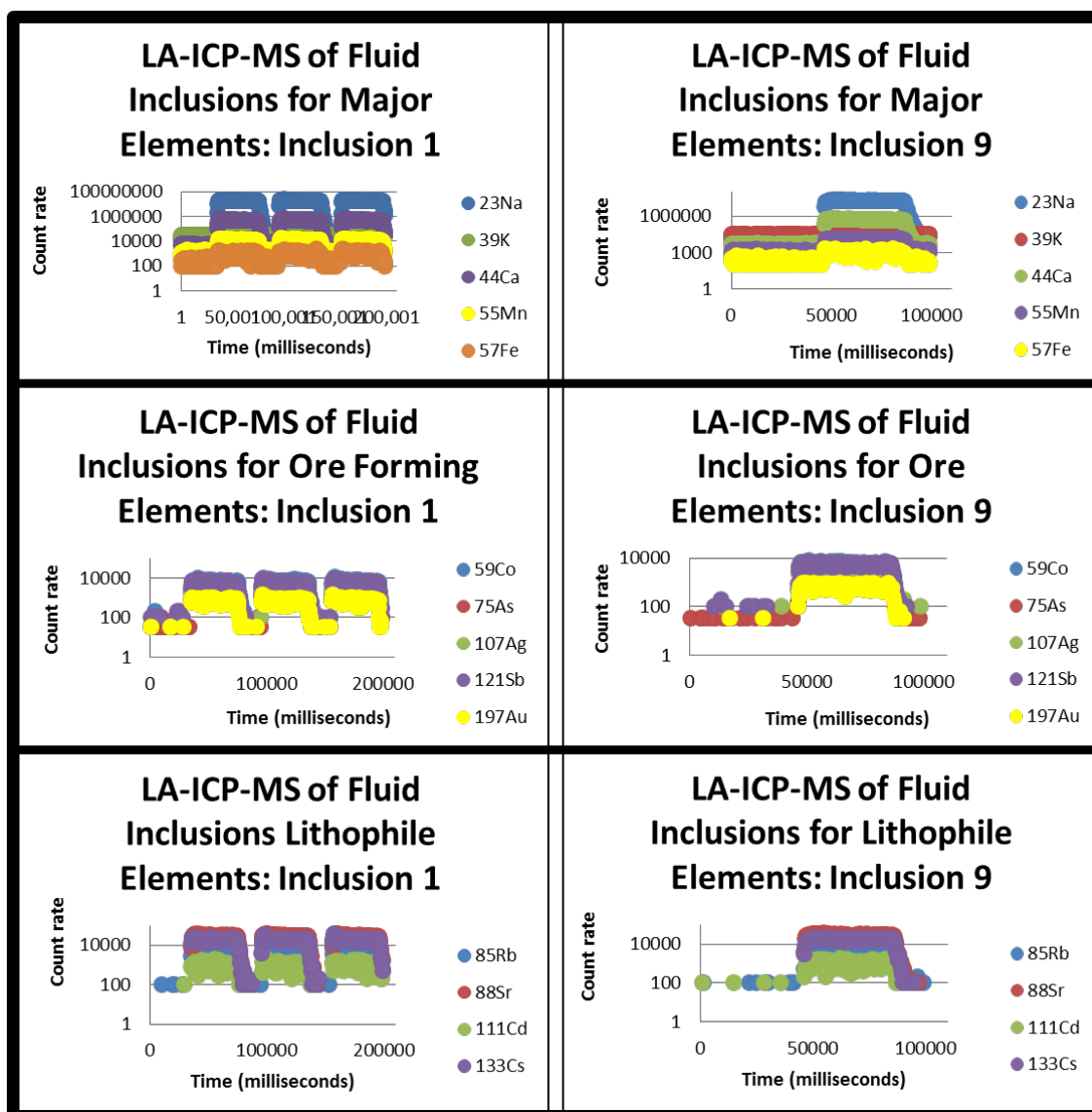
Figure 4.12 Raw LA-ICP-MS count rate data of fluid inclusions 1 and 9. Fluid inclusion 1 shows three peaks, each peak represents ablation of an inclusion. The troughs before and between peaks are background count rates in quartz. Fluid inclusion 9 is a single fluid inclusion. The elevated values of the elements are hosted within the fluid inclusion indicating the fluid is enriched in these elements rather than the host quartz.
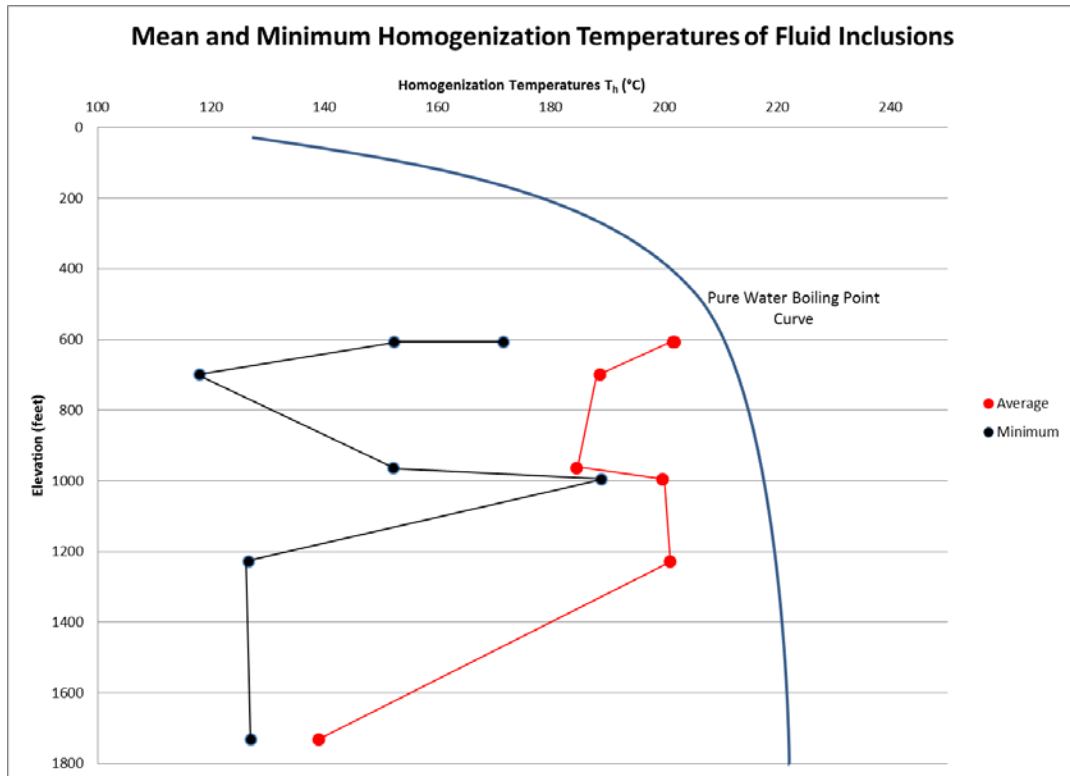
Figure 4.13 Homogenization temperatures versus true depths of drill holes. Drill hole depths were adjusted by the dip the drill hole was drilled. The homogenization temperatures of fluid inclusions represent the average and minimum homogenization temperatures. Since the surface depth is unknown at Rattlesnake Hills, a minimum depth is used as a constraint for the pure water boiling point curve given that all fluid inclusions homogenized to the liquid.
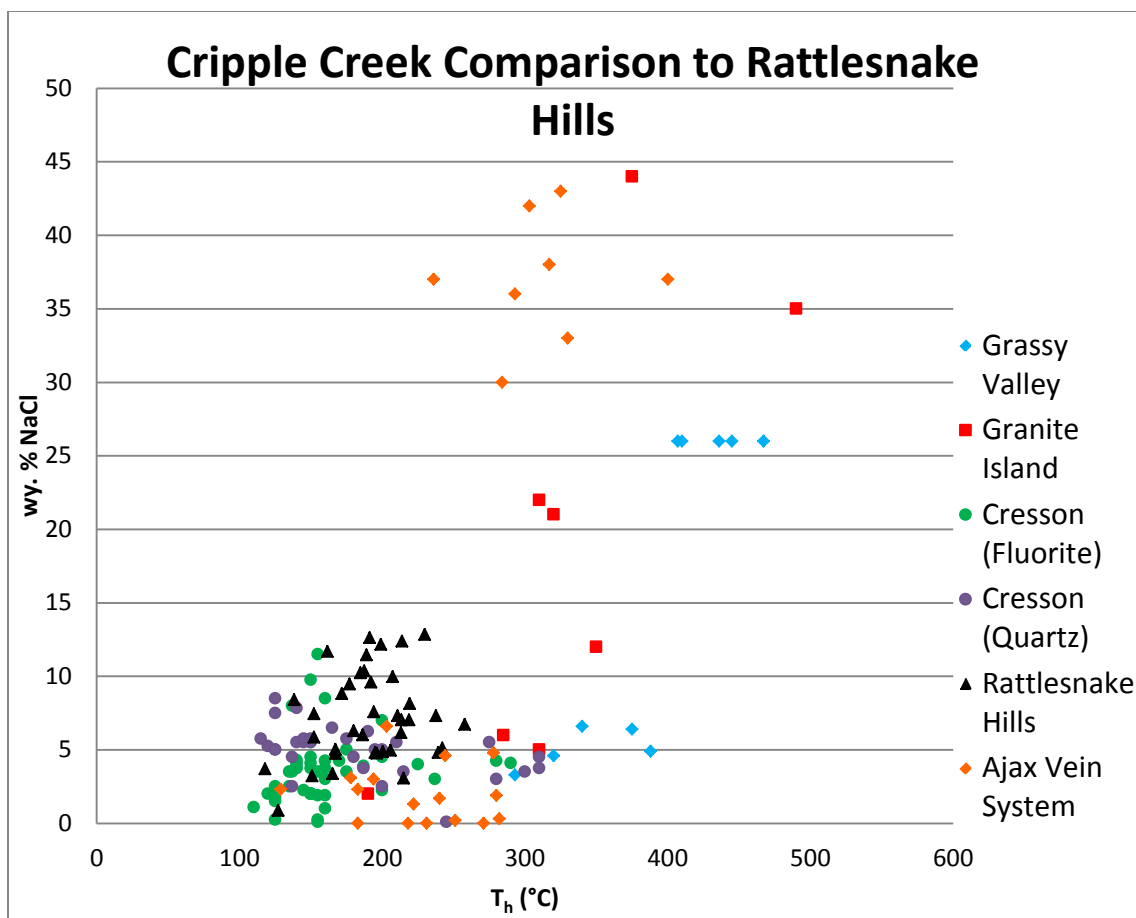
Figure 4.14 Scatterplot of fluid inclusion properties of combined Cripple Creek fluid

inclusion studies (Dwelley, 1984; Burnett, 1995; Rosdeutscher, 1996; Mote, 2000).
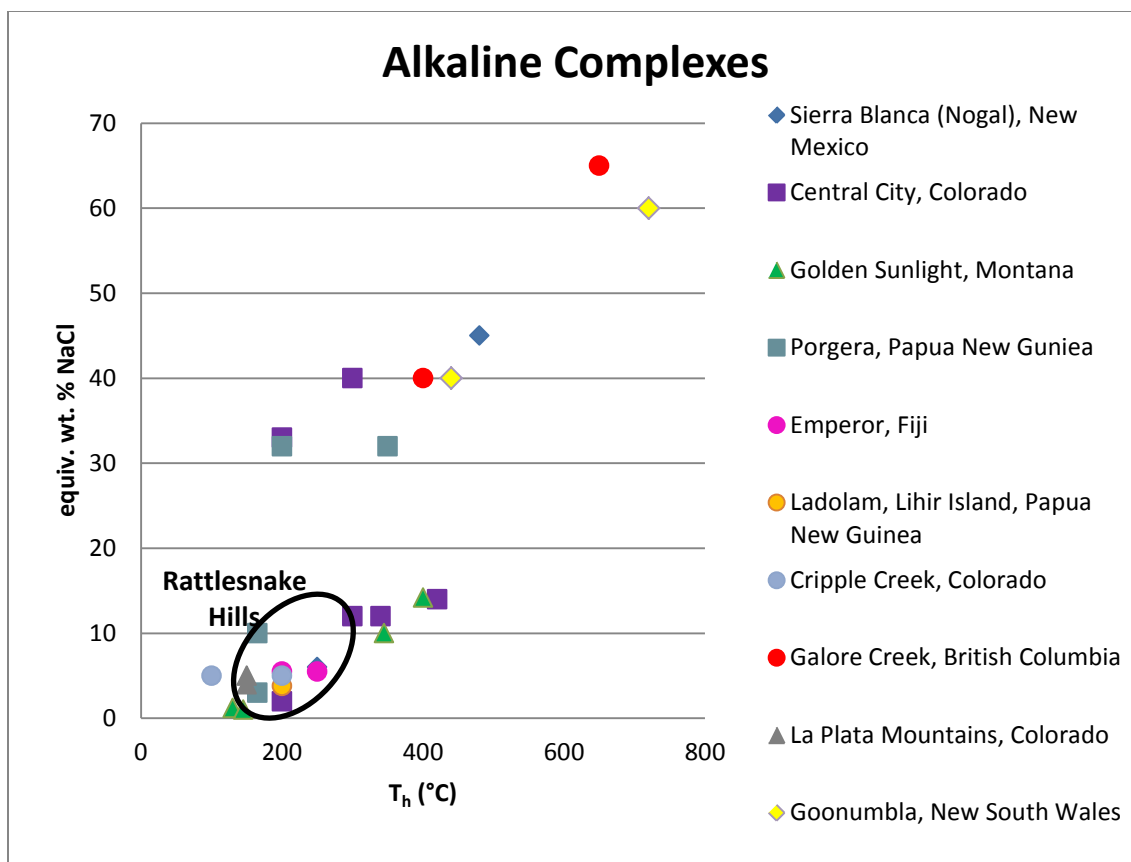
Figure 4.15 Comparison of fluid inclusion properties of alkaline hosted gold complexes in the Colorado Mineral Belt and global world-class gold alkaline systems (adapted from Jensen and Barton, 2000).

Fluid Inclusion Summary					
Hole	**Depth**	**Rock Type**	**Au (ppm)**	**Inclusions**	**Vein Color**
RSC-003	743B	Schist	18.1	n=6	Grey
RSC-004	431.5	Porphyry	0.1	n=3	White-Grey
RSC-004	1112.3	SchBx	0.273	n=10	White
RSC-014	995.2	HIBx	0.361	n=2	White-Grey
RSC-015	1272.7	SchBx	0.142	n=15	White-Grey
RSC-020	646.5	Schist	1.39	n=11	Clear
RSC-027	2001	SchBx	3	n=3	Grey
RSC-054	859	Schist	0.556	n=9	Clear

Table 4.1 Summary of samples used for fluid inclusion microthermometry analysis. See Figure 4.1 for drill hole locations. SchBx is a monolithic schist breccias and HIBx is a heterolithic breccias with schist and igneous clasts. RSC-015 1272.7' is the sample used for LA-ICP-MS and Laser Raman.

5. ISOTOPE ANALYSIS OF CARBONATE VEINS

Carbon and oxygen isotope analysis was completed on 38 carbonate samples (Appendix 2). Each sample was drilled from the puck for thin sections. The carbonates were extracted from veins, amygdules, and late stage open spaced vugs from a variety of depths and rock units present at North Stock. Carbonates are not distinguished as calcite or dolomite due to the fine grain (μm-scale) intergrown nature of carbonates. However, the samples were further categorized by the color of the vein and the generations of carbonate present. Some veins contained multiple generations of carbonate and care was taken to separate the generations for individual analysis. Three duplicate samples were selected prior to analysis at the Department of Geology at Colorado School of Mines and one duplicate selected at the time of testing to ensure accuracy. Each sample was powdered and sent to Colorado School of Mines Stable Isotope Laboratory for analysis. The duplicate samples fall within 2 standard deviations. One sample did not have enough material to measure. All sample results are expressed relative PDB (carbon) and SMOW (oxygen).

5.1 OXYGEN AND CARBON ISOTOPE GEOCHEMISTRY

The carbonates show a constrained range in the oxygen isotopes with a wide range of carbon isotopic compositions (Figure 5.1). The data clusters with $\delta^{13}C_{PDB}$ between -2.22‰ and -13.45‰ where as $\delta^{18}O_{SMOW}$ ranges from 8.70‰ to 14.84‰.

Recalculating isotopic compositions as fluid compositions, the recalculated $\delta^{18}O_{SMOW}$ ‰ ratios range from -1.49 to +4.65 and $\delta^{-13}C$ ‰ range from -14.30 to -3.07 assuming a temperature of 475 K (Chacko et al., 1991). The oxygen and carbon isotopic compositions overall show two intersecting trends: 1) large cluster with positive covariation of oxygen and carbon and 2) a scatter to strongly negative $\delta^{13}C_{PDB}$ values (Figure 5.2). Isotope compositions were assessed based on specific criteria: rock type, vein color, vein edges compared to vein centers, and depth of samples to examine any correlation that may explain these trends.

The rock units with carbonate sampled include: schist, porphyry, phonolite, heterolithic igneous and metamorphic breccias, and carbonate veins of calcite and dolomite >3 inches wide. There are no distinctive trends of isotope compositions with respect to rock type (Figure 5.3). The schist has a wider carbon and oxygen spread; while the carbonate veins and phonolite have a narrow oxygen variation with slightly larger spread of carbon isotopic compositions. The other rock units do not have enough data to define a trend. Additionally, there appears to be no distinctive cluster associated with any one rock type. The low $\delta^{13}C$ values are not within a specific rock type, but are confined to heterolithic igneous and metamorphic breccias (HIMBx) and schist.

The vein types are classified by the color: white, clear, yellow, and grey. While the color is not always helpful, at Rattlesnake Hills vein color can be attributed to sulfides and hence to gold mineralization. Grey veins contain the most disseminated sulfides, while clear and white veins have significantly less sulfides. Yellow veins are notable due to the FeOx content, but tend to be late carbonate veins in the system. However, no colors

of vein show isotopic differentiation (Figure 5.4). Since there is no differentiation of the vein types, the vein with multiple generations of carbonate growth were separated into edges and centers. There are eight samples where the edges and centers were analyzed separately (Figure 5.5). There is no contextual pattern with generation. Four of the samples show the edges have a more negative carbon isotopic ratio than the center of the veins. Two samples show the centers have a more negative carbon isotopic ratio than the edges. However, two samples show little or no variation from the center to edge. During sampling, different generations might not have been separated completely. The implications of sample mixing would create an erroneous isotopic ratio, potentially mixing two separate sources. No trend is however interpreted.

Lastly, the data was separated by the depth of the sample (Figure 5.6). Shallow samples are 0' to 750', intermediated samples are 750' to 1500', and deep samples are 1500' to 2600'. Note the depths used for isotope analysis are different than fluid inclusion analysis depths in Ch. 4. Shallow samples have a large spread that is offset to a more positive $\delta^{18}O$ than the intermediate or deep samples. Intermediate and deep samples have a narrow oxygen and carbon spread, but fall within the larger overall spread. The cluster of strongly negative $\delta^{13}C$ samples, are all of an intermediate depth.

5.2 CARBON AND OXYGEN ISOTOPE DISCUSSION

Overall, most of the samples plot within or close to the defined magmatic isotopic ratio box. However, to explain the covariation and the scatter to negative $\delta^{13}C$ ratios, other processes will be discussed in more detail. There are several possible processes that could have created the isotopic trends observed at Rattlesnake Hills. There are four likely

processes: magmatic fractionation, progressive magmatic degassing, interaction of magmatic and meteoric waters, and the incorporation of country rock.

The strongly negative $\delta^{13}C_{PDB}$ values from some carbonate veins could reflect fluids interacting with organic matter from pyroclastic or sedimentary units, influx of meteoric water mixing with magmatic fluids, or magmatic degassing. A similar steep trend of decreasing carbon isotopic ratios with decreasing oxygen isotope ratios was observed at the Cobalt Embayment in Ontario, Canada (Potter and Taylor, 2010). The trend is the result of an influx of meteoric water interacting with magmatic fluids (Potter and Taylor, 2010). However, Oliveria Cordeiro et al. (2011) attributed a negative slope with heavier oxygen and lighter carbon compositions, to CO_2 degassing. The degassing of CO_2 came from a carbonatite melt is most likely coupled with decompression melting (Oliveria Cordeiro et al., 2011). While carbonatites have not been identified in the study area, it is possible they are present but undocumented. However, in view of the low $\delta^{13}C$ values and higher $\delta^{18}O$ values (covariation trend) this most likely reflects fluids interacting with pyroclastic or sedimentary units with organic carbon. There are pyroclastic units located on the west side of North Stock. The pyroclastic units are near surface deposits containing organic material and formed in a maar-type setting (Evolving Gold Corp., 2009).

The systematic positive covariation of oxygen and carbon isotopic compositions can be attributed to several processes: fluid mixing, wallrock interaction, or CO_2 degassing from an underlying magma chamber (Potter and Taylor, 2010; Zheng, 1990). The large cluster of samples shows a wider range of oxygen than carbon isotopic ratios.

According to Potter and Taylor (2010) the wider $\delta^{18}O$ values are due to loss of oxygen in degassing both CO_2 and H_2O. This change in oxygen isotopic compositions could alternatively be caused by mixing with meteoric fluids (Oliveria Cordeiro et al., 2011). However, Zheng (1990) proposed that covariation trends would not be created by mixing of two fluids, because the end composition of oxygen and carbon isotopes would be similar. Alternatively, the covariation trend could be a product of decreased temperatures and a change in the dissolved carbon species (Matsuhisa et al., 1985).

The fluid inclusions at Rattlesnake Hills show no evidence of boiling (CO_2 degassing) (see Chapter 4). However, it is possible that there had to have been a magma chamber below the level of exploration, which has undergone CO_2 degassing. In a low-sulfidation epithermal style deposits, CO_2 degassing is the primary process for gold deposition (Hedenquist et al., 2000). Additionally, the covariation trend, ignoring the negative cluster of data, has a low horizontal positive slope. The slope of the isotopic data in the Rattlesnake Hills complex is 0.289±0.03 while most carbonatites are 0.40 (Marks et al., 2009) (Figure 5.2). Carbonatite systems with steeper trends tend to be water rich. Magmatic systems generally have shallow slopes due to crystal fractionation (Marks et al., 2009).

The center and edges of carbonate veins show differing trends of heavier and lighter carbon isotopic compositions both with increasing and decreasing oxygen ratios with up to 2‰ $\delta^{18}O$ variation. There is no consistent pattern. One possibility is incomplete sampling due to μm-scale oscillations. The sampling is restricted to ~2mm scale (size of diamond drill bit) and oscillations are possibly smaller than this scale of

93

sampling (Figure 3.6). The shifts can be explained by assimilation of crustal material, magmatic degassing, meteoric fluid interactions, or alteration (Oliveria Cordeiro et al., 2011; Marks et al., 2009). Alteration of wallrock can cause the precipitation of calcite or in a more carbonate-rich system low temperature alteration of carbonates would cause the fluid to show little change in carbon isotopic values but show changes in oxygen isotopic compositions (Oliveria Cordeiro et al., 2011; Marks et al., 2009).

5.3 CARBON AND OXYGEN ISOTOPE INTERPRETATIONS

While there are several alternative explanations for the two distinct isotopic trends, the regional and local geology narrow the feasible theories. It is unlikely that either signature is from mixing with meteoric water or from degassing of carbonatites. Although the isotopic compositions at Rattlesnake Hills fit the box of carbonatite isotopic compositions $\delta^{18}O_{SMOW}$ 6‰ to 8.5‰ and $\delta^{13}C_{PDB}$ of -8‰ and -5‰, there is no known carbonatite on site (Taylor et al., 1967). This fit only implies that Rattlesnake Hills is dominated by a mantle-derived magma.

Published estimates of the isotopic signatures of Eocene meteoric values from the Wind River Basin and Bighorn Basin located in central Wyoming were compared to Rattlesnake Hills to determine if there is a similar composition. Eocene estimates were used for comparison since Rattlesnake Hills is an Eocene alkaline complex. The Wind River Basin samples are significantly different than Rattlesnake Hills (Figure 5.7). The Eocene precipitation is estimated as -6.8±1.9‰ ($\delta^{18}O_{SMOW}$), ground water as -16.6±.5‰ ($\delta^{18}O_{SMOW}$), and paleosols as -7.0±2.0‰ ($\delta^{13}C_{PDB}$) (Fan et al., 2011). Groundwater from highlands, not from precipitation, is proposed to cause the large variation in oxygen

isotopic compostions in the Wind River Basin (Fan et al., 2011). However, different basins in Wyoming have different Eocene meteoric waters values. Sage Creek Basin located along the southeastern border of Montana has meteoric waters more closely resembling isotopic signatures at Rattlesnake Hills (Kent-Corson et al., 2010). Yet, it is improbable that meteoric waters from other basins influenced the isotopic compositions at Rattlesnake Hills. Paleogeographic reconstructions of Wyoming are continental interior of ~40°N. Overall, it is important to note there is no trend toward strongly negative $\delta^{18}O$ meteoric compositions at Rattlesnake Hills; hence there is no evidence of meteoric fluids mixing with magmatic fluids.

The covariation signature is most likely caused by magmatic degassing at depth within the magma chamber causing the progressive release of CO_2 rich fluids which then resulted in the precipitation of carbonate. The changes from rim to core of veins are most likely to be a product of wallrock or carbonate alteration, assimilation of crustal material or wallrock, or μm-scale oscillations formed during the degassing of an underlying magma chamber. These changes imply that the magma is complex and multi-phase. The strongly negative $\delta^{13}C$ is indicative of incorporation of organic carbon most likely from pyroclastic rocks or schist. Additionally, there is no evidence that there is a cooling trend within the magmatic system. Lastly, the lack of systematic variation with depth implies CO_2 most likely passed through the system from the magma chamber and vented at the surface, rather than all crystallizing as carbonate veins.
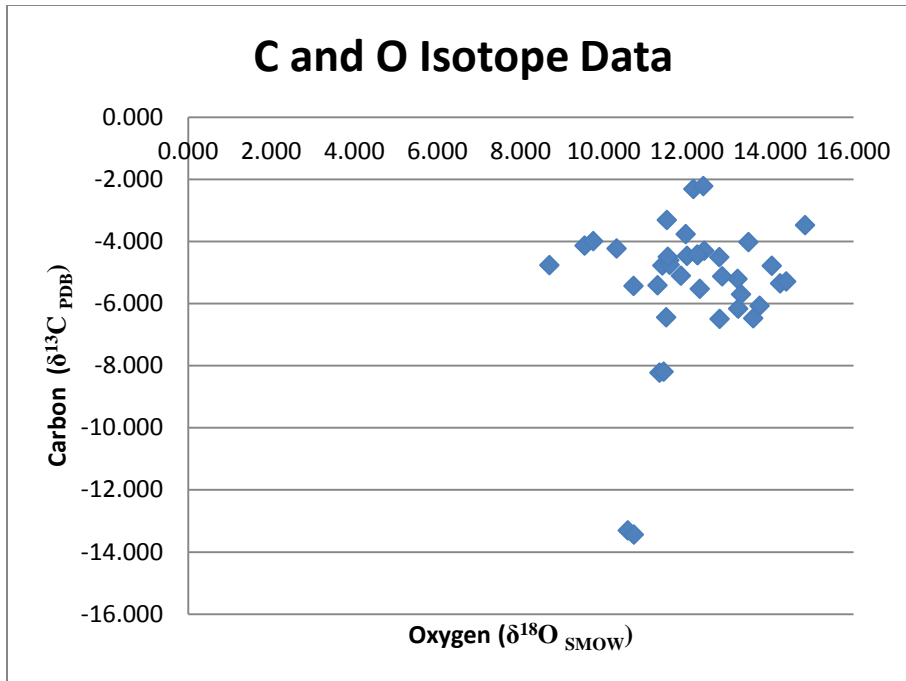
Figure 5.1 Carbonate stable isotope data at Rattlesnake Hills.

C and O Isotope Data

y = 0.2896x - 8.8945
R² = 0.0307

Carbon ($\delta^{13}C_{PDB}$)

Oxygen ($\delta^{18}O_{SMOW}$)
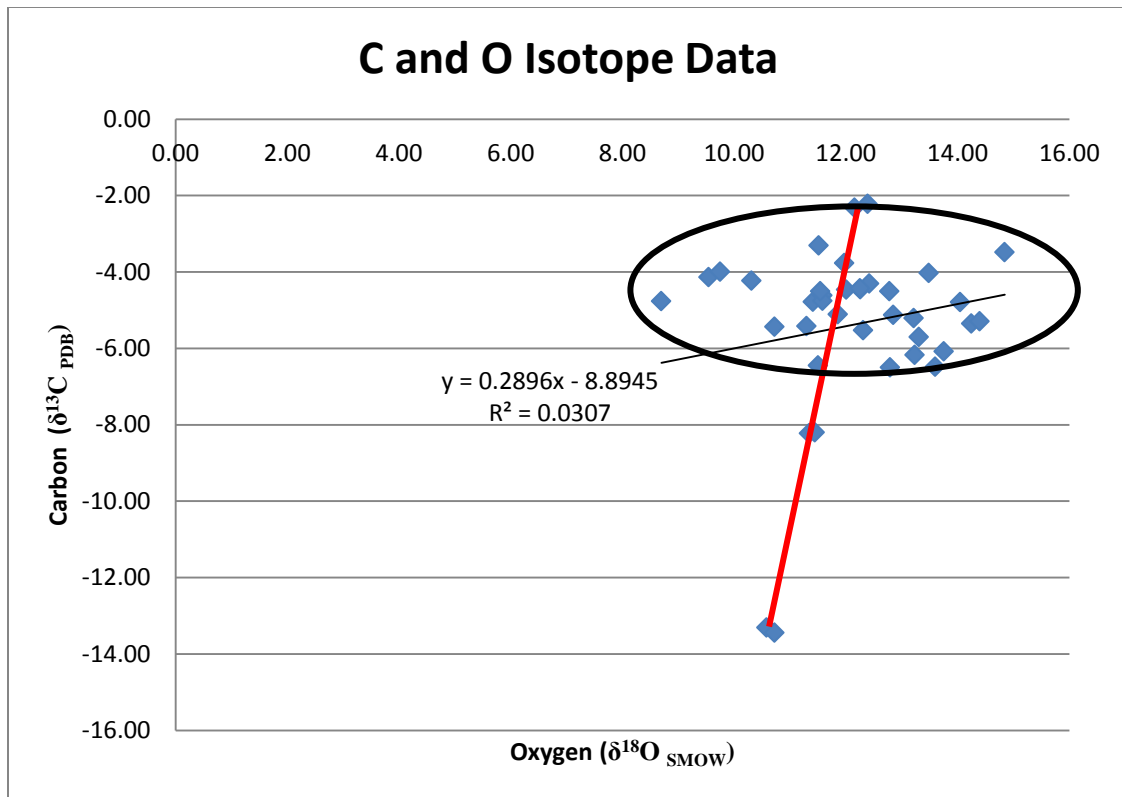
Figure 5.2 Diagram showing the two trends: covariation (black circle), the slope of isotopic trend with the statistics, and the scatter to strongly negative $\delta^{13}C$ values (red line).
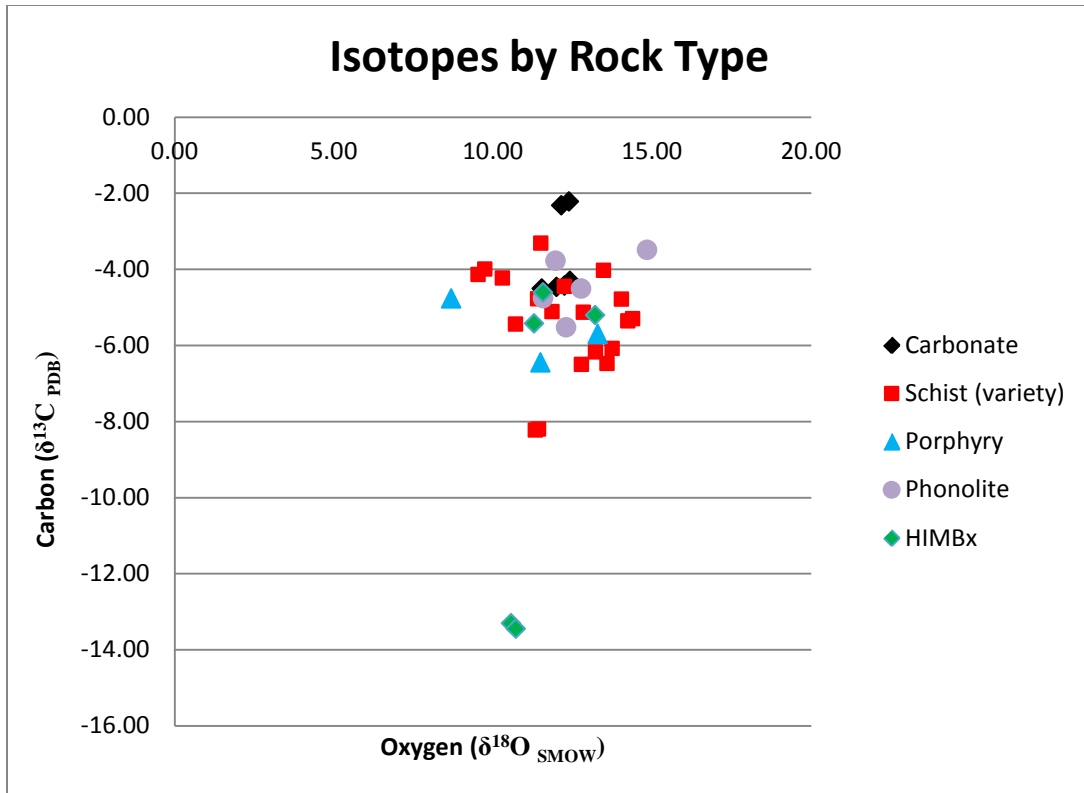
Figure 5.3 Stable isotope data separated by rock type. Carbonate is carbonate veins of calcite and dolomite >3 inches. Schist (variety) includes schist, monolithic schist breccias, and schist with unidentified igneous intrusions. HIMBx are heterolithic igneous and metamorphic (schist clast) breccias.
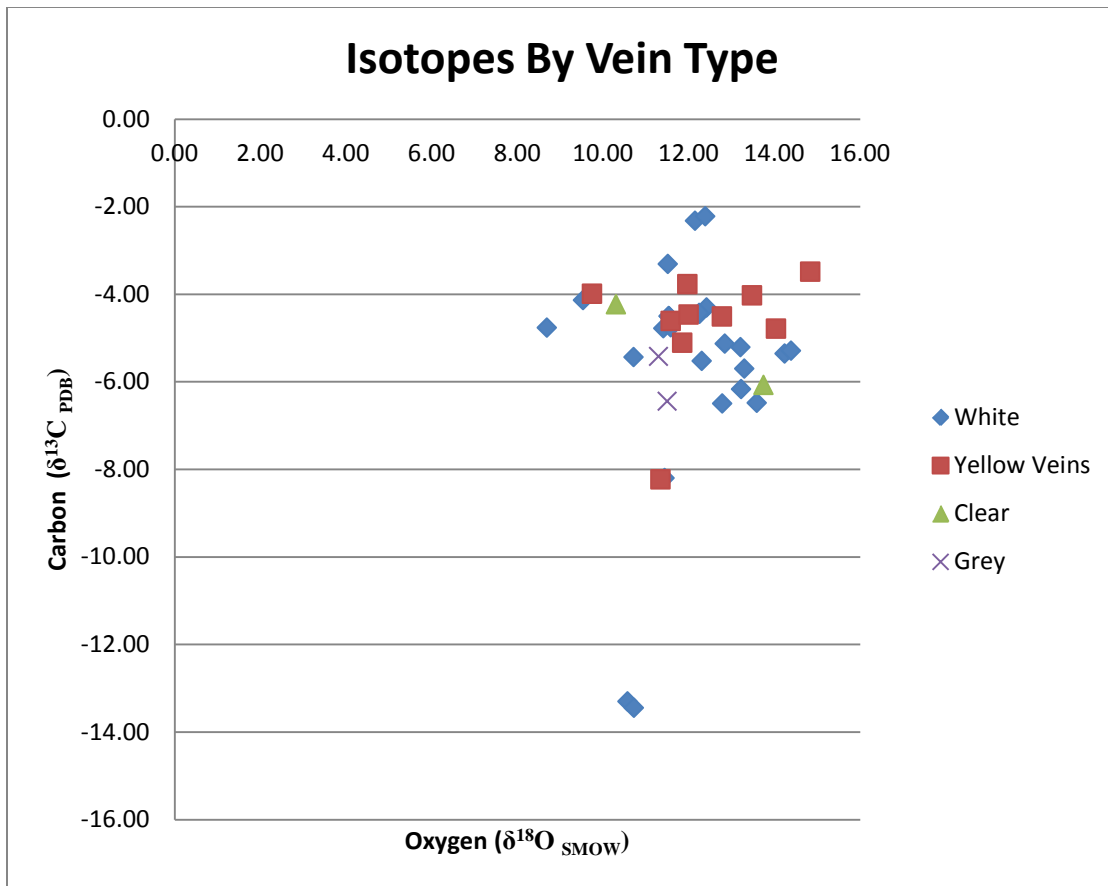
Figure 5.4 Stable isotope data separated based on the color of the vein analyzed.
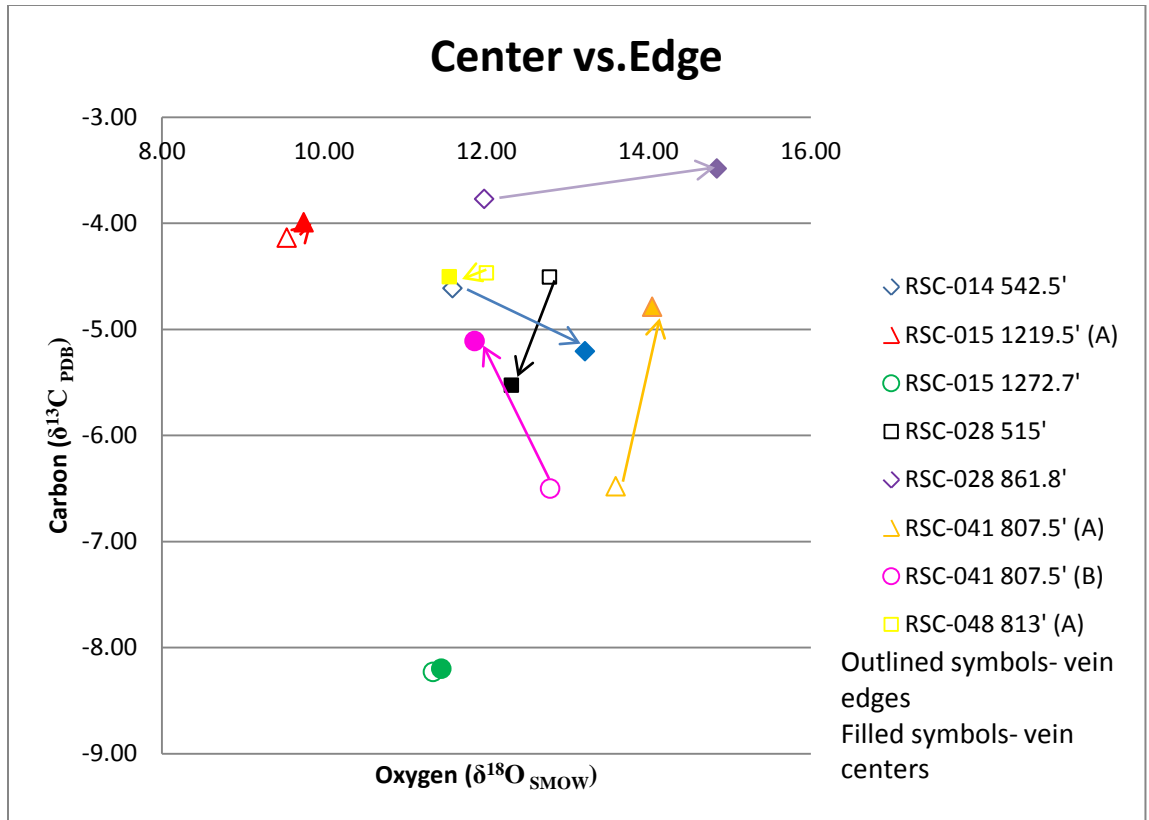
Figure 5.5 Stable isotopes data showing the variation from centers (filled in symbols) to edges of veins (open symbols). Since there is no systematic trend with regard to the direction of core vs. edge implies multiple processes.

Figure 5.6 Stable isotope data is separated by depth: shallow (0-750'), intermediate (750-1500'), deep (1500-2600').
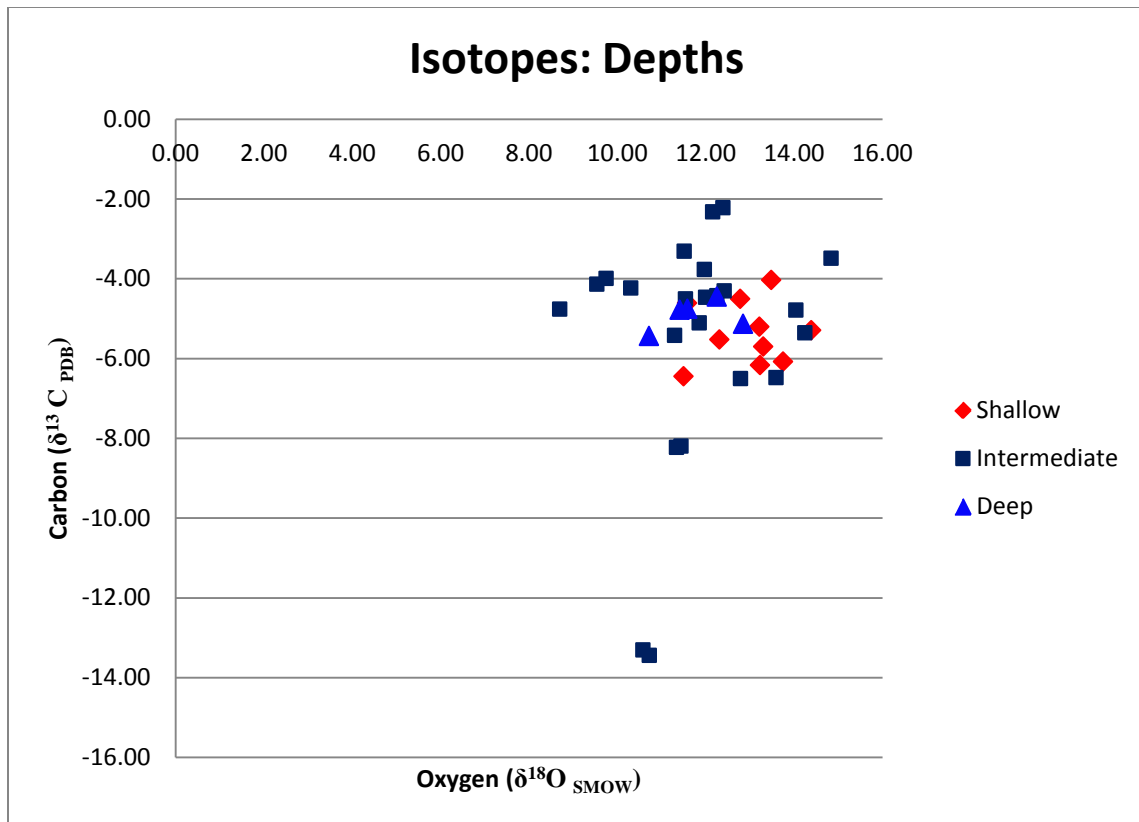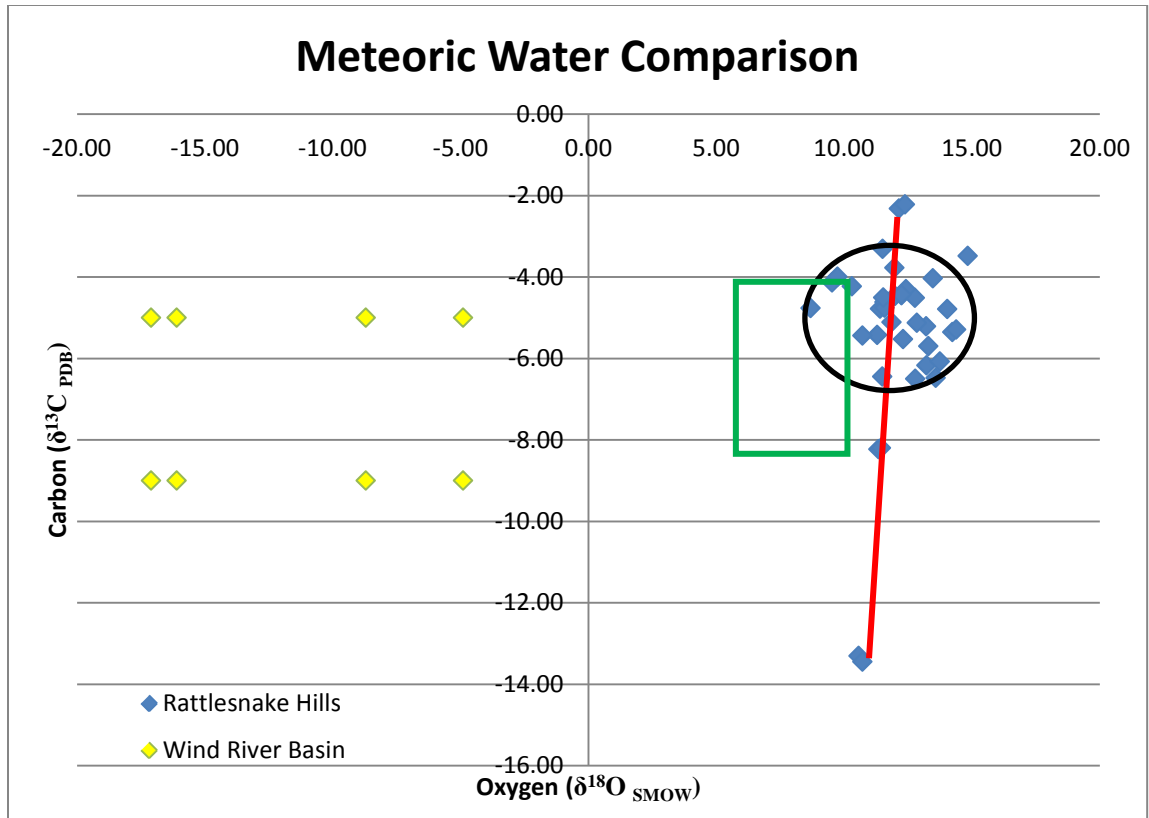
Figure 5.7 Comparison of Rattlesnake Hills stable isotope compositions to meteoric water values of stable isotopes from the Wind River Basin (adapted from Fan et al., 2011). The two trends of Rattlesnake Hills are emphasized: red line is strongly negative $\delta^{13}C$ and black circle represents the covariation. The green box outlines the primary carbonatite field (Demeny et al., 2004). Note the lack of the scatter towards a meteoric composition.

6. ORE PETROGRAPHY MINERALOGY AND MINERAL CHEMISTRY

6.1 ORE PETROGRAPHY

The ore petrography of 44 thin sections show simple ore mineralogy, the ore minerals listed in relative abundance from most abundant to least are: pyrite, marcasite, leucoxene, electrum, chalcopyrite, and sphalerite. However, there are other ore minerals that are recognized in scanning electron microscope (SEM) and QEMSCAN® that were not identified using microscope (i.e. cobaltite, cassiterite, unidentified Ag+Bi and Ag+Pb minerals, arsenopyrite, arsenian pyrite, naumanite, and bismuthinite, electrum, silver, galena, bismuthinite, cobaltite, gersdorffite, and molybdenite). Ore minerals are found in schist, breccias, phonolite, porphyries, and pyroclastic rocks. However, not all rock units have significant mineralization, in particular phonolites. The non-ore petrography of the various rock types is discussed in detail in Chapter 3 and a full description of the ore petrography of each thin section is in Appendix 2. This chapter describes the abundances and relationship of each of the ore minerals.

6.1.1 Ore Minerals and Their Petrography

Pyrite is the most abundant ore mineral and occurs in most of the thin sections. Pyrite grains are sub- to euhedral with cubic or octrahedral forms (Figure 6.1). Some pyrite grains appear zoned, pitted or weakly transparent. SEM analysis shows pyrite grains are compositionally zoned with bands ~3-7μm wide (Figure 6.2). Pitting, weak

anisotropy in reflected light, and weak transparency in transmitted light are other occasional characteristics of pyrite. However, these grains can occasionally be identified based on unusual coloration (appear whiter than typical pyrite grains) in reflected light.

Pyrite grains are hosted in calcite+dolomite carbonate veins and within country rock. Individual grains vary in size from <10μm to >50μm. Occasionally, pyrite is associated with leucoxene. Leucoxene occurs as cores to pyrite grains or is intergrown with pyrite creating a myrmekitic-like texture (Figure 6.1G).

Marcasite is the second most abundant ore mineral and occurs in more than half of the samples. Marcasite grains have several forms: bladed/wispy, blocky, and snowflake (Figure 6.3). The marcasite grains range significantly in size from <10μm to >50μm. Blocky and snowflake marcasite grains have significant patchy zonation while bladed/wispy marcasite has a much more subdued zonation. Patchy zonation of individual marcasite grains and intergrown grains is seen in polarized reflected light (Figure 6.3 I). Some of the individual blades of marcasite are twinned, but this is uncommon. Marcasite grains occur in a variety of rock types, but are most abundant in calcite+dolomite carbonate veins. Some marcasite grains show strong anisotropic colors of blue, greens, and greys.

Marcasite occurs only under limited conditions and is indicative of an environment. Murowchick and Barnes (1986) suggested that marcasite formed in "either mildly oxidizing or (conditions that) went through a change from reduced, sulfidic conditions to more oxidized conditions." Marcasite forms under 240°C and pH < 5.0 (Murowchick and Barnes, 1986). However, to transform marcasite into pyrite, the

temperature needs to exceed 673 K (400°C) but this is not a complete transformation and the half-life of replacement (Lennie and Vaughan, 1992). If the temperature is 473K, the half-life of the pyrite to marcasite transformation is 3×10^6 yr while even lower temperatures increase the half-life transformation (i.e. 433 K the transformation is 1.3×10^9 yr) (Lennie and Vaughan, 1992).

Pyrite forms pseudomorphs after marcasite and less commonly marcasite overgrows pyrite. These pseudomorphs occur in most samples and are distinguishable based on anisotropy and shape. Pyrite belongs to an isotropic system, whereas, marcasite is anisotropic. Therefore, grains that appear isotropic but are marcasite shapes (bladed/wispy, blocky, or snowflake) are most likely pseudomorphic pyrite after marcasite. Likewise, if pyrite appears weakly anistropic it is likely overgrowths of marcasite after pyrite.

It is difficult with reflected light to determine if an irregular grain is a pseudomorphic pyrite grain after marcasite or primary marcasite. There are some grains in which marcasite appears partially replaced, while others appear completely replaced. Due to the lack of cross-cutting relationships or overgrowth patterns between marcasite, pyrite, and pseudomorphs it is impossible to determine a paragenetic sequence of these ore minerals. However, it is most likely that pyrite and marcasite are the first phase. There is a second phase of pseudomorphic pyrite after marcasite and marcasite overgrowths after pyrite. A much later oxidation phase of goethite replacing sulfides occurs.

Leucoxene is a replacement mineral of titanium-bearing minerals which were most likely magnetite, biotite, hornblende, and titanite or sphene, and is considered here as an ore mineral because it is closely associated with ore minerals at Rattlesnake Hills; therefore, it is discussed in more detail. Leucoxene occurs in ore and mineralized samples, in wallrocks and veins. It occurs as cores within pyrite grains or rims outlining pseudomorphed mafic mineral sites (Figure 6.5).

While visible electrum only occurs in four samples (RSC-003 743', RSC-006 581.5' A and B, and RSC-020 702'), there are many grains of electrum within each of these samples. SEM and ore petrography show visible electrum is not hosted in pyrite but all visible electrum is associated/hosted in marcasite grains. Electrum grains range in size from <5μm to >30μm (Figure 6.6). There are slight color variations of the electrum grains indicating that there might be compositional variations (Figure 6.7). The timing of electrum is associated with the marcasite of the first phase; it is unsure if the mineralization occurred concurrently or later than the marcasite that hosts it. It is difficult to determine if the electrum precipitated at the same time as the marcasite or late on the surface of marcasite grains. However, it is clear that the pseudomorphs of pyrite after marcasite and rarer marcasite overgrowths after pyrite are not associated with any visible electrum.

Chalcopyrite and sphalerite were observed infrequently in the polished thin sections. Chalcopyrite grains are small (<10μm), typically associated with carbonate, most notable by the brassy color, and only occurs in 15 samples (Figure 6.8). Sphalerite

has been observed more frequently in hand sample, but only occurs in one thin section sample (RSC-003 1374') (Figure 6.9).

6.2 SCANNING ELECTRON MICROSCOPE MINERAL ANALYSIS

Seven samples were analyzed and imaged with SEM-EDAX (scanning electron microscopy with energy dispersive spectrometry) at the USGS microbeam lab in Denver. The seven samples selected for analysis cover the variety of depth, rock type, and known gold grade. All grains were analyzed using point or spot analysis using EDAX, X-ray microanalysis, and imagery using backscatter electron detection. Individual spot analysis determines elemental composition, approximate weight percent of elements, and the atomic percent of each element. As the analyses are approximate, for the purpose of this study arsenian pyrite refers to pyrite with low As content (less than 5 weight percent), while arsenopyrite is iron-sulfide with elevated As content measured at greater than 20 weight percent.

Pyrite grains were observed in four of the seven samples analyzed. Nine euhedral pyrite grains that were both zoned and unzoned were analyzed. Analysis of 46 spots indicated that pyrite grains are zoned relative to As content. Zoning of pyrite grains varies from arsenian pyrite and arsenopyrite intergrowths depending on the amount of As. The rims or zones are approximately 2-5μm thick. However, not all pyrite grains are zoned. Pyrite grains from samples with <1ppm Au, are unremarkable grains with little or no As zoning. Additionally, pyrite grains that appear zoned in reflected light are not all detectably zoned compositionally. This lack of elemental zoning could be caused by overgrowth or defect in the lattice structure of pyrite grains, such as formed by

replacement of marcasite. Approximately half of all pyrite grains have zoning or pitting, the pitting could also be created by impurities or defects in the crystals.

The variation of minor elements within pyrite grains is significant, even from the same sample. From the SEM, most pyrite grains have a 2:1 sulfur to iron ratio, but can also have cobalt, magnesium, lead, copper, and zinc. The variation of trace elements detected using LA-ICP-MS (section 6.3) was greatest with vanadium, magnesium, cobalt, nickel, copper, zinc, gallium, molybdenum, antimony, tellurium, titanium, lead, and bismuth. Pyrite trace element compositions can be used to determine the type of ore forming process (Ho et al., 1995). Based on a pyrite trace element study from two deposits in New South Wales determined "Co, Cu, Ni, and Zn in pyrite are derived from wall-rock and reflect host rock contributions, whereas, Au, Ag, As, Bi, and Pb are most likely introduced by the ore fluids" (Ho et al., 1995). From the trace elements present at Rattlesnake Hills, there are significant influences by both the host-rock and ore fluids.

Marcasite grains were observed in five of the sections analyzed. Multiple forms of marcasite were analyzed: bladed/wispy, blocky, and snowflake. Approximately 20 individual grains were analyzed with 94 point analyses. Most marcasite grains show variable patchiness using back scatter electron imagery. Overall, the patches can be characterized as irregular and approximately 1-10μm in size. Dark patches in back-scatter images are end-member marcasitic compositions of FeS_2, intermediate patches are FeS_2 that are As rich (1-5 weight percent), and bright patches are more enriched in As (20-35 weight percent or arsenopyrite intergrowths). However, not all colors (dark, intermediate, and bright) of patches are present in all marcasite grains. In general, pyrite grains have

108

higher As content than marcasite grains. All forms of marcasite have similar compositions and patchiness, but blades are typically less patchy than blocks and snowflakes. Additionally, marcasite shows no consistent sense of growth zonation in respect to type of grain habits (wisps, blocky, or snowflake) or composition.

Due to the limitations of the SEM equipment, it is impossible to determine compositions of grains to differentiate pyrite from marcasite grains. Some pyrite grains analyzed might be pseudomorphic pyrite after marcasite; however, these samples were avoided since they can only be identified with a reflected light microscope based on shape and colors in cross-polars.

Samples with higher Au assay values generally have more As-rich phases such as arsenopyrite. Two high grade samples, RSC-003 743'B (18.1ppm) and RSC-006 581.5' A and B (12.0 ppm), have multiple grains/inclusions of electrum hosted in marcasite. RSC-003 743' A and B has 9 marcasite grains with multiple, smaller (2-10µm) grains of electrum. RSC-003 743' B has several larger (2-100µm) grains of electrum and naumanite. The samples with intermediate gold values (1.34, 1.380, and 1.80ppm) have arsenian pyrite and arsenopyrite intergrowths but no electrum grains while the sample with 0.011ppm has no eletrum grains and zones with some As in pyrite.

The arsenian pyrite and arsenopyrite (and/or marcasite) intergrowths can be used as a geothermometer in a qualitative sense. A total of 69 spots analyzed in pyrite and marcasite are used to determine if the system is high temperature or low temperature. There were twice as many spots that indicated a low temperature system; most of these spots were hosted in pyrite grains and were most likely arsenian pyrite. For 23 spots, a

high temperature system was implied; most of these spots were hosted in marcasite and occasionally spatially associated with gold and silver grains (Barnes, 1997).

Electrum grains were observed and analyzed in three samples. Analysis of 25 spots of electrum showed that all grains have similar compositions, Au:Ag ratios, and no zonation within grains. From 22 point analysis, 20 electrum grains have a 2:1 Au:Ag ratio corresponding to a fineness of ~700. Electrum grains range in size from ~1 to 100μm and are irregularly shaped. Most electrum is hosted in marcasite grains. There is only one instance where the electrum occurs as a free grain.

Small grains of a silver selenides, Naumanite, were observed in one sample (RSC-003 743' B) hosted in a marcasite grain. Naumanite grains are 1-5μm, irregularly shaped, and have 50-65 weight percent Ag (Figure 6.10). It is impossible to determine how naumanite is related to the paragenesis of Rattlesnake Hills.

6.3 LASER ABLATION INDUCTIVELY COUPLE PLASMA MASS SPECTROMETRY (LA-ICP-MS)

The seven samples analyzed using the SEM, were also analyzed using LA-ICP-MS. Pyrite and marcasite grains were analyzed to determine where the gold and silver is located within grains and to determine the trace element chemistry. From SEM analysis, microscopic gold and silver grains 1-100μm in size are dominantly on marcasite grain surfaces while there is no gold associated with pyrite. However, mineralization is not uniform. Samples with known gold mineralization from Evolving Gold Corp assay results do not all have visible grains of gold or silver. For these samples, it is possible that

gold and silver are hosted as nanonuggets within pyrite and marcasite or within the crystal lattice.

Most pyrite grains are zoned with respect to As content. Most pyrite rims are enriched in As while the cores are depleted. Nine core and rim pairs were analyzed and, show cores have low to moderate As (390-9914ppm) while the rims are elevated in As (21,083-70,143ppm) (Figure 6.11). Not all pyrite grains have different core and rim compositions but in general, there is a strong correlation between enriched rims and depleted cores with increased gold and arsenic values. Additionally, some pyrite grains have cobalt enriched cores (5-650ppm). Gold in the pyrites range from below detection limits (<2ppm) to 890ppm. The higher As concentrations in pyrite are correlated to higher gold concetrations (Figure 6.12). However, high gold assays show a weak trend to increased pyrite gold and arsenic values (Figure 6.13). The gold occurs with variable Au:Ag ratios in both pyrite and marcasite, ranging from 95:1 to 1:1; however, some samples have higher silver concentrations than gold concentrations. The gold and silver might be lattice bound or nanonuggets. Lattice bound mineralization is shown by constant count rate during ablation while nanonuggets are sharp spikes. Most of the gold count rates were constant during ablation, but there were rare sharp spikes of nanonuggets. Silver occurs as sporadic nanonuggets and has no correlation to increased gold values.

Marcasite grains have two distinct compositional groups: 1) high As to gold ratios and 2) low As to gold ratios (Figure 6.14). Some marcasite grains exhibit rims of higher As; however, not all grains have As-rich rims. Additionally, some marcasite grains have

111

intergrowths of arsenopyrite which might be responsible for the compositional patchiness

of marcasite. Some marcasite grains have zones enriched in molybdenum (6-8,500 ppm),

which may be occurring as nanonuggets, lattice bound, or a combination of both. There is

variable gold (1-17,961ppm) and silver (9-22,656ppm) content in the marcasite grains.

The large variations in the abundance of gold and silver could reflect nanonuggets of both

gold and silver.

The mineralization at Rattlesnake Hills is dominantly hosted in the sulfide grains.

The amounts of sulfides hosting gold mineralization (pyrite and marcasite) were

determined from petrographic work as the modal percentage for each type of sulfide

(Table 6.2). The average and highest recorded Au values from LA-ICP-MS for each

sample was used to calculate the tenor. Tenor is the amount of gold present in the

sulfides. The tenor is multipled by the modal abundance of the sulfides to determine the

calculated Au values. Most of the samples show comparable results with the assay values

determined by Evolving Gold Inc. The implication is that gold mineralization is hosted

within sulfide grains and can be used a vector for future gold exploration.

6.3.1 Interpretation of Trace-Element Compositions of Ore Minerals

- Silver concentrations cannot be used to distinguish marcasite generations

  due to their variability but can be used to separate pyrite and marcasite

  grains (Figure 6.14). In general, marcasite has a lower Ag:Au ratio than

  pyrite does.

- Pyrite and marcasite in samples without known gold mineralization from

  assay results, do not have elevated As and Au values (Figures 6.12 and

  6.13).

- There are two trends of gold and arsenic in pyrite and marcasite grains: 1) higher gold values with high arsenic and 2) low gold and intermediate arsenic values (Figure 6. 11, 6.12, and 6.14). Both trends occur in the same samples and no further interpretations can be made.

- The grade is strongly correlated to sulfides. For most samples, the gold assay values correlate to the amount of calculated gold in marcasite and pyrite grains. Where a trend cannot be observed, are most likely nuggets of free gold in carbonate veins and wallrock. Evolving Gold Corp standard operating procedure for assaying samples, is a 5' composite of core or smaller composites if mineralization or rock type change are present (Table 6.2).

- Rims of pyrites are enriched in As and cores are depleted in As. There is a general correlation between As and Au.
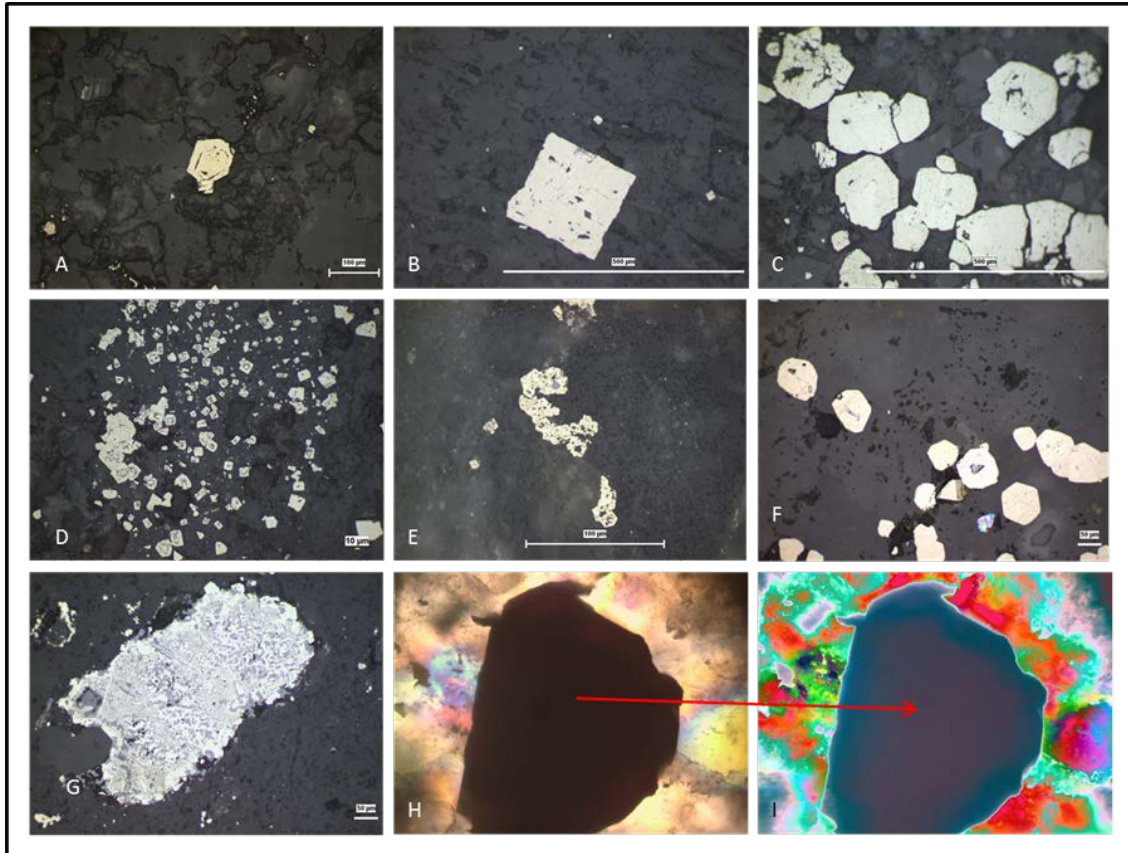
Figure 6.1 Photomicrographs of pyrite grains. All photomicrographs are in reflected light unless otherwise stated. A) Euhedral pyrite grain from RSC-015 1272.7' with pitting mimicking the euhedral shape in a carbonate vein, B) cubic, euhedral pyrite grain with black pits from sample RSC-020 1202.5' hosted in carbonate vein, C) sub to euhedral grains of pyrite from RSC-014 542.5' hosted in carbonate vein, D) zoned appearance created by pitting within euhedral pyrite grains hosted in a carbonate vein from RSC-003 1266.9', E) a cluster of fine grains of pyrite hosted in a carbonate vein that nucleated on magnetite (or other mafic mineral site) RSC-003 1374', F) pyrite grains in the wallrock of a monolithic schist breccias that nucleated on a mafic mineral RSC-028 2587.5', G) pyrite and leucoxene intergrown creating a myrmekitic texture hosted in a carbonate vein from RSC-027 1754', H & I) RSC-006 1760' samples hosted in carbonate vein H) pyrite grain in plane polarized light, the edges appear weakly transparent, and I) false-colored image of H to enhance the reflection color contrast.
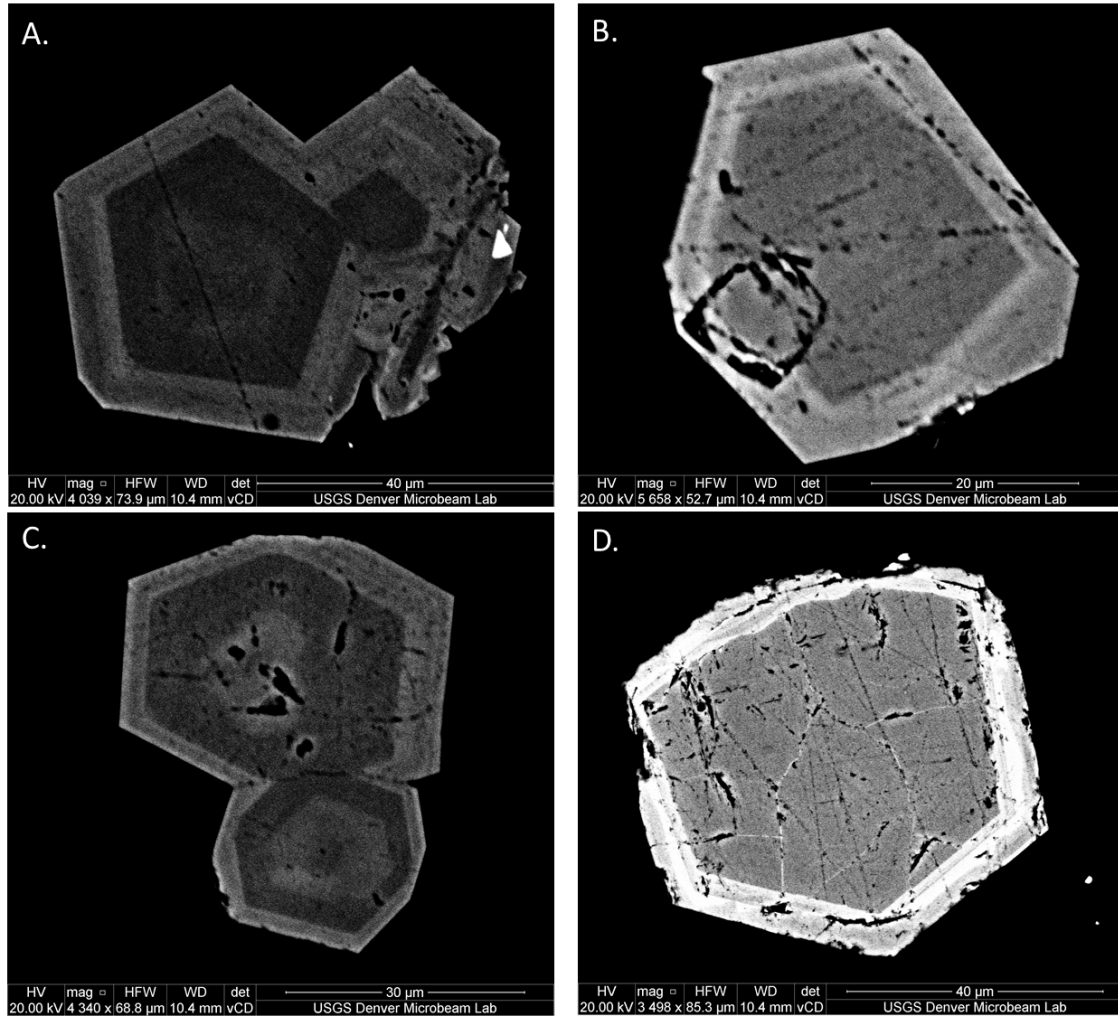
Figure 6.2 Backscatter electron SEM images of euhedral pyrite grains with concentric zones of varying compositions. Brighter color zones are more arsenic rich than the darker color zones. Images A, B, and C are from RSC-003 1266.9' and D is RSC-006 1769'A.
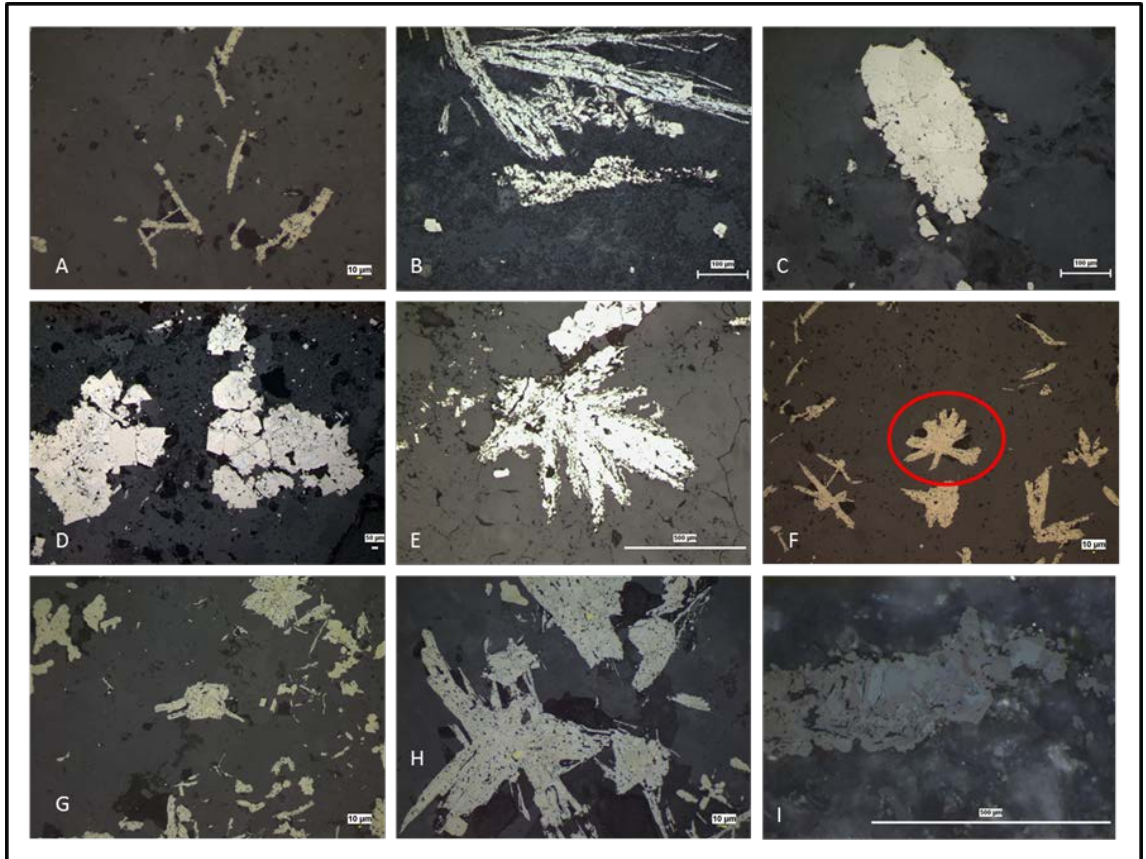
Figure 6.3 Photomicrographs of marcasite grains. All photomicrographs are in reflected light unless otherwise stated. Large marcasite grains are comprised of smaller grains that have different extinction angles creating a "patchy" appearance, some of this appearance can be attributed to marcasite twins. A) Bladed/wispy marcasite grains from sample RSC-003 743' A, B) bladed marcasite grains from RSC-020 503' A, C) Blocky marcasite with patchy zonation from RSC-020 702', D) Blocky marcasite from RSC-028 1331.5', E) snowflake marcasite from sample RSC-054 859', F) snowflake marcasite (red) with multiple blades/wisps of marcasite from RSC-003 743' A, G and H) marcasite with multiple intergrown/included electrum grains from RSC-006 581.5' A, and I) blocky marcasite under crossed-polar of reflected light, note the strong anisotropic colors of blues, greens, and greys from sample RSC-004 1112.3'.

116
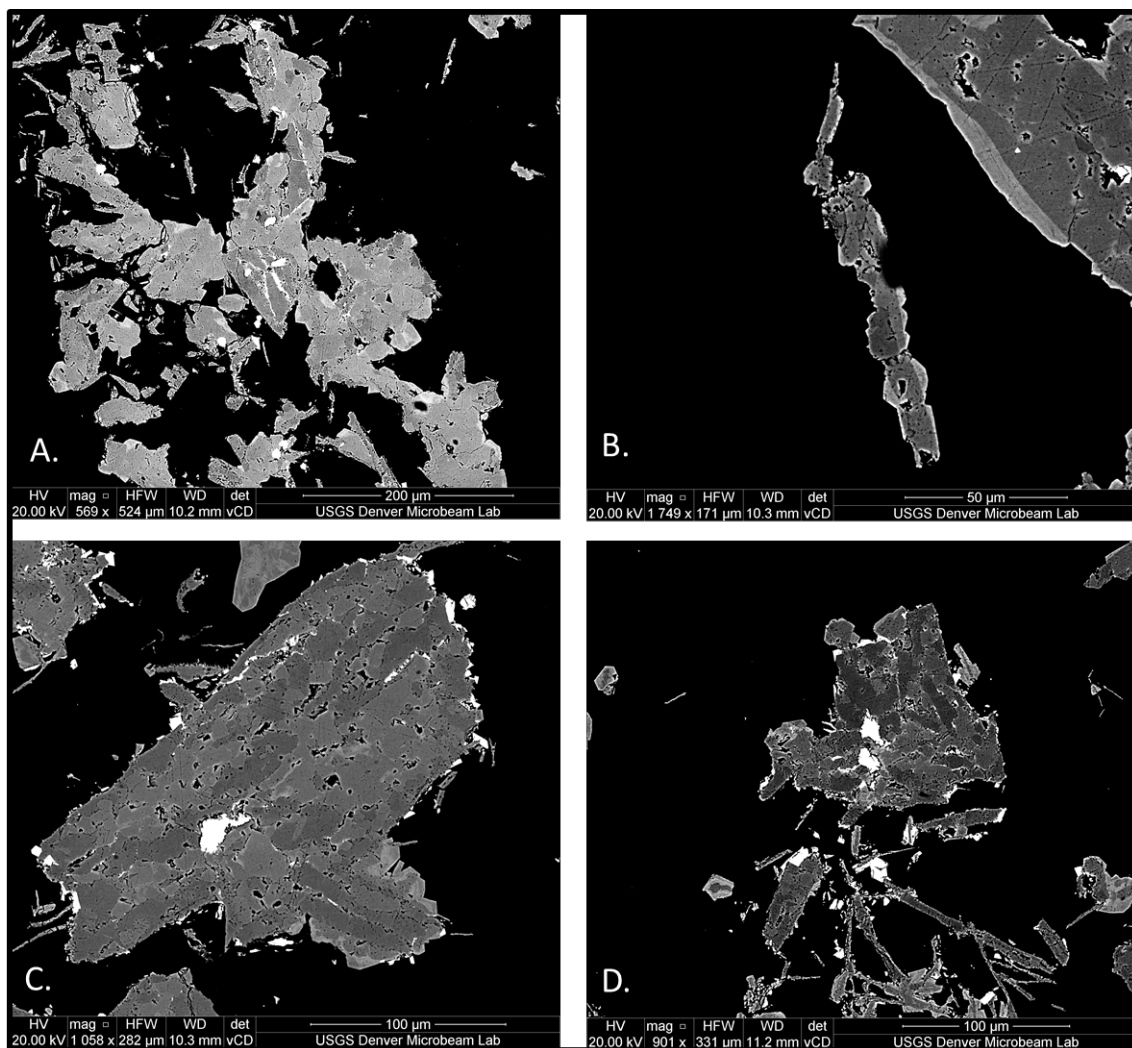
Figure 6.4 Backscatter images of marcasite grains with zones of varying compositions. Brighter color zones are more arsenic rich than the darker color zones in images A and B (RSC-006 581.5' A). Images C and D have very bright spots in the core of the marcasite grains, gold and silver (electrum), and a variety of gray patches with compositions that have different contents of arsenic.
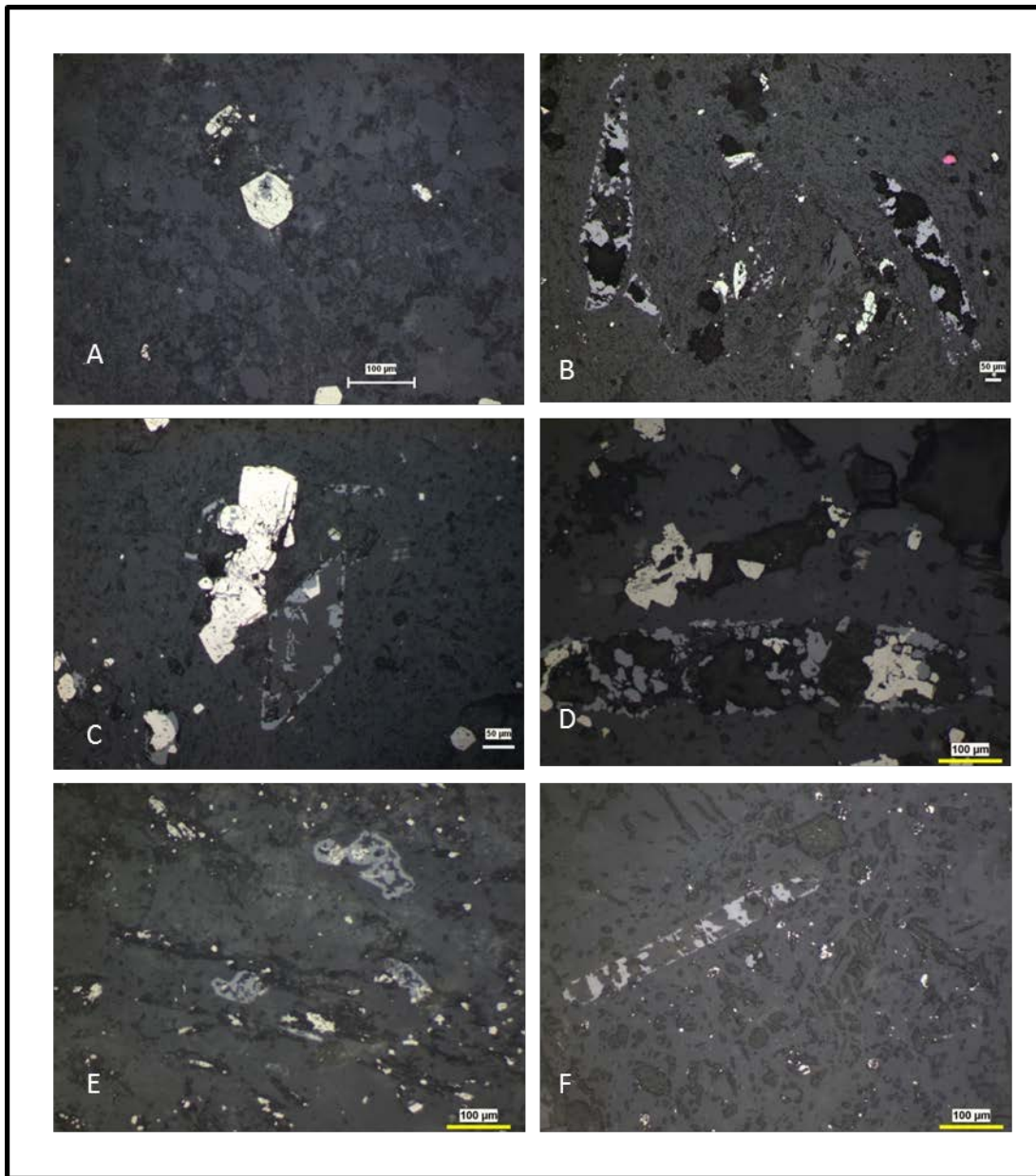
Figure 6.5 Photomicrographs of leucoxene. All photomicrographs are in reflected light unless otherwise stated. A) Pyrite nucleated on a mafic mineral that is being replaced by leucoxene RSC-020 503' C hosted in a schist; B) leucoxene replacing mafic mineral sites from RSC-028 1331.5' hosted in a schist with small pyrite grains; C) leucoxene replacing mafic mineral sites and pyrite nucleated on mafic mineral from RSC-033 582' hosted in medium grained porphyry; D) leucoxene replacing mafic mineral sites from RSC-080 890.7' hosted in porphyritic sample with amygdules; E) leucoxene replacing mafic mineral sites from RSC-006 1760' hosted in schist with abundant small pyrite grains; F) leucoxene replacing mafic mineral sites from RSC-101 1348.8' hosted in heterolithic igneous and metamorphic breccia with occasional pyrite grains.
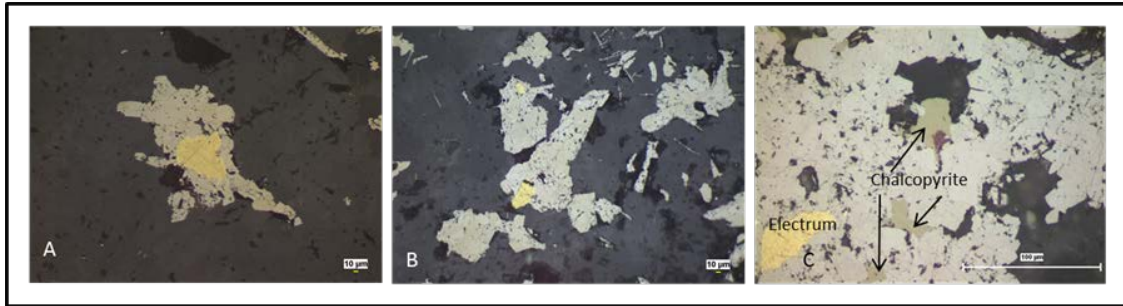
Figure 6.6 Photomicrographs of marcasite with intergrown visible electrum grains. All photomicrographs are in reflected light. A) from RSC-003 743'; B and C) from RSC-020 702'. C) Large marcasite grain with electrum, chalcopyrite, and unidentified purple mineral in plane polarized reflected light.
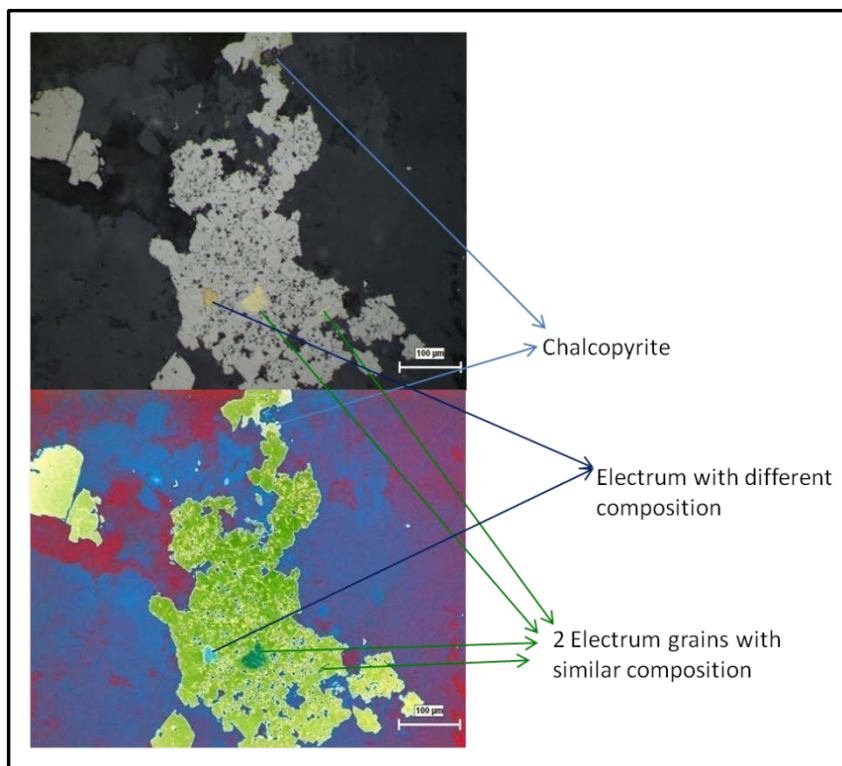
Figure 6.7 Photomicrographs of blocky marcasite with multiple grains of electrum showing different reflection of colors. The top photomicrograph is in plane reflected light, and the bottom photomicrograph is the same grains in false-color image. SEM showed there are no composition variations of electrum grains, regardless of color differences.
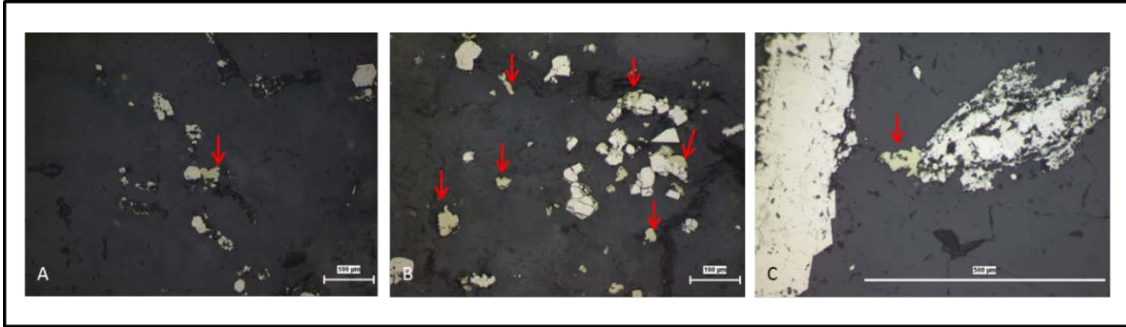
Figure 6.8 Photomicrographs of chalcopyrite grains. All photomicrographs are in reflected light. The red arrows point to chalcopyrite grains in each photomicrograph. A) Chalcopyrite grains around and immediately adjacent/growing on subhedral pyrite grains from RSC-015 1219.5' A, B) Chalcopyrite grains with subhedral pyrite grains from RSC-020 702', C) Chalcopyrite grains with blocky marcasite grains from RSC-054 859'.
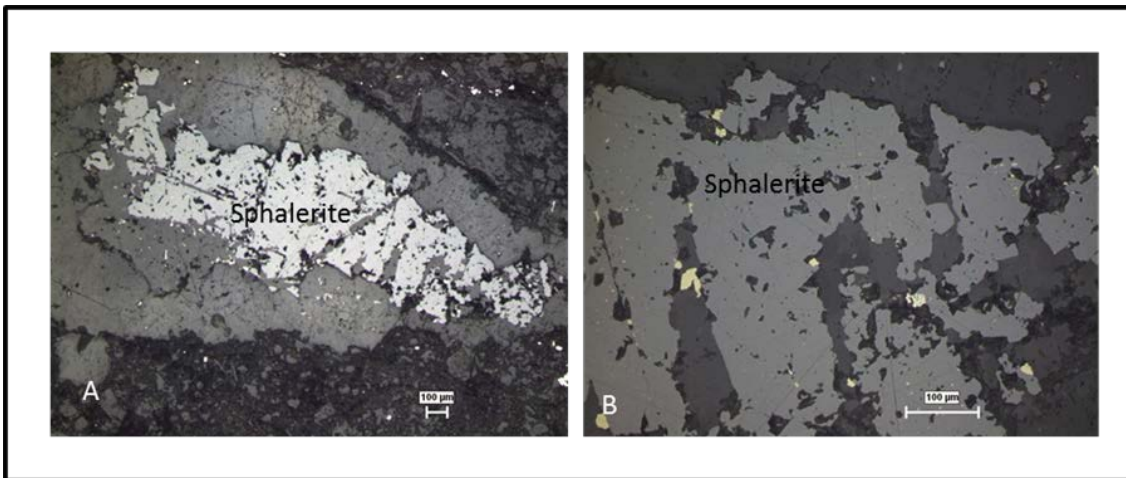
Figure 6.9 Photomicrographs of sphalerite from RSC-003 1374'. Both photomicrographs are taken in reflected light. A) Large sphalerite grain hosted in a carbonate vein, B) same sphalerite grain at higher magnification with brassy chalcopyrite.
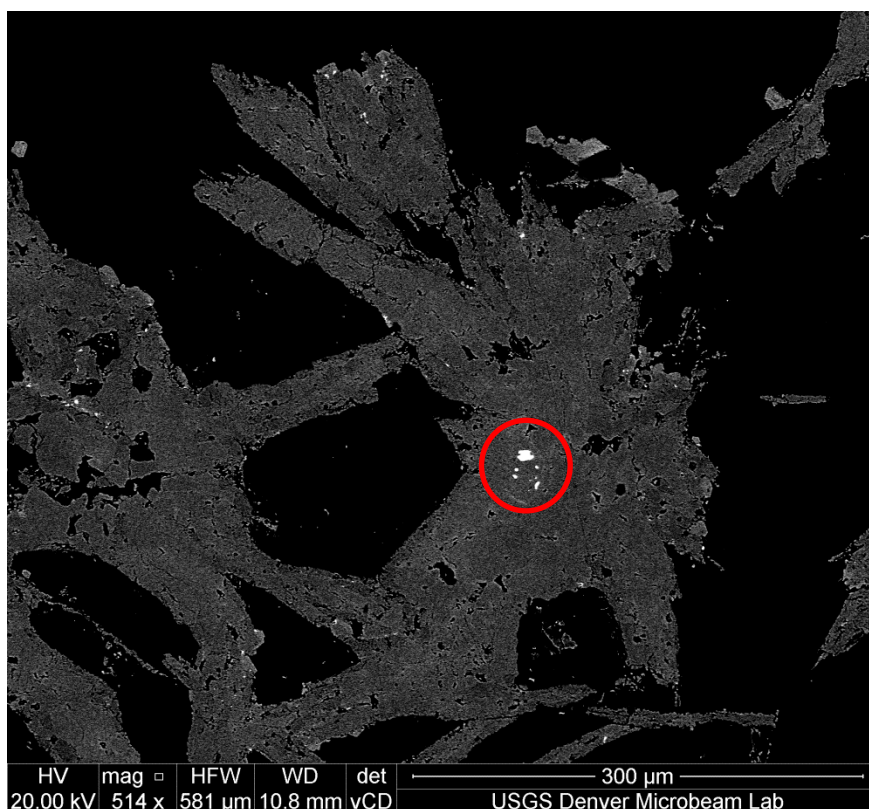
Figure 6.10 Backscatter image of sample RSC-003 743' B. The image shows a marcasite

grain with patchy weak compositional differences and a cluster of bright spots in the

core. The bright spots circled are naumanite.
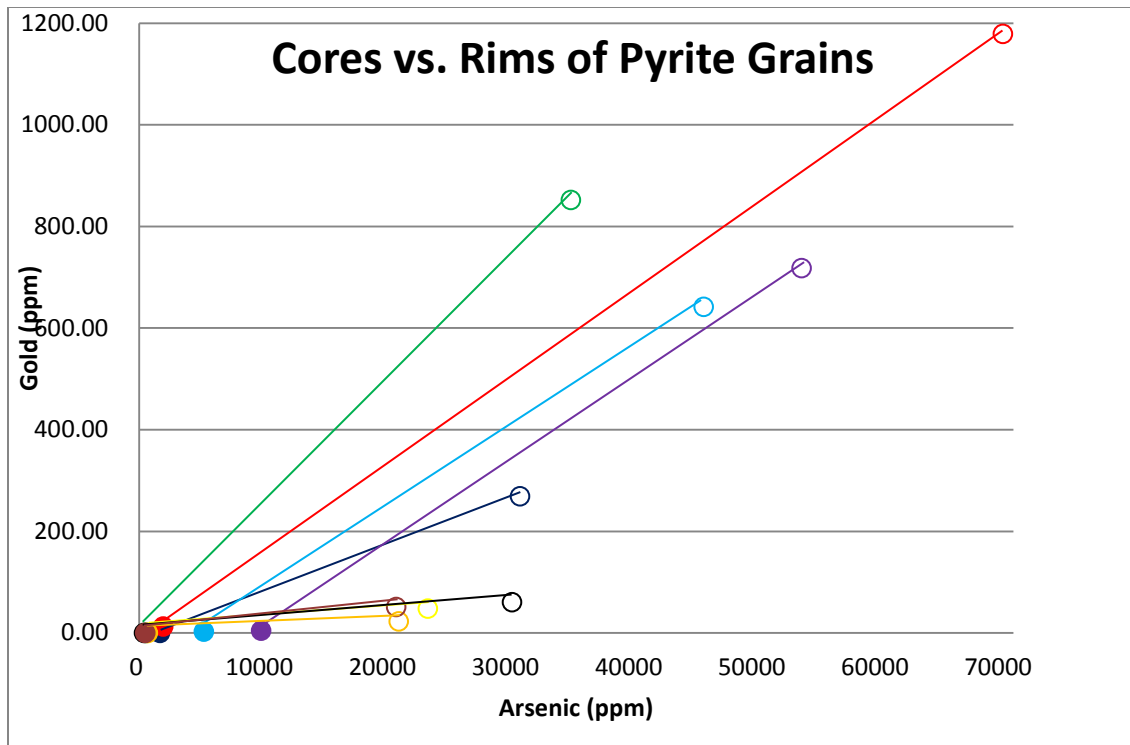
Figure 6.11 Scatterplot of core and rim measurements of 9 pyrite grains analyzed with

LA-ICP-MS. The cores are the filled in circles while the rims are the open circles.

Overall, there is enrichment of gold and arsenic in all cores to rims. There are two trends:

1) high gold and arsenic values, and 2) lower gold values with intermediate arsenic
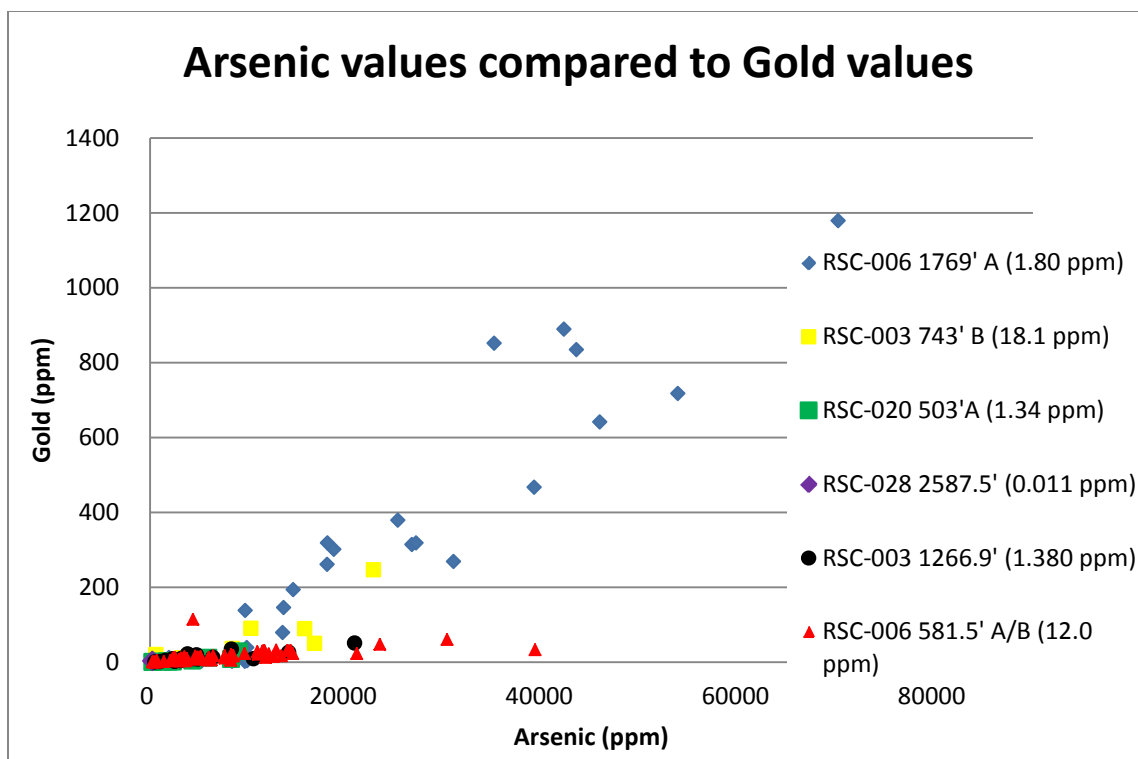
values.

Figure 6.12 Scatterplot of arsenic and gold values of pyrite and marcasite grains from

LA-ICP-MS. There is a trend between increasing gold and arsenic values.

Figure 6.13 Distribution of gold values of laser ablation samples compared to assay values of a composite sample. For RSC-006 581.5' A/B there was one measurement that is indicative of an electrum nugget that is not plotted on the figure (17,961 ppm). There is no trend interpreted.
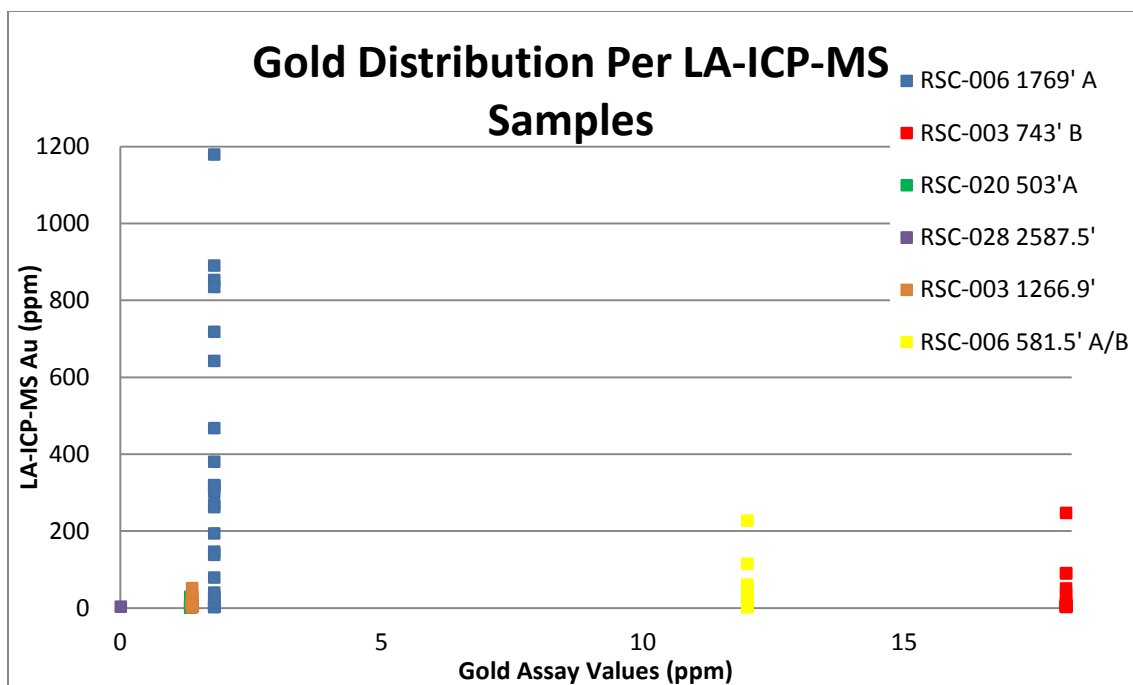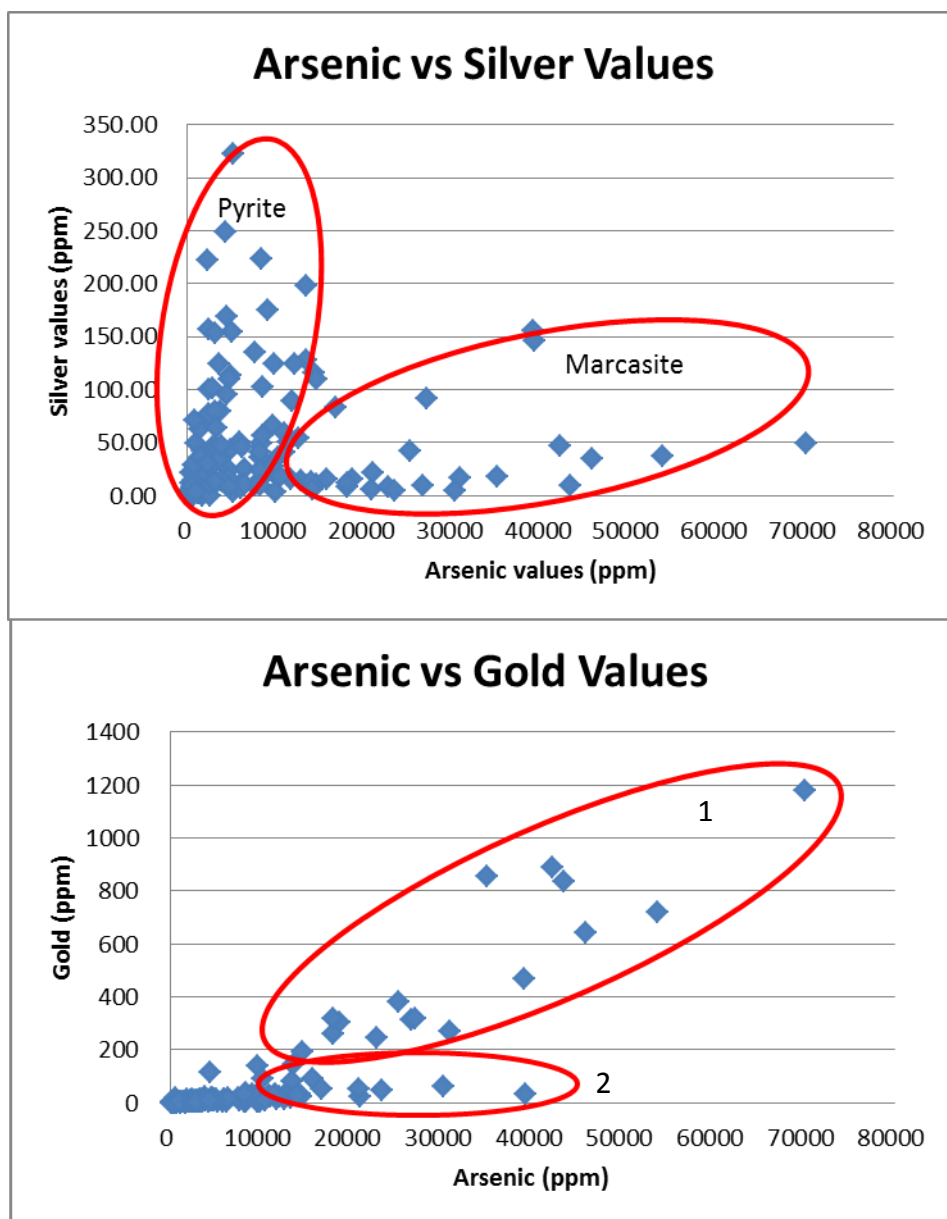
Figure 6.14 Scatterplots of arsenic vs silver and gold concentrations in pyrite and marcasite from LA-ICP-MS. For the scatterplot of arsenic vs silver, the data easily distinguishes pyrite grains from marcasite grains; however, the arsenic vs gold scatterplot shows little separation. The arsenic vs gold values show the 2 populations of marcasite: high As to Au ratios and low As to Au ratios.

Modal Abundance of Oxide and Sulfide

Minerals

Mineral	Percentage
Pyrite	50
Marcasite	30
Leucoxene	15
Chalcopyrite	3
Gold/Electrum	2
Goethite	>1
Sphalerite	>1

Table 6.1 List of total percentage of oxide and sulfide minerals at Rattlesnake Hills. This table represents a general estimate and composite of all the thin sections.

Pyrite Concentrations

Sample	Depth	Modal %	**Average ppm Au**	Tenor	Calculated Au	Assay Results
RSC-003	1266.9'	20%	13.64	2.728	0.5456	1.38
RSC-006	581.5' A/B	2%	47.46	0.9492	0.018984	12
RSC-006	1769' A	3%	324	9.72	0.2916	1.8
RSC-020	503 'A	2%	8.46	0.1692	0.003384	1.34
RSC-028	2587.5'	1%	2.87	0.0287	0.000287	0.011

Sample	Depth	Modal %	**Highest ppm Au**	Tenor	Calculated Au	Assay Results
RSC-003	1266.9'	20%	50.75	10.15	2.03	1.38
RSC-006	581.5' A/B	2%	47.46	0.9492	0.018984	12
RSC-006	1769' A	3%	1179	35.37	1.0611	1.8
RSC-020	503 'A	2%	28.63	0.5726	0.011452	1.34
RSC-028	2587.5'	1%	2.87	0.0287	0.000287	0.011

Marcasite Concentrations

Sample	Depth	Modal %	**Average ppm Au**	Tenor	Calculated Au	Assay Results
RSC-003	743' B	30%	34	10.2	3.06	18.1
RSC-003	1266.9'	3%	8.97	0.2691	0.008073	1.38
RSC-006	581.5' A/B	15%	340.12	51.018	7.6527	12
RSC-006	1769' A	2%	159.78	3.1956	0.063912	1.8
RSC-020	503 'A	2%	2.06	0.0412	0.000824	1.34

Sample	Depth	Modal %	**Highest ppm Au**	Tenor	Calculated Au	Assay Results
RSC-003	743' B	30%	247	74.1	22.23	18.1
RSC-003	1266.9'	3%	21.35	0.6405	0.019215	1.38
RSC-006	581.5' A/B	15%	17961	2694.15	404.1225	12
RSC-006	1769' A	2%	467	9.34	0.1868	1.8
RSC-020	503 'A	2%	3.8	0.076	0.00152	1.34

Combined Concentrations

Sample	Depth	**Average Calculated Au**	**Highest Calculated Au**	Assay Results
RSC-003	1266.9'	0.553673	2.049215	1.38
RSC-006	581.5' A/B	7.671684	404.141484	12
RSC-006	1769' A	0.355512	1.2479	1.8
RSC-020	503 'A	0.004208	0.002344	1.34

Table 6.2 Estimates of the gold content of each sample in pyrite and marcasite based on the average and highest Au ppm. Tenor is the gold concentrations within the sulfides. Most of the samples fall within the average and highest calculated gold values; however, there are two samples that do not have corresponding calculated values and assay results (RSC-020 503' A and RSC-028 2587.5'). It can be interpreted that most of the gold mineralization is as nanonuggets in or the crystal lattice of sulfides.

7. DISCUSSIONS AND SUMMARY

7.1 SUMMARY OF SETTING

Rattlesnake Hills is a smaller, gold-bearing alkaline igneous complex that is part of a larger volcanic field. The larger volcanic field, Rattlesnake Hills Alkaline Complex (RHAC) consists of over 50 individual igneous stocks or plugs with compositions ranging from rhyolite to phonolite to medium grained feldspar porphyry intruded into Archean basement. The igneous rock units of the smaller complex consists of barren phonolite, quartz monzodiorite with low grade halos of Au mineralization, and feldspar porphyry with narrow zones of high grade Au. However, mineralization is not limited to the intrusive bodies, but extends into the adjacent diatreme breccias. Most of the units in the alkaline igneous complex are silica undersaturated, but this is not true of all the units. Quartz occurs in the groundmass of some of the igneous bodies (quartz monzodiorite) and locally intergrown with carbonate in veins.

The alkaline igneous complex is shallowly intruded (0-3000'), is Eocene age, and the ores share similarities with epithermal and porphyry-style alkaline hosted precious metal deposits throughout the world.

The veins are mostly carbonate with some containing intergrowths of euhedral quartz. It is difficult to visually determine if veins are barren or mineralized, but the color of veins or breccia cement indicates the abundance of sulfides present. Barren

carbonate veins are white and can be translucent, while sulfide rich veins are light grey. Most of the mineralization is at vein contacts with adjacent wallrock. There are two generations of carbonate within veins: early Fe-rich phase and late Mg-rich phase; but there is no isotopic difference between the cores and edges of veins.

There is variable alteration throughout the alkaline complex. In general, there is potassic alteration overprint for the entire system. Most of the Archean basement rocks have undergone amphibolite grade metamorphism.

7.2 HYDROTHERMAL FLUID CHARACTERISTICS

7.2.1 Fluid Inclusions Characteristics

Fluid inclusions are predominately hosted in carbonate veins, there is only one sample (RSC-015 1272.7') where inclusions were present and were analyzed in euhedral quartz intergrown into carbonate. Dolomite and calcite intergrowths comprise the carbonate veins. The intergrowths might be micro-scale oscillations, but generally show evolution from Mg-rich to Fe-rich carbonate. The hydrothermal system at Rattlesnake Hills was dominated by low to moderate salinity aqueous fluids (~4.0 to 12.8wt % eq. NaCl) and low to moderate homogenization temperatures of fluid inclusions (118°C to 257°C). The fluid inclusions at Rattlesnake Hills show no evidence of boiling or vapor-rich phase. Overall there is a lack of vertical or horizontal gradient, no spatial variation in temperatures and salinities. Lastly, there is evidence of discrete amounts of CO_2 that are undetectable by normal fluid inclusion microthermometry methods since it is insufficient to nucleate a CO_2 phase at room temperature but are detected by clathrates. Additionally,

there are rare euhedral to cubic solids with high relief to the fluid and low relief to the host carbonate minerals.

Laser Ablation Inductively Couple Plasma Mass Spectrometry (LA-ICP-MS) and Raman analysis of the fluid inclusions confirmed low salinity inclusions with an average of 4.3% salinity (n=5). There was no CO_2 detected during these two analyses. It is important to note that there is evidence of Au and Ag in fluid that is detected up to 2.1 and 8.9 ppm. The gold and silver content of the fluid from the fluid inclusions is comparable to other epithermal systems. Magmatic gases discharged from active volcanoes with high sulfidation hydrothermal activity have variable gold compositions ranging from not detectable to rates 1,200 kg/year (Hedenquist and Lowenstern, 1994). Geothermal fluids from low sulfidation epithermal deposit, Ladolam, and active geothermal wells in New Zealand, have concentrations up to ~20ppb and fluxes of 4.7 kg/year (Brown, 1986; Simmons and Brown, 2006). Rattlesnake Hills has fluids have a lower Au content, similar to low sulfidation epithermal deposits or the lower end of high sulfidation epithermal deposits.

7.2.2 Oxygen and Carbon Isotopic Fluid Characteristics

The oxygen and carbon isotopic geochemistry data clusters with $\delta^{13}C_{PDB}$ between -2.22‰ and -13.45‰ where as $\delta^{18}O_{SMOW}$ ranges from 8.70‰ to 14.84‰. There are two distinct trends in the oxygen and carbon isotope data: 1) large cluster with positive covariation of oxygen and carbon and 2) a scatter to strongly negative $\delta^{13}C_{PDB}$ values. The covariation signature is most likely caused by magmatic degassing at depth within the magma chamber causing the progressive release of CO_2 rich fluids which then

130

resulted in the precipitation of carbonate. The strongly negative $\delta^{13}C$ is indicative of incorporation of organic carbon most likely from pyroclastic rocks or schist. It is important to note that meteoric water interaction is not likely.

7.2.3 Ore Mineral Paragenesis

The main ore minerals at Rattlesnake Hills are marcasite and pyrite. There are very few cross-cutting or overprinting relationships, making determination of ore paragenesis difficult. The basic paragenesis is: mafic minerals replaced by leucoxene followed by pyrite and/or marcasite phase with subsequent pseudomorphs of marcasite overgrowths of pyrite and pyrite replacing marcasite with the last phase of goethite replacing sulfides. There is increasing concentrations of As in the pyrite and marcasite with time.

7.2.4 Gold Setting

Most gold grains (less than 5μm to greater than 40μm) are hosted in or on marcasite grains. Analysis shows gold mineralization with other precious metals: pyrite, silver sulfides, silver-antimony sulfates, cobaltite, cassiterite, unidentified Ag+Bi and Ag+Pb minerals, arsenopyrite, arsenian pyrite, naumanite, and bismuthinite.

LA-ICP-MS analysis shows nanonuggets or lattice bound gold in marcasite and pyrite grains. Pyrite grains are typically zoned with respect to gold concentration with trace amounts of gold in the core (several ppm) with elevated values in the rims (up to 20,000ppm). The elevated rims correlate to arsenian pyrite and intergrowths with

arsenopyrite. Pyrite with arsenian pyrite rims are associated with muscovite-sericite alteration zones that form as halos around veins.

The presence of marcasite and gold nanonuggets or nanoparticles provides clear limits for the conditions of mineralization. Marcasite forms under specific pH and temperature conditions. Murowchick and Barnes (1986) determined that the occurrence of marcasite implies

> "1. The mineralizing fluids were acidic, with pH <5.0; 2. The temperature of deposition was below 240°C and post-depositional temperatures have remained below 160°C; 3. H_2S_n species were present, and because of their limited persistence in warm solutions, must have been formed close to the site of deposition; and 4. Sulfides species were partially oxidized, ore reacted with more-oxidized sulfur species ($S_2O^{2-}_3$, HSO^-_3, etc.) to form the required polysulfides."

While marcasite provides a vital key piece of evidence, nanonuggets or nanoparticles of gold might represent a primary form of gold mineralization at Rattlesnake Hills which is comparable to gold deposition in the Carlin Trend deposits, Nevada. Palenik et al. (2004) suggested that nanoparticles form in two ways: "a) when the solubility limit of Au in arsenian pyrite (0.5% Au at 10 wt. % As) was exceeded locally during crystallization of the arsenian pyrite rims, resulting in deposition of elemental Au; or b) that the Au nanoparticles exsolved from a metastable arsenian pyrite matrix during later stages in the evolution of the deposit." Based on results from LA-ICP-MS of As:Au ratios in pyrite grains, the maximum measured gold nanoparticles most likely formed by the first

process because the maximum gold to arsenic ratio in marcasite is approximately 0.1 and >5,000 ppm. Palenik et al. (2004) also observed that mineralized areas of As-rich pyrite have a different texture than barren zones. Gold bearing areas have a polycrystalline matrix of Au nanoparticles in the As-rich matrix (Palenik et al., 2004). This observation could explain why some samples do not have high enough gold concentrations in pyrite (and marcasite) grains to equal the assay results. However, some samples have similar gold concentrations in pyrite grains equivalent to the assay results.

7.3 COMPARISON OF RATTLESNAKE HILLS TO OTHER WORLD CLASS DEPOSITS

7.3.1 Barren vs. Mineralized Alkaline Gold Deposits

While Rattlesnake Hills is mineralized, not all alkaline complexes are gold bearing. What separates gold bearing complexes with barren complexes? Audetat et al. (2008) compared magmatic mineralized and barren systems and determined that the initial exsolved aqueous fluid is single phase low salinity (RSH has comparable salinities). The authors concluded that "the metal content of magmatic, low-salinity fluids correlates positively with the type and amount of mineralization in the associated intrusions…this implies that a significant part of the geochemical signature of these deposits was determined during processes operating at the magmatic stage" implying an evolved magma (Audetat et al., 2008). LA-ICP-MS of fluid inclusions at Rattlesnake Hills have elevated levels of trace elements Zn, As, Cs, and Rb. The fluid inclusions do have trace amounts of Ag and Au present but the Au is as high as recorded in any hydrothermal deposit to date.

7.3.2 Comparison to World Class Alkaline Deposits

Overall the hydrothermal fluid at Rattlesnake Hills is low to moderate salinity, low to moderate homogenization temperatures, magmatic without meteoric water component interactions, low pH and low temperature of deposition is deduced from the crystallization of marcasite, and mostly low temperature arsenopyrite compositions. Rattlesnake Hills is comparable to alkaline igneous/diatreme gold complexes in the CMB and throughout the world, and also has similarities to epithermal style gold deposits, and porphyry style deposits. Rattlesnake Hills is most comparable to Cripple Creek and other alkaline complexes in the CMB. Rattlesnake Hills has a similar age, style of mineralization, environment/tectonic setting but it is still unclear if these deposits all formed in the same setting and environment. Rattlesnake Hills has comparable fluid characteristics, but lacks a higher homogenization temperature and higher salinity phase as seen at Cripple Creek, Colorado hence Cripple Creek is a deeper or hotter system than Rattlesnake Hills.

World-class gold deposits hosted in alkaline complexes throughout the world are still not well understood. There is still not a clear understanding as to what distinguishes a mineralization alkaline system and a barren system. It is possible that the composition (alkaline vs. calc-alkaline), environment, style of deposit (epithermal or porphyry style deposit), or age could control the gold mineralization and grade. Without having the constraints on which parameters control gold mineralization, it makes it difficult to understand if Rattlesnake Hills is an extension of the CMB and alkaline complex trend along the North American Cordilleran. Comparing Rattlesnake Hills to other world class

deposit types: Au (Te) epithermal systems, mafic-intermediate (Cu/Au) porphyry style systems, and intermediate-felsic (Mo/Au) porphyry style provide insights.

Au (Te) epithermal systems (Porgera, Emperor, Ladolam, and Cripple Creek) have a wide range of ages from 0.018 to 30 Ma, form in island arcs areas of back arc subduction, and crustal extension (Jensen and Barton, 2000). Mineralization is associated with veins with the ore minerals including: Au, Au tellurides, electrum, Au bearing pyrite and arsenopyrite, and copper minerals (Jensen and Barton, 2000). The fluid inclusions range from a lower homogenization temperature of 100-200°C and higher temperature of 200-400°C with equiv. wt. % NaCl ranging from ~3-10 (Jensen and Barton, 2000). The oxygen isotope compositions range from 2-10 per mil with the fluids mostly consisting of magmatic fluids with some meteoric waters (Jensen and Barton, 2000).

Mafic-intermediate (Cu/Au) porphyry style systems (Galore Creek, La Plata Mountains, and Goonumbla) have a wide range in ages from 435Ma to Jurassic with each location having a slightly different tectonic setting from island arc to intra-continental Laramide Orogeny (Jensen and Barton, 2000). The style of mineralization varies from finely disseminated to skarn to porphyry style with stockwork veins with the main ore minerals including: chalcopyrite, bornite, Au, and tellurides (Jensen and Barton, 2000). The fluid inclusions for two of the systems are hot 400-720°C with 40-65 equiv. wt. % NaCl while one system is 150°C with 4-5 equiv. wt. % NaCl (Jensen and Barton, 2000).

The intermediate-felsic (Mo/Au) porphyry style systems (Sierra Blanca, Central City, and Golden Sunlight) range in age from 80 to58 Ma and range in tectonic settings

from extensional rifts to regional upwarping (Jensen and Barton, 2000). The main style of mineralization is Mo porphyry style with the main ore minerals: copper, molybdenum, Au, and tellurides (Jensen and Barton, 2000). The fluid inclusions range from 130-420°C with 2-12 equiv. wt. % NaCl (Jensen and Barton, 2000). For the systems for which evidence is available, the source of the fluid was magmatic and meteoric mixed (Jensen and Barton, 2000).

Rattlesnake Hills is Eocene in age (42Ma) and in an interior edge of a continental orogenic belt setting associated with the Laramide Orogeny. The main style of mineralization is low grade finely disseminated Au in the wallrock and narrow high grade zones that might be associated with carbonate veins. The ore minerals are pyrite, marcasite, and electrum. The fluids responsible for the mineralization are low temperature with low equiv. wt. % NaCl and magmatic. These are more characteristic of the Au (Te) epithermal style deposits.

7.3.3 Comparison of Porphyry-Style and Epithermal-Style Alkaline Gold Deposits to Rattlesnake Hills

Porphyry-style gold deposits are typically Jurassic or younger aged, form in a variety of tectonic settings but porphyry-Au deposits tend to form in continental-arc settings (Sinclair, 2007). Since most porphyry-style deposits are hot and have highly saline fluid, it is unlikely Rattlesnake Hills fits a porphyry-style gold deposit model. Rattlesnake Hills follows an epithermal-style gold deposit model with low temperature, low salinity, hosted in an island arc type tectonic setting, and similar fluid inclusions with other epithermal deposits.

136

Rattlesnake Hills thus tends to be more closely related to epithermal style mineralization than to porphyry style mineralization. One of the largest and well-studied epithermal gold-silver deposits in the world is the Hauraki Goldfield, New Zealand. The Hauraki Goldfield is comprised of over 50 smaller Miocene and Pilocene deposits in a subduction related magmatic arc with mineralization primarily contained in andesite and dacite units (John, 2011). The main difference between Rattlesnake Hills and Hauraki Goldfield is that mineralization is confined to quartz veins in andesite and dacite at Hauraki (John, 2011), while Rattlesnake Hills is silica-undersaturated with most veins are carbonate. At the Hauraki goldfield, it is proposed that individual deposits formed from multiple, overlapping hydrothermal systems that migrated but gold mineralization was restricted to a 1 million year interval (Mauk et al., 2011).

It is important to determine if Rattlesnake Hills is a low sulfidation or high sulfidation epithermal style system. Low sulfidation systems tend to be more distant from the magmatic center, shallow and low salinity fluids. High sulfidation systems are shallow, closer to magmatic source, and can be diatreme hosted. Rattlesnake Hills has similarities with both types of epithermal systems.

Overall, most epithermal deposits form at lower temperatures and shallower depths with a pervasive fluid flow. Porphyry style deposits are hotter, deeper and have a fluid flow through veins (typically quartz veining). Rattlesnake Hills more closely fits the criteria of an epithermal deposit than a porphyry deposit.

REFERENCES

Audetat, A., Pettke, T., Heinrich, C.A., and Bodnar, R., 2008, The composition of magmatic-hydrothermal fluids in barren and mineralized intrusions: Economic Geology: Special Paper, v. 103, p. 877-908.

Bakker, R.J., 1997, CLATHRATES: Computer programs to calculate fluid inclusion V-X properties using clathrate melting temperatures: Computers and Geosciences, v. 28, p. 1-18.

————2003, Package FLUIDS 1: Computer programs for analysis of fluid inclusion data and for modeling bulk fluid properties: Chemical Geology, v. 194, p. 3-23.

Bodnar, 2003, Introduction to aqueous-electrolyte fluid inclusions. In *Fluid Inclusions*: Analysis and interpretation (eds. I. Samson, A. Anderson, and D. Marshall). Mineralogical Association of Canada Short Course, v. 23, p. 81-100.

Bourdet, J. and Pironon, J., 2008, Strain response and re-equilibration of CH_4-rich synthetic aqueous fluid inclusions in calcite during pressure drops: ScienceDirect Geochimica et Cosmochimica Acta, v. 72, p. 2946-2959.

Brown, K.L., 1986, Gold Deposition from geothermal discharges in New Zealand: Economic Geology, v. 81, p. 979-983.

Burnett, W.J., 1995, Fluid chemistry and hydrothermal alteration of the Cresson disseminated gold deposit, Cripple Creek, Colorado: Masters Thesis, Colorado State University, Fort Collins, p. 168.

Carman, G.D., 2003, Geology, mineralizational, evolution of the Ladolam Gold Deposit, Lihir Island, Papua New Guinea: Society of Economic Geologists Special Publication, v. 10, p. 247-284.

Cerny, P., 1991, Rare-element pegmatites. Part 1: Anatomy and internal evolution of pegmatite deposits: Geoscience Canada, v. 18, no. 2, p. 49-67.

CC&V (Cripple Creek and Victor Gold Mining Company), 2005, Geology of the Cripple Creek Mining District: http://ccvgoldmining.com/Geology/geology.html (May 2010).

Chacko, T., Mayeda, T.K., Clayton, R.N., and Goldsmith, J.R., 1991, Oxygen and carbon isotope fractionations between CO_2 and calcite: Geochimica et Cosmochimica Acta, v. 55, p. 2867-2882.

Demeny, A., Sitnikova, M.A., and Karchevsky, P.I., 2004, Stable Cand O isotope compositions of carbonatite complexes of the Kola Alkaline Province: phoscorite-carbonatite relationships and source compositions. In *Phoscorites and Carbonatites from mantle to min: the Key example of the Kola Alkaline Province* (F. Wall and A.N. Zaitsev, eds.) Mineralogical Society Series, v. 10.

Durk, K., 2011, personal communication, ongoing Masters Thesis Reseach, Idaho State University, Pocatello.

Dwelley, P.C., 1984, Geology, mineralization, and fluid inclusion analysis of the Ajax Vein System, Cripple Creek, Colorado: Masters Thesis, Colorado State University, Fort Collins, p. 166.

Evolving Gold Corp., 2009, The geology and gold mineralization at the Rattlesnake Hills Property, Natrona County, Wyoming, USA: A National Instruments 43-101Technical Report for Evolving Gold Corp., p. 68.

———2011, Evolving Gold and Agnico-Eagle Joint venture, Rattlesnake Hills project Wyoming: http://www.evolvinggold.com/news/news2011/news-release-2011-05-09.html (May 2011).

———2012, New gold targets identified at Rattlesnake Hills project: http://www.evolvinggold.com/news/2012news/news-20120326.html-2012-03-26 (May 2012).

Fan, M., DeCelles, P.G., Gehrels, G.E., Detterman, D.L., Quade, J., and Peyton, S. L., 2011, Sedimentology, detrital zircon geochronology, and stable isotope geochemistry of the lower Eocene strata in the Wind River Basin, central Wyoming: GSA Bulletin, v. 123, no. 5/6, p. 979-996.

Frost, C.D., Fruchey, B.L., Chamberlain, K.R., and Frost, B.R., 2006, Archean crustal growth by lateral accretion of juvenile supracrustal belts in the south-central Wyoming Province: Can. J. Earth Sci, v. 43, p. 1533-1555.

Goldstein, R.H., and Reynolds, T.J., 1994, Systematics of fluid inclusions in diagenetic minerals: SEPM short course 31, p. 199.

Gottlieb, P., Wilkie, G., Sutherland, D., Ho-Tun, E., Suthers, S., Perera, K., Jenkins, B., Spencer, S., Butcher, A., and Rayner, J., 2000, Using quantitative electron microscopy for process mineralogy applications: JOM- Journal of Minerals, Metals and Materials Society, v. 52, p. 24-25.

Grace, R.L.B., Chamerlain, K.R., Frost, B.R., and Frost, C.D., 2006, Tectonic histories of the Paleo- to Mesoarchean Sacawee block and Neoarchean Oregon Trail structural belt of the south-central Wyoming Province: Can. J. Earth Sci., v. 43, p. 1445-1466.

Hausel, W.D., 1996, Geology and gold mineralization of the Rattlesnake Hills, Granite Mountains, Wyoming: Wyoming State Geological Survey Report of Investigations, no. 52, 28p.

———1998, The Rattlesnake Hills: Wyoming's little known gold district: International California Mining Journal, v. 68, no. 4, p. 44-46.

Hedenquist, J.W., Arribas, A.J., and Gonzales-Urien, E., 2000, Exploration for epithermal gold deposits. In *Gold*, 2000 (S.G. Hagemann and P.E. Brown, eds). Reviews Economic Geology, v. 13, p. 245-277.

Hedenquist, J.W., and Lowenstern, 1994, The role of magmas in hydrothermal ore deposits: Nature, v. 370, p. 519-527.

Ho, S.E., McQueen, K.G., NcNaughton, N.L., and Groves, D.I., 1995, Lead isotope systematics and pyrite trace element geochemistry of two granitoid associated

mesothermal gold deposits in the southeastern Lachlan fold belt: Economic Geology, v. 90, p. 1818-1830.

Hoch, A.R., 1991, Petrological and geochemical evolution of the Rattlesnake Hills alkaline-intrusive complex, Natrona County, Wyoming: M.S. dissertation, University of Wyoming, Laramie, 140p.

Hoch, A.R., and Frost, C.D., 1993, Petrographic and geochemical characteristics of mid-Tertiary igneous rocks in the Rattlesnake Hills, central Wyoming, with a comparison to the Bear Lodge intrusive suite or northeastern Wyoming, In *Geology of Wyoming* (Snoke, A.W., Steidtmann, J.R., and Roberts, S.M. , eds.): Memoir Geological Survey of Wyoming, no. 5, p. 508-528.

Houston, R.S., 1969, Aspects of the geologic history of Wyoming related to the formation of the uranium deposits: Contribution to Geology Wyoming Uranium Issue, v. 8, no. 2, pt. 1, p.67-79.

Jensen, E.P., and Barton, M.D, 2000, Gold deposits related to alkaline magmatism: SEG Reviews, v. 13, p. 279-314.

———2007, Geology, petrochemistry, and time-space evolution of the Cripple Creek district, Colorado: Geological Society of America Field Guide 10, p. 63-78.

John, D.A., 2011, Epithermal gold-silver deposits of the Hauraki goldfield, New Zealand: An introduction: Economic Geology, v. 106, p. 915-919.

Kelley, K.D., and Ludington, S., 2002, Cripple Creek and other alkaline-related gold deposits in the southern Rocky Mountains, USA: Influence of regional tectonics: Mineralium Deposita, v. 37, p. 38-60.

Kelley, K.D., Romberger, S.B., Beaty, D.W., Pontius, J.A., Snee, L.W., Stein, H.J., and Thompson, T.B., 1998, Geochemical and geochronological constraints on the genesis of Au-Te deposits at Cripple Creek, Colorado: Economic Geology, v. 93, p. 981-1012.

Kent-Corson, M.L., Mulch, A., Graham, S.A., Carroll, A.R., Ritts, B.D., and Chamberlain, C.P., 2010, Diachronous isotopic and sedimentary responses to topographic change as indicators of mid- Eocene hydrologic reorganization in the western United States: Basin Research, v. 22, p. 829-845.

Love, J.D., 1970, Cenozoic geology of the Granite Mountains area, central Wyoming: U.S. Geological Survey Professional Paper 494-C, 154 p.

Marks, M.A.W., Neukirchen, F., Vennemann, T., and Markl, G., 2009, Textural, chemical, and isotopic effects of late-magmatic carbonatitic fluids in the carbonatite-syenite Tamazeght complex, High Atlas Mountains, Morocco: Miner. Petrol., v. 97, p. 23-42.

Matsuhisa, Y., Morishita, Y., Sato, T., 1985, Oxygen and carbon isotope variations in gold-bearing hydrothermal veins in the Kushikino mining area, southern Kyushu, Japan: Economic Geology, v. 80, p. 283-293.

Mauk, J.L., Hall, C.M., Chesley, J.T., and Barra, F., 2011, Punctuated evolution of a large epithermal province: the Hauraki goldfield, New Zealand: Society of Economic Geology, v. 106, p. 921-943.

140

Mote, A.S., 2000, Fluid inclusion study of veins within Granite Island, Cripple Creek mining district, Cripple Creek, Colorado: B.A. honors thesis, University of Georgia, Athens, 8 p.

Murowchick, J.B. and Barnes, H.L., 1986, Marcasite precipitation from hydrothermal solutions: Geochemica et Cosmochimica Acta, v. 50, p. 2615-2629.

Mutschler, F.E., Mooney, T.C., and Johnson, D.C., 1991, Precious metal deposits related to alkaline igneous rocks-A space-time trip through the Cordillera: Fourth Western Regional Conference on Precious Metals and the Environment, p. 304-309.

Oliveira Cordeiro, P.F., Brod, J.A., Santos, R.V., Dantas, E.L., Oliveira, C.G., and Barbosa, E.S.R, 2011, Stable (C,O) and radiogenic (Sr, Nd) isotopes of carbonates as indicators of magmatic and post-magmatic processes of phoscorite-series and carbonatites from Catalao I, central Brazil: Contrib Mineral Petrol, v. 161, p. 451-464.

Palenik, C.S., Utsunomiya, S., Reich. M., Kesler, S.E., Wang, L., and Ewing, R.C., 2004, "Invisible" gold revealed: Direct imaging of gold nanoparticles in a Carlin-type deposit: American Mineralogist, v. 89, p. 1359-1366.

Pekarek, A.H., 1977, The structural geology and volcanic petrology of the Rattlesnake Hills, Wyoming:Wyomng Geological Association Earth Science Bulletin, v. 10, no. 4, p. 3-30.

———1978, Stratigraphy and structural geology of the Rattlesnake Hills, Wyoming: Wyoming Geological Association Guidebook, v. 30, p. 239-253.

Pekarek, A.H., Marvin, R.F., and Mehnert, H.H., 1974, K-Ar ages of the volcanic in the Rattlesnake Hills, Central Wyoming: Geology, v. 2, p. 283-285.

Pontius, J.A., and Butts, R.A., 1991, Geology and gold mineralization of the Cresson Deposit, Cripple Creek, Colorado: 97th Annual Northwest Mining Association Convention, 10 p.

Potter, E.G., and Taylor, R.P., 2010, The stable and radiogenic isotopic attributes of the precious-metal-bearing polymetallic veins from the Cobalt Embayment, Northern Ontario, Canada: Genetic and exploration implication: The Canadian Mineralogist, v. 48, no. 2, p. 391-414.

Reinhard, A.W., Epis, R.C., and Scott, G.R., 1976, Reconnaissance geologic map of the Cripple Creek-Pikes Peak area, Teller, Fremont, and El Paso counties, Colorado: U.S. Government Printing Office.

Roedder, E., 1984, Fluid Inclusions: Mineralogical Society of America Reviews in Mineralogy, v. 12, 644p.

Rosdeutscher, J.A., 1999, Geology and stable isotope geochemistry of the Grassy Valley AU deposit, Cripple Creek District, Colorado: Evidence for magmatic fluids: Masters thesis, University of Georgia, Athens, 89 p.

Shepherd, T.J., Ranklin, A.H., and Alderton, D.H.M., 1985, A pratical guide to fluid inclusion studies: Blackie, Glasgow and London, 239 p.

Shive, P.N., Pekarek, A.K., and Zawislak, R.L., 1977, Volcanism in the Rattlesnake Hills of central Wyoming: A paleomagnetic study: Geology, v. 5, p. 563-566.

Sillitoe, R.H., 2008, Major gold deposits and belts of the North and South American Cordillera: Distribution, tectonomagmatic settings, and metallogenic considerations: Economic Geology Special Paper, v. 103, p. 663-687.

Simmons, S.F., and Brown, K.L, 2006, Gold in magmatic hydrothermal solutions and the rapid formation of a giant ore deposit: Science, v. 314, p. 288-291.

Sinclair, W.D., 2007, Porphyry deposits, In *Mineral Deposits of Canada: A synthesis of major deposit-types, district metallogeny, the evolution of geological provinces, and exploration methods* (Goodfellow, W.D., ed.): Geological Association of Canada, Mineral Deposits Division, Special Publication, no. 5, p. 223-243.

Slack, P.B., 1981, Paleotectonics and hydrocarbon accumulation: Powder River Basin: American Association of Petroleum Geologist, v. 65.

Taylor, H.P., Frechen, J, Degens, E.T., 1967, Oxygen and carbon isotope studies of carbonatites from the Laacher See District, West Germany and the Alno District, Sweden: Geoch Cosm Acta, v. 31, p. 407-430.

Todorov, T., Koenig, A., and Marsh, E.E., 2009, Integrated Raman microspectroscopy laser ablation inductively coupled plasma mass spectrometry (LA-ICP-MS) system for the analysis of fluid and melt inclusions: Geological Society of America Abstracts with Programs, v. 41, no. 7, p. 332.

Ujiie, K., Yamaguchi, A., and Taguchi, S., 2008, Stretching of fluid inclusions in calcite as an indicator of frictional heating on faults: The Geological Society of America, v. 36, no. 2, 111-114.

Vityk, M.D., and Bodnar, R.J., 1995, Textural evolution of synthetic fluid inclusions in quartz during reequilibration: With applications to tectonic reconstruction: Contrib Mineral Petrol, v. 121, p. 309-323.

Vaughan, D.J., and Craig, J.R., 1997, Sulfide ore mineral stabilities, morphologies, and intergrowth textures. In *Geochemistry of hydrothermal ore deposits* (ed. Barnes, H.L): New York: John Wiley & Sons,3rd ed., p. 972.

Zheng, Y. –F., 1990, Carbon-oxygen isotopic covariation in hydrothermal calcite during degassing of CO2: A quantitative evaluation and application to the Kushikino gold mining area in Japan: Mineralium Deposita, v. 25, p. 246-250.

APPENDIX 1: DESCRIPTION OF THIN SECTION SAMPLES

RSC-002 849.8': White carbonate vein (possible carbonatite), euhedral green fluorite with lesser purple fluorite and trace sulfides. Sulfides are cubic and octahedral pyrite and chalcopyrite. Chalcopyrite and pyrite in this sample are hosted in two different gangues. Cannot tell determine paragensis for this sample. Fluid inclusions are difficult to see, hosted in carbonate. Most inclusions are two-phase (l+v) with rare three phase inclusions (l+v+s) with the average sizes ranging from 6.7-18 μm. Most inclusions occur as clusters or individual inclusions. This sample is from South Stock.

RSC-003 743' A and B: The sample is schist with amphibolite grade metamorphism with multiple carbonate+adularia+pyrite veinlets. The primary ore and oxide minerals are: marcasite, leucoxene, and pseudomorphic pyrite after marcasite. 95% of sample is radial/bladed marcasite. The marcaste is coarse blades in wallrock and smaller, finer blades in carbonate vein. The marcasite is later than the gangue, the marcasite cross-cuts the cleavage. The paragensis is: 1) Marcasite and followed by 2) Pseudomorphc pyrite after marcasite. The fluid inclusions are very small and dark. Most inclusions are two phase (l+v) with rare three phase inclusions (l+v+s) with the average sizes ranging from 6.9-10.5μm. The solids are accidental solids. Most inclusions occur as clusters or individual inclusions. These samples are from North Stock.

RSC-003 1266.9': The sample is of spherical, carbonate amygdule that is compositionally zoned and hosted in heterolithic igneous and metamorphic breccia (HMBx). The main ore and oxide minerals are: leucoxene, pyrite, and marcasite. Most pyrite grains are subhedral to euhedral cubes in matrix/wallrock with lesser pyrite in amydule. There are growth pits within the pyrite. The carbonate amygdule contains mostly bladed marcasite. Not all marcasite is anisotropic, this might represent partial to complete replacement by pyrite. The paragenesis of ore minerals in the wallrock/breccia matrix: 1) Marcasite and later 2) Pyrite. The paragenesis within the amygdule is indeterminate. Some of the sulfides present in this sample are partially (weakly) transparent. There are no useable fluid inclusions. This sample is from North Stock.

RSC-003 1374': The sample is of schist with amphibolite grade metamorphism. The main ore and oxide minerals are: pyrite, marcasite, leucoxene, sphalerite, and chalcopyrite. Pyrite is euhedral. Pyrite and marcasite hosted together and the grain boundaries blurred. The sphalerite is irregular shaped with small individual grains of chalcopyrite and is late stage. The paragenesis is: 1) Marcasite and 2) Pyrite. There were no useable fluid inclusions. This sample is from North Stock.

RSC-004 431.5': The sample is of two phases of carbonate: 1) irregular shaped body with carbonate+sulfides and 2) thin white carbonate vein hosted in medium grained porphyry. The main ore and oxide minerals are: pseudomorphic pyrite after marcasite, leucoxene, and marcasite. The pyrite occurs as subhedral, replacement after marcasite. The marcasite

is wispy, well formed, weakly anisotropic, and hosted within the carbonate vein. Most of the marcasite has been partially or fully replaced by pyrite. The fluid inclusions are hosted in a thin, late stage vein. Inclusions are two-phase (*l+v*) with some rare one phase inclusions (*l*) and three phase inclusions (*l+v+s*). Most of the solids appear to be accidental or trapped, with some of the solids occurring within the vapor. The fluid inclusions range in size from 3.8-19.2µm. This sample is from North Stock.

RSC-004 1112.3': The sample is white carbonate vein/breccia cement in monolithic crackle schist breccia. Most of the sulfides are concentrated in the carbonate, not in the host rock. The main ore and oxide minerals are: marcasite, pyrite, and leucoxene. Marcasite occurs as blades, blocky aggregates, and rare twins. The blocky marcasite grains are larger and show paragenesis within the grains: centers, radiating grains, with a thin outer edge with the radiating crystals nucleating on the center. The fluid inclusions are two phase (*l+v*). Most inclusions are irregular shaped and hosted in pockets of carbonate. Fluid inclusion sizes range from 2.7-41.1µm. This sample is from North Stock.

RSC-006 581.5' A and B: The sample is of a carbonate+sulfide vein hosted in a feldspar porphyry. The main ore and oxide minerals are: pyrite, gold, marcasite, chalcopyrite, leucoxene. Some of the pyrite grains appear to have zoning or rims—possible arsenopyrite rims. Marcasite occurs are twins, wisps, and blocky aggregates. Gold is associated with blocky marcasite at the vein edge. Almost all sulfides are associated with a later replacement/partial replacement by fluids carrying pyrite, marcasite, and pyrite+marcasite. There are no useable fluid inclusions. This sample is from North Stock.

RSC-006 1760' A and B: The samples are intensely potassically altered schist with cross-cutting carbonate veins. The main ore and oxide minerals are: leucoxene, marcasite, and pyrite. Marcasite occurs are blades and radial grains with partial replacement by pyrite. Pyrite is euhedral and some grains are pitted. The sulfide grains are weakly transparent in plane polarized light. There are no useable inclusions. This sample is from North Stock.

RSC-006 1769' A and B: The sample is intensely potassically altered schist with adularia veins. Sulfides are concentrated along veins. The main ore and oxide minerals are: pyrite, marcasite, chalcopyrite, and leucoxene. Pyrite occurs are euhedral grains with rare pitting. Marcasite occurs as blocky aggregates, snowflakes, and blades. Marcasite has partial replacement by pyrite. The samples are from North Stock.

RSC-006 1785' A and B: The sample is intensely potassically altered schist with adularia veins. The main ore minerals are: marcasite and pyrite. Pyrite occurs as euhedral grains in the carbonate veins. Marcasite only occurs in trace amounts. The sample is from North Stock.

RSC-012 1557.1': The sample is a white carbonate vein hosted in altered schist. The vein appears zoned. The main ore and oxide minerals are: chalcopyrite, pyrite, marcasite, and leucoxene. Pyrite grains are anhedral and some are pitted. Increased amounts of pyrite grains are spatially associated with small veinlets and within the schist, elongated grains follow the foliation. Marcasite is not well formed and occurs as ribbons. The fluid

inclusions are two phase (*l+v*) and rare one phase (*l*). Most of the inclusions are irregular and hosted within carbonate vein. The sizes of the fluid inclusions range from 3.9-39.0µm. This sample is from North Stock.

RSC-014 542.5': The sample is of a symmetrical carbonate vein hosted in heterolithic igneous and metamorphic breccia (HIMBx). The breccia has increased amounts of biotite; this may be secondary biotite alteration. The main ore and oxide minerals are: marcasite, pyrite, leucoxene, and goethite. Marcasite grains are partially replaced by pryite. Pyrite occurs are small, eudhral cubic grains with occassional grains being pitted and filled with leucoxene. Leucoxene is in/around pitted pyrite grains and is replacing mafic minerals in brecciated sections. On the carbonate vein edge, there is goethite. The goethite is a late replacement of sulfides. There are no useable fluid inclusions. This sample is from North Stock.

RSC-014 995.2': The sample is a heterolithic igneous breccia (HIBx) with vuggy alteration. The breccia cement is carbonate+sulfide. The main ore and oxide minerals: pyrite, leucoxene, and marcasite. Leucoxene occurs as rims and cores of pyrite grains, replacement of mafic minerals with the replacement forming in a diamond to arrow-head shape. There are only trace amounts of marcasite with some grains partially replaced by pyrite. The paragenesis of this sample is: 1) Leucoxene, 2) Pyrite and/or Marcasite, and 3) Pseudomorphic pyrite after marcasite. There is no clear relationship between the primary pyrite and marcasite. The fluid inclusions are hosted in carbonate. Most of the fluid inclusions are small, dark trails with most two phase inclusions (*l+v*) with rare three phase inclusions (*l+v+s*) where solids are either accidental or daughter minerals. Rare solids occur in the vapor bubble of the fluid inclusion. The fluid inclusions range in size from 3.8-17.4µm. This sample is from North Stock.

RSC-015 1219.5' A and B: The samples are of a white carbonate vein hosted in schist; white carbonate vein has multiple generations with trace purple fluorite and some rare vugs. The main ore and oxide minerals are: pyrite, marcasite, chalcopyrite, and leucoxene. The chalcopyrite appears be to filling voids around pyrite or growing on pyrite. It occurs in both the wallrock and carbonate vein. The marcasite occurs as aggregate blocks and blades. The marcasite grains have partial replacement by pyrite. Pyrite occurs are cubic, euhedral grains at the contact of the vein and the wallrock. Leucoxene occurs in both the wallrock and carbonate vein; however, leucoxene is more abundant in schist than carbonate vein. The parageneis present in this sample is: 1) Pyrite and 2) Chalcopyrite. There are no useable fluid inclusions. This sample is from North Stock.

RSC-015 1272.7': The sample has multiple generations (at least 2) of carbonate vein/breccia that is white, cream, grayish hosted in schist. The main ore and oxide minerals are: pyrite, chalcopyrite, leucoxene, and trace marcasite. Pyrite occurs are well formed, euhedral grains. The fluid inclusions in this sample are two phase (*l+v*) and rarer three phase (*l+v+s*). There are large, dark inclusions. Most of the inclusions occur as individual inclusions or small clusters. The sizes of the fluid inclusions range from 3.7-57.6µm. This sample is from North Stock.

RSC-020 503' A, B, and C: Thin section A is of schist that appears bleached with minor clay alteration. Thin section B is of schist with minor bleaching and amphibolite grade metamorphism. Thin section C is of schist with minor amphibolite grade metamorphism and bleaching with a white carbonate vein. The main ore and oxide minerals are: pyrite, leucoxene, and marcasite. Pyrite occurs are small, euhedral grains with rare grains having leucoxene cores. Paragenesis is difficult to determine because the pyrite and marcasite are intergrown with no present grain boundaries. The marcasite and pyrite are weakly transparent in plane-polarized light. Thin section A has no useable fluid inclusions. Thin section B has small, two phase ($l+v$) and one phase (l) inclusions. The inclusions are irregular shaped and occur as primary clusters and secondary trails cross-cutting grain boundares. The average size of the fluid inclusions is 6.5µm. Thin section C has more inclusions that the previous two thin section but most inclusions are small and dark. Most inclusions are two phase ($l+v$) and occur as pseudosecondary trails and larger primary inclusions. The fluid inclusions range in size from 5.2-28.9µm. This sample is from North Stock.

RSC-020 646.5': The sample is a carbonate+sulfides vein hosted in green schist with spider pyrite veins. There is trace purple fluorite. The carbonate vein is boytrodial and is depleted in sulfides compared to surrounding rock. There are very few sulfides in vein. The main ore and oxide minerals are: marcasite, pyrite, chalcopyrite, gold, and leucoxene. Marcasite forms as blades with minor partial replacement by pyrite. Pyrite occurs as euhedral, cubic grains and as pseudomorphic pyrite after marcasite. Gold is hosted in marcasite with partial replacement by pyrite. The fluid inclusions are two phase ($l+v$), one phase (l), and three phase ($l+v+s$). The inclusions occur as secondary trails and larger, individual, primary inclusions. The sizes range from 3.9-9.5µm. This sample is from North Stock.

RSC-020 702': The sample is a zoned carbonate with euhedral carbonate grains hosted in strongly altered schist (amphibolite grade metamorphism and bleached) with sulfides present. The carbonate veins shows multiple generations. The handsample has visible gold. The main ore and oxide minerals are: pyrite, marcasite, chalcopyrite, and hematite. Pyrite and marcasite occur as blocky to euhedral intergrowths. Gold occurs in blocky marcasite. Gold grains show color variations. Fluid inclusions occur in translucent pockets of carbonate, are two phase ($l+v$), and are small. Most inclusions occurs as pseudosecondary trails. The average size of the inclusions range from 3.2-11.2µm. The sample is from North Stock.

RSC-020 1202.5': The sample is a white carbonate vein hosted in schist; the carbonate vein is overprinting adularia (?). The main ore and oxide minerals are: marcasite, chalcopyrite, pyrite, and leucoxene. Marcasite occurs as blades, aggregates of blocks, and some has been partially replaced by pyrite. Leucoxene is replacing mafic minerals. The sulfides show weak transparency in plane polarized light. There are no useable fluid inclusions. The sample is from North Stock.

RSC-027 1754': The sample is phonolite with a carbonate+sulfide+fluorite vein. The fluorite is purple. The main ore and oxide minerals are: leucoxene, pyrite, and marcasite. Pyrite occurs in the phonolite groundmass and as very small grains. Marcasite is replaced by pseudomorphic pyrite; however, there are a few patches of marcasite left. Not all the marcasite has been completely replaced pyrite. Pyrite and leucoxene occur intergrown forming a myrmekitic texture. Marcasite occurs are blades, twins, blocky aggregates, and rare grains with boytrodial shape. There are no useable fluid inclusions. The sample is from North Stock.

RSC-027 2001': The sample is of schist breccia (SCHBx) with carbonate+sulfide breccia cement. There are trace amounts of purple fluorite. The main ore and oxide minerals are: pyrite, marcasite, chalcopyrite, and leucoxene. Pyrite occurs as euhedral cubes and pseudomorphic pyrite after marcasite. Marcasite occurs as blades and blocky aggregates with both forms with partial replacement by pyrite. Chalcopyrite occurs in the schist, not in the breccia cement. The fluid inclusions are two phase ($l+v$), three phase ($l+v+s$), and one phase (l). Large irregular shaped inclusions and most inclusions are concentrated at the edge of calcite+walllrock (schist). The fluid inclusions range in size from 1.7-15.2μm. The sample is from North Stock.

RSC-028 515': The sample is an iron-rich carbonate vein in phonolite. The main ore and oxide minerals are: marcasite, goethite, pyrite, and leucoxene. Pyrite and marcasite has been replaced by goethite. Goethite is not homogeneous but has lighter colored bands indicative of composition change. Goethite occurs as sulfide replacement with preferential replacement of marcasite and lining/filling voids. There are no useable fluid inclusions. This sample is from North Stock.

RSC-028 861.8': The sample is of a white carbonate vein with late stage carbonate with very minor open spaces preserved in the center of vein hosted in phonolite. The main ore and oxide minerals are: leucoxene, pyrite, marcasite, and goethite. Leucoxene occurs as replacement of mafic minerals. Marcasite occurs as blocky aggregates. The wallrock has more blocky marcasite than the carbonate vein. The goethite occurs as stringers that are cross-cut by later calcite vein. The vein has very few sulfides. Fluid inclusions are too small to be measured. The sample is from North Stock.

RSC-028 1331.5': The sample is of a porphyry breccia with vuggy carbonate (+trace sulfides) as cement. The main ore and oxide minerals are: pyrite, leucoxene, and marcasite. Pyrite occurs are euhedral and cubic. Leucoxene is replacing mafic minerals. There are two generations of marcasite: blocky and bladed/twinned. The blocky aggregates of marcasite are greyer in color and occur at the edge of the vein while the bladed marcasite is whiter with trace yellow coloration and in the center of the carbonate vein. The paragenesis of the sample is: 1) Ti bearing mineral phase (or mafic mineral), 2) Leucoxene replacing Ti mineral phase, 3) Pyrite, 4) Bladed Marcasite (bladed nucleated on the pyrite and grew within the pit of the pyrite), and 5) Blocky Marcasite. The fluid inclusions are dark, two phase ($l+v$), and occur as primary individual inclusions. The inclusions range in size from 4.4-14.7μm. The sample is from North Stock.

RSC-028 2587.5': The sample is a white carbonate vein with euhedral carbonate crystals within vein that is hosted in schist/igneous intrusion. There are occasional to rare sulfides in this sample. The main ore and oxide minerals are: chalcopyrite, pyrite, marcasite, leucoxene, and hematite. Pyrite grains are euhedral. Leucoxene and/or hematite centers with pyritic edges implying euhedral pyrite grew or nucleated on leucoxene or hematite. Vein of hematite and pyrite where the pyrite is older than hematite. The fluid inclusions are two phase ($l+v$) and range in size from 3.8 to 10.0µm. The sample is from North Stock.

RSC-033 582': The sample is carbonate and sulfide amydules hosted in medium grained porphyry. The main ore minerals are: pyrite, chalcopyrite, and leucoxene. The amygdules are zones with pyritic edges and more carbonate center. Pyrite occurs as euhedral cubes with leucoxene cores. No useable fluid inclusions. This sample is from North Stock.

RSC-041 807.5' A and B: The sample is intensely altered schist clasts within carbonate with multiple generations of carbonate. The main ore and oxide minerals are: pyrite, marcasite, and goethite. Pyrite occurs are euhedral cubes, rare grains appear zoned. Marcasite occurs as blades with partial replacement by pyrite. Dolomite is the dominant carbonate in the sample. No useable fluid inclusions. The samples are from North Stock.

RSC-048 813' A and B: The sample is a carbonate+sulfide vein with some preserved open spaces and intergrown crystals. The main ore minerals are: marcasite, pyrite, and chalcopyrite. The pyrite is large, euhedral cubes with rare pitting. All sulfides in this section are contained in/adjacent to the vein. The pyrite and marcasite are intergrown, making paragenesis difficult.

RSC-054 859': The sample is of late stage, open spaced filling quartz, with minor carbonate hosted in schist. There is early adularia+sulfides, later quartz, then carbonate+sulfides (carbonates include dolomite and calcite). The main ore and oxide minerals are: pyrite, marcasite, leucoxene and chalcopyrite. Pyrite occurs as euhedral grans with some pseudomorphic pyrite after marcasite. Marcasite occurs as blades and snowflakes. The fluid inclusions are two phase ($l+v$) with irregular shapes. Some inclusions occur in pseudosecondary trails and larger individual primary inclusions. Fluid inclusion sizes range from 2.7 to 18.6µm. The sample is from North Stock.

RSC-080 890.7': The sample is of carbonate irregular amygdules in feldspar porphyry. The main ore and oxide minerals are: pyrite and leucoxene. There is significantly more leucoxene in this thin section than in other samples. Leucoxene occurs as replacing mafic mineral sites. Sulfides are not hosted in amygdules but in the porphyry. There are no useable fluid inclusions. The sample is from North Stock.

RSC-101 1348.8' A and B: The samples are a heterolithic breccia (HIMBx) with dark, sooty sulfides. There is carbonate with open space preserved on fracture surface. The carbonate shows multiple generations. The main ore and oxide minerals are: pyrite, marcasite, and leucoxene. Pyrite occurs as euhedral grains and pseudomorphic pyrite after marcasite. Marcasite occurs as blades and blocky aggregates. Marcasite grains have

been partially replaced by pyrite. There is no clear paragenetic relationship. Leucoxene occurs as replacement of mafic mineral sites and is intergrown with pyrite or pseudomorphic pyrite. There are no useable fluid inclusions. The samples are from North Stock.

RSC-105 1466' A and B: The sample is heterolithic breccia zone (?) with fluidized textures with pyrite concentration at clast contacts. The main ore and oxide minerals are: chalcopyrite, marcasite, pyrite, goethite, and leucoxene. Pyrite occurs as euhedral grains and are weakly transparent in plane polarized light. Marcasite is irregular and partially replaced by pyrite. Leucoxene is replacing mafic mineral site. Goethite is present with pyrite and leucoxene. There are no clear paragenetic relationships. No useable fluid inclusions. The sample is from North Stock.

RSC-105 1533': The sample is a heterolithic breccia zone (?) with fluidized textures with carbonate veins. The main ore minerals are: pyrite and marcasite. Marcasite occurs as blocky aggregates with rare pitting and partial pyrite replacement. Pyrite grains are small, euhedral, and have a rare light brown coloration. No useable fluid inclusions. The sample is from North Stock.

RSC-105 1870.2': The sample is tye-dye phonolite with interesting alteration rims surrounding carbonate veins. The main ore and oxide minerals are: leucoxene and marcasite. There are rare sulfides with marcasite partially being replaced by pyrite. No useable fluid inclusions. The sample is from North Stock.

APPENDIX 1: ANALYTICAL TECHNIQUES

QEMSCAN® ANALYSIS

Of the thirteen samples, ten samples were prepared as doubly polished thin sections.

Three samples were cut into 3x4x1 cm sized blocks. Then the blocks were ground and

polished. All samples where carbon coated to create an electrically conductive surface.

Each sample was analyzed using the basic SEM capabilities. Based on the results, then

the samples were analyzed using QEMSCAN for overall modal abundances at 20µm.

Next, samples were analyzed at a resolution of 2µm for a detailed imagery. Lastly,

samples were analyzed using specific mineral search for mineralizing phases. Samples

were analyzed at the Advanced Mineral Research Center at Colorado School of Mines.

Table A-1 : Results of QEMSCAN® analysis

Sample Hole	Depth (ft)	Description	Resolution µm	Albite %	Ankerite ? %	Amphibole %	Apatite %	Arsenian Pyrite %	Biotite/Phlogopite %	Calcite %
RSC-001	436.5	Quartz Monzodiorite	20			6.8	1.5		4.1	
RSC-001	436.5	Quartz Monzodiorite	2			2.5	0.4		1.9	
RSC-002	772.5	Schist	15	5.6			0.4		7.4	23.3
RSC-003	504.5	Porphyry-Schist Breccia	10				0.2		6.4	
RSC-003	702.7	Schist	15	5.5			0.2		0.3	0.2
RSC-003	775	Schist	15	0.3					0.2	
RSC-003	968	Schist	Backscatter only							
RSC-005	1663	Porphyry	20			1.4	0.5		4.4	5.9
RSC-006	1786	Schist	2				0.2	0.4	3	
RSC-006	1786	Schist	5				0.3	0.2	4.8	
RSC-007	540	Schist	15	0.2			0.2		0.8	
RSC-012	1769	Phonolite	20		2.1		0.3		2.5	0.1
RSC-013	124.3	Pyroclastic	20			0.4	0.4		3.2	
Handsample North Stock		Phonolite	20			2.2			0.4	
Handsample North Stock		Schist Breccia	20		0.2	1.5	1.1		6.1	11

Sample Hole	Depth (ft)	Description	Limonite %	Muscovite/Sericite %	Nepheline %	Others %	K-Spar %	Plag %	Pyrite %	Pyroxene %
RSC-001	436.5	Quartz Monzodiorite	1.4	0.4		3.8	24.3	21.6	3.2	
RSC-001	436.5	Quartz Monzodiorite	2.1	0.3		3.3	23.4	10.9	9.1	
RSC-002	772.5	Schist		0.8		1.2	45.4		0.7	
RSC-003	504.5	Porphyry-Schist Breccia		4.3		1.4	55.8		7.4	
RSC-003	702.7	Schist		0.2		0.9	23.3		7.5	
RSC-003	775	Schist		0.3		0.8	25.1		7.2	
RSC-003	968	Schist	Backscatter only							
RSC-005	1663	Porphyry		0.3		3.1	60.7	15.8		
RSC-006	1786	Schist		18.3		2.5	47.8	10.1	5.2	
RSC-006	1786	Schist		14.9		2.2	38.2	12.6	2.8	
RSC-007	540	Schist		0.2		3.1	26.7		4.7	
RSC-012	1769	Phonolite		1.4			83.6	4.1	4.7	
RSC-013	124.3	Pyroclastic		0.6		4.3	47.8	19.7	3.3	
Handsample North Stock		Phonolite			24.5	0.6	66.3	4.4		0.6
Handsample North Stock		Schist Breccia		0.6		3.4	43	15.1	0.2	

Table A-1 Cont. : Results of QEMSCAN® analysis

Sample		Description	Resolution	Calcite (Fe, Mg bearing)	Chlorite	Dolomite	Dolomite (Fe)	Fe-Mg Silicate	FeOx/Hydrox
Hole	Depth (ft)		µm	%	%	%	%	%	%
RSC-001	436.5	Quartz Monzodiorite	20	7.2				8.5	4.1
RSC-001	436.5	Quartz Monzodiorite	2	17.9				18.7	1.4
RSC-002	772.5	Schist	15	6.2	1.1	1.7			0.3
RSC-003	504.5	Porphyry-Schist Breccia	10	22.9	0.4				
RSC-003	702.7	Schist	15	9.8	0.1	46.7	4.9		
RSC-003	775	Schist	15	1.8		43	15.5		
RSC-003	968	Schist	Backscatter only						
RSC-005	1663	Porphyry	20		1				2.5
RSC-006	1786	Schist	2		1.6				
RSC-006	1786	Schist	5		5.6				
RSC-007	540	Schist	15		0.2	22.4	7.9		32.6
RSC-012	1769	Phonolite	20						0.1
RSC-013	124.3	Pyroclastic	20		2.9				
Handsample North Stock		Phonolite	20						0.5
Handsample North Stock		Schist Breccia	20		7.2				3.1

Sample		Description	Limonite	Quartz	Silicate ?	Silver	Sphene	Ti-Minerals	Kaolinite
Hole	Depth (ft)		%	%	%	%	%	%	%
RSC-001	436.5	Quartz Monzodiorite	1.4	8.1	1			4	
RSC-001	436.5	Quartz Monzodiorite	2.1	5.8	1.3			1.2	
RSC-002	772.5	Schist		4.1				1.1	
RSC-003	504.5	Porphyry-Schist Breccia		0.2				1	
RSC-003	702.7	Schist						0.3	
RSC-003	775	Schist		5.4					
RSC-003	968	Schist	Backscatter only						
RSC-005	1663	Porphyry		3.8				0.6	
RSC-006	1786	Schist		9.8				0.9	
RSC-006	1786	Schist		16.8				1.6	
RSC-007	540	Schist				0.5		0.3	
RSC-012	1769	Phonolite						0.6	
RSC-013	124.3	Pyroclastic		14.2				1.1	0.5
Handsample North Stock		Phonolite					0.4		
Handsample North Stock		Schist Breccia		6.2				1	0.3

OXYGEN AND CARBON ISOTOPES

Approximately 90 ug of carbonate sample material was weighed into individual sample vials. Samples were quantitatively acidified in vacuo in an on-line autosampler with 100% orthophosphoric acid at 90°C. After cryogenic purification of the generated carbon dioxide, the gas was analyzed simultaneously for stable carbon and oxygen isotopes in a Micromass Isoprime stable isotope ratio mass spectrometer, located at the Colorado School of Mines Stable Isotope Laboratory, using traditional dual-inlet techniques. Laboratory standard reference gas has been calibrated against a laboratory working calcium carbonate powder derived from the Colorado Yule Marble (CYM). The composition of CYM has been calibrated against NBS-18 and NBS-19 standard reference materials obtained from the National Institute of Standards and Technology. Sample data are reported as a per mil difference from the Vienna PeeDee Belemnite (VPDB) international reference. Precision determined through repeated analyses of CYM and blind duplicate analysis of samples is 0.05‰ for carbon and 0.08‰ for oxygen. All data are corrected for the contribution of 17O using the correction factors from Craig (1950).

*Note the yellow highlighted samples were selected prior to analysis to be duplicate samples. The orange highlighted samples were selected at Colorado School of Mines for an internal duplicate. One sample, AR-17, did not have enough carbonate to measure.

Table A-2: Results of Oxygen and Carbon Isotope
Analysis

Run Number	Sample ID	Depth	d^{18}(‰VPDB)	d^{18} (‰SMOW)	d^{13}C (‰VPDB)	Recalculated SMOW	
						d^{18}(‰SMOW)	d^{13}C (‰VPDB)
AR-1	RSC-002	849.8A	-18.705	12.155	-2.321	1.965	-3.171
AR-2	RSC-002	849.8B	-18.469	12.391	-2.221	2.201	-3.071
AR-3	RSC-003	1266.9	-19.563	11.297	-5.420	1.107	-6.270
AR-4	RSC-004	431.5A	-17.557	13.303	-5.701	3.113	-6.551
AR-5	RSC-004	431.5B	-19.361	11.499	-6.449	1.309	-7.299
AR-6	RSC-004	1112.3	-16.617	14.243	-5.354	4.053	-6.204
AR-7	RSC-006	1769A	-18.606	12.254	-4.451	2.064	-5.301
AR-8	RSC-012	1557.1	-19.450	11.410	-4.780	1.220	-5.630
AR-9	RSC-014	542.5A	-19.279	11.581	-4.612	1.391	-5.462
AR-10	RSC-014	542.5B	-17.645	13.215	-5.208	3.025	-6.058
AR-11	RSC-015	1219.5AA	-21.321	9.539	-4.136	-0.651	-4.986
AR-12	RSC-015	1219.5AB	-21.113	9.747	-3.991	-0.443	-4.841
AR-13	RSC-015	1219.5B	-19.346	11.514	-3.311	1.324	-4.161
AR-14	RSC-015	1272.7A	-19.517	11.343	-8.228	1.153	-9.078
AR-15	RSC-015	1272.7B	-19.417	11.443	-8.199	1.253	-9.049
AR-16	RSC-020	503C	-16.469	14.391	-5.294	4.201	-6.144
AR-18	RSC-020	720A	-17.378	13.482	-4.030	3.292	-4.880
AR-19	RSC-020	720B	-17.629	13.231	-6.170	3.041	-7.020
AR-20	RSC-020	720C	-17.109	13.751	-6.076	3.561	-6.926
AR-21	RSC-027	1754	-19.277	11.583	-4.756	1.393	-5.606
AR-22	RSC-028	515A	-18.081	12.779	-4.508	2.589	-5.358
AR-23	RSC-028	515B	-18.553	12.307	-5.528	2.117	-6.378
AR-24	RSC-028	861.8	-16.018	14.842	-3.486	4.652	-4.336
AR-25	RSC-028	861.8B	-18.888	11.972	-3.772	1.782	-4.622
AR-26	RSC-028	1331.5	-22.165	8.695	-4.766	-1.495	-5.616
AR-27	RSC-028	2587.5A	-20.141	10.719	-5.439	0.529	-6.289
AR-28	RSC-028	2587.5B	-18.014	12.846	-5.129	2.656	-5.979
AR-29	RSC-041	807.5AA	-16.816	14.044	-4.787	3.854	-5.637
AR-30	RSC-041	807.5AB	-17.266	13.594	-6.479	3.404	-7.329
AR-31	RSC-041	807.5BA	-19.004	11.856	-5.111	1.666	-5.961
AR-32	RSC-041	807.5BB	-18.073	12.787	-6.500	2.597	-7.350
AR-33	RSC-048	813AA	-18.857	12.003	-4.468	1.813	-5.318
AR-34	RSC-048	813AB	-19.317	11.543	-4.504	1.353	-5.354
AR-35	RSC-048	813BA	-18.441	12.419	-4.303	2.229	-5.153
AR-36	RSC-048	813BB	-18.609	12.251	-4.430	2.061	-5.280
AR-37	RSC-054	859	-20.553	10.307	-4.231	0.117	-5.081
AR-38	RSC-101	1348.8A	-20.283	10.577	-13.306	0.387	-14.156
AR-38	RSC-101	1348.8A	-20.137	10.723	-13.446	0.533	-14.296
AR-17	RSC-020	646.5	Not Enough to Measure				

154

FLUID INCLUSION MICROTHERMOMETRIC DATA

All the tables represent the microthermometric data collected from the Olympus BX51 microscope with a Linkham THMS 600 stage. Fluid inclusion data below is sub-divided into 3 tables. The first table A-3a is a table of microthermometrc results. Table A-3b is table of microthermometrc results from LA-ICP-MS sample. Table A-3c table of microthermometric results of complex fluid inclusions. If the data was not collected, the cell of the table is shaded grey.

Table A-3a: Fluid Inclusion Measurements for Two-Phase Inclusions

Hole-Inclusion	Depth ft	T$_{eutectic,}$ First Ice Melt °C	T$_{m, ice}$ Last Ice Melt °C	T$_{h,}$ vapor °C	L:V Ratios	Volume %	NaCl %	Density (g/cc)
RSC-003-2	743B	-56.1	-4.4	218.7	15	85	7.02374	0.90311
RSC-003-3	743B	-54.3	-5.4	138.4	7.5	92.5	8.41084	0.980594
RSC-003-4	743B	-59.4	-4.4	213.3	10	90	7.02374	0.908878
RSC-003-5	743B	-61.3	-3.7	186.2	50	50	6.00912	0.928098
RSC-003-6	743B	-57.1	-4.2	257.8	15	85	6.73758	0.852737
RSC-003-10	743B		-2.2	118	10	90	3.708	0.96776
RSC-004-2	1112.3	-48.4	-8.4	199	1.5	98.5	12.1634	0.95953
RSC-004-3	1112.3	-61.9	-2.9	195.1	15	85	4.80386	0.910496
RSC-004-4	1112.3	-55.2	-6.6	207.3	10	90	9.98278	0.937249
RSC-004-5	1112.3	-64	-6.8	184.6	30	70	10.2353	0.958274
RSC-004-10	1112.3	-56.2	-6.3	192.1	10	90	9.59898	0.947839
RSC-004-15	1112.3	-59.9	-3.6	152.2	15	85	5.86116	0.955828
RSC-004-16	1112.3	-49.8	-8	161.7	3.5	96.5	11.6964	0.984743
RSC-014-2	995.2	-61.9	-4.6	210.6	1	99	7.30694	0.913924
RSC-014-3	995.2	-57.9	-7.8	188.9	3.5	96.5	11.4592	0.962937
RSC-027-4	2001	-54.4	-1.9	150.9	20	80	3.22626	0.940935
RSC-027-5	2001	-51.4	-0.5	127.1	5	95	0.87902	0.94644
RSC-020-3	646.5	-50.7	-2	165.1	10	90	3.38766	0.948627
RSC-020-4	646.5	-64.7	-8.6	213.9	3.5	96.5	12.3933	0.929632
RSC-020-5	646.5	-45.3	-3.9	180.1	2	98	6.30276	0.935693
RSC-020-6	646.5	-55	-1.8	215	1.5	98.5	3.06404	0.873292
RSC-020-7	646.5	-49.7	-2.9	239.1	5	95	4.80386	0.858278
RSC-020-8	646.5	-41.3	-8.8	191.3	7.5	92.5	12.6207	0.968706
RSC-020-9	646.5	-48.8	-4.7	152.3	7.5	92.5	7.44745	0.965299
RSC-020-11	646.5	-42.9	-3.8	213.2	2	98	6.15632	0.901944
RSC-020-15	646.5	-50	-5.2	219.3	2	98	8.13915	0.911591
RSC-020-16	646.5	-45.5	-4.6	237.7	5	95	7.30694	0.883989
RSC-020-17	646.5	-45.5	-4.8	194.2	2	98	7.58723	0.931924
RSC-054-2	859	-43.5	-9	229.7	1	99	12.8459	0.937862
RSC-054-5	859	-34.5	-5.7	171.7	5	95	8.81309	0.959199

Hole-Inclusion	Depth ft	T eutectic °C	T m, ice °C	T h, vapor °C	L:V Ratios	Volume %	NaCl %	Density (g/cc)
RSC-054-9	859	-51.4	-3.1	242	20	80	5.10983	0.857431
RSC-054-11	859	-46.7	-6.2	177.1	25	75	9.4697	0.959207
RSC-054-12	859	-31.1	-6.9	187.3	7.5	92.5	10.3606	0.956936

Table A-3b: Fluid Inclusion Measurements for Two-Phase Inclusions for LA-ICP-MS Sample

Hole-Inclusion	Depth ft	$T_{eutectic,}$ First Ice Melt °C	$T_{m, ice}$ Last Ice Melt °C	$T_{h, vapor}$ °C	L:V Ratios	Volume %	NaCl %	Density (g/cc)
RSC-015-1	1272.7	-37.8	-3.3		20	80		
RSC-015-2	1272.7	-32.4	-6	148.1	2	98	9.205948	1.06484
RSC-015-3	1272.7	-27.3	-5	243	5	95	7.860858	1.054909
RSC-015-4	1272.7	-32.4	-5.4	281.3	7	93	8.406921	1.058931
RSC-015-5	1272.7	-43.2	-4	236.7	5	95	6.446805	1.044555
RSC-015-6	1272.7	-32.1	-2.2	70.9	5	95	3.712453	1.024759
RSC-015-7	1272.7	-37.7	-4.5	262.1	7	93	7.162735	1.049786
RSC-015-8	1272.7	-37.7	-1.6	252	7	93	2.742669	1.0178
RSC-015-9	1272.7	-34.3	-4	168.7	7	93	6.446805	1.044555
RSC-015-10	1272.7	-38	-3.1	254	15	85	5.111323	1.034852
RSC-015-11	1272.7	-32.1	-2.5	253	10	90	4.18603	1.028168
RSC-015-12	1272.7	-33.2	-2.3	249.1	7	93	3.871137	1.025901
RSC-015-13	1272.7	-42.7	-6.6	214.6	7	93	9.9817	1.070604
RSC-015-14	1272.7	-49.8	-4.5		5	95		
RSC-015-15	1272.7	-34.4	-8.2	126.7	3	97	11.94301	1.085307

Table A-3c: Fluid Inclusion Measurements of Complex Inclusions-Clathrates

Hole Inclusion	Depth ft	$T_{eutectic,}$ First Ice Melt °C	$T_{m, ice}$ Last Ice Melt °C	$T_{h, vapor}$ °C	$T_{h,}$ clathrate °C	L:V Ratios	Volume %	%NaCl	Density (g/cc)
RSC-004-7	1112.3	-64.3	-9.4	196.2	6.1	3.5	96.5	4.760189	0.962088
RSC-004-9	1112.3	-62.4	-2.5	205.7	5.2	12.5	87.5	4.958469	0.961726
RSC-004-12	1112.3	-56.6	-3.6	200.5	6.8	3.5	96.5	4.885423	0.962511
RSC-027-3	2001	-48	0	167.3	6.9	3.5	96.5	5.02178	0.962631
RSC-054-8	859	-42.7	-11.1	219.8	9.5	25	75		0.961796
RSC-054-15	859	-45.1	-3.8	167.2	8.2	2	98	4.749491	0.963866
RSC-015-16	1272.7	-30.6	-5.7	130	7.1	3	97	4.781608	0.990993
RSC-015-17	1272.7	-30.6	-5.2	126.7	7.1	3	97	4.798233	0.862103

LASER ABLATION INDUCTIVELY COUPLE PLASMA MASS SPECTROMETRY (LA-ICP-MS) OF FLUID INCLUSIONS

The sample was analyzed at the USGS Laser Ablation ICP-MS Laboratory in Denver for multielemental composition. The sample selected for LA-ICP-MS has the largest inclusions observed from all samples. The standards used to calibrate the LS-ICP-MS ,achine are listed at the top with the detection limits. The beam size column refers to the size of the beam (or concentration) of the beam used to ablate the fluid inclusions. In addition to the fluid inclusions measured, 7 matrix and host rock spots were analyzed.

Table A-4: LA-ICP-MS of Fluid Inclusions from RSC-015 1272.7'
Results

		23 Na ppm	24 Mg ppm	27 Al ppm	29 Si ppm	39 K ppm	44 Ca ppm	55 Mn ppm	57 Fe ppm	59 Co ppm
Standard	Beam Size (µm)	<	<	<	<	<	<	<	<	<
1	44	30	2	6	2000	40	400	5	50	0.5
2	32	50	4	10	4000	70	800	10	100	0.9
3	24	90	8	20	7000	100	1000	20	200	2
Inclusions	Beam Size (µm)									
4	24	17500	11700	<20	<7000	3180	<1000	<20	<200	<2
5	24	17500	8170	<20	<7000	2480	<1000	<20	<200	<2
6	32	17500	4580	<10	<4000	4180	<800	<10	<100	<0.9
7	32	17500	19300	<10	<4000	4710	<800	490	8100	11
9	24	17500	7740	<20	<7000	3760	<1000	140	490	<2
10	24	17500	10700	<20	<7000	<100	<1000	<20	5600	<2
11	44	17500	2120	<6	<2000	4240	5400	<5	<50	<0.5
12	44	17500	1470	<6	<2000	8920	<400	<5	<50	<0.5
13	44	17500	5270	<6	<2000	<40	<400	<5	<50	<0.5
14	44	17500	278	<6	<2000	2200	<400	<5	<50	<0.5
16	44	17500	401	<6	<2000	3120	760	6.1	220	<0.5
18	24	17500	2820	<20	<7000	2840	<1000	<20	<200	<2
19	24	17500	17600	<20	<7000	11200	<1000	940	2500	<2
20	44	17500	1930	<6	<2000	5170	5400	200	800	<0.5
24	44	17500	8390	<6	<2000	6170	11000	410	1200	9.5
Calcite 5	32	89.6	<4	69.4	467000	100	<800	<10	<100	<0.9
Feldspar 6	44	108	<2	107	466000	1540	<400	<5	<50	<0.5
Matrix 1	24	<90	<8	90.9	467000	<100	<1000	<20	<200	<2
Matrix 2	44	<30	<2	177	467000	<40	<400	<5	<50	<0.5
Matrx 3	32	<50	<4	1480	466000	<70	<800	<10	<100	<0.9
Matrix 4	44	<30	<2	144	467000	<40	<400	<5	<50	<0.5
Matrix 5	44	54.6	<2	81.1	467000	<40	<400	<5	<50	<0.5

Table A-4 cont. : LA-ICP-MS of Fluid Inclusions from RSC-015 1272.7' Results

	Beam Size (μm)	65Cu ppm	66Zn ppm	75As ppm	85Rb ppm	88Sr ppm	89Y ppm	95Mo ppm	98Mo ppm	107Ag ppm	111Cd ppm	121Sb ppm
Standard		<	<	<	<	<	<	<	<	<	<	<
1	44	3	4	2	0.3	0.2	0.1	2	1	0.5	2	0.9
2	32	5	8	4	0.5	0.3	0.2	3	2	1	3	2
3	24	9	10	7	1	0.5	0.4	6	3	2	6	3

Inclusions	Beam Size (μm)	65Cu	66Zn	75As	85Rb	88Sr	89Y	95Mo	98Mo	107Ag	111Cd	121Sb
4	24	<9	<10	<7	28		<0.4	<6	<3	<2	<6	<3
5	24	<9	<10	<7	<1	<0.5	<0.4	<6	<3	<2	<6	<3
6	32	<5	<8	<4	29	<0.3	<0.2	<3	<2	<1	<3	<2
7	32	270	120	46	<0.5	<0.3	<0.2	<3	<2	<1	<3	<2
9	24	<9	<10	<7	37	<0.5	<0.4	<6	<3	<2	<6	<3
10	24	<9	670	210	1000		<0.4	<6	<3	<2	<6	<3
11	44	<3	170	47	21	6.3	<0.1	<2	<1	<0.5	<2	<0.9
12	44	<3	900	30	27	3.4	<0.1	<2	<1	<0.5	<2	<0.9
13	44	<3	1400	<2	53	<0.2	<0.1	<2	<1	<0.5	<2	<0.9
14	44	<3	250	<2	24	<0.2	<0.1	<2	<1	<0.5	<2	<0.9
16	44	<3	75	20	25	3.3	<0.1	<2	<1	1.7	3	<0.9
18	24	<9	<10	<7	<1	<0.5	<0.4	<6	<3	<2	<6	<3
19	24	380	1100	130	<1	72	<0.4	<6	<3	<2	<6	<3
20	44	30	460	24	23	22	<0.1	<2	<1	<0.5	<2	<0.9
24	44	36	97	50	33	69	<0.1	<2	<1	8.9	<2	<0.9
Calcite 5	32	<5	<8	<4	<0.5	<0.3	<0.2	<3	<2	<1	<3	30
Feldspar 6	44	<3	<4	<2	<0.3	<0.2	<0.1	<2	<1	<0.5	<2	30
Matrix 1	24	<9	<10	<7	<1	<0.5	<0.4	<6	<3	<2	<6	24.2
Matrix 2	44	<3	<4	<2	<0.3	<0.2	<0.1	<2	<1	<0.5	<2	27.3
Matrx 3	32	<5	<8	<4	<0.5	<0.3	<0.2	<3	<2	<1	<3	5.01
Matrix 4	44	<3	<4	<2	<0.3	<0.2	<0.1	<2	<1	<0.5	<2	26.7
Matrix 5	44	<3	<4	<2	<0.3	<0.2	<0.1	<2	<1	<0.5	<2	7.25

Table A-4 cont. : LA-ICP-MS of Fluid Inclusions from RSC-015 1272.7' Results

Standard	Beam Size (µm)	133Cs ppm <	137Ba ppm <	197Au ppm 1	208Pb ppm 1	209Bi ppm 1
1	44	0.1	0.8	0.2	0.5	0.1
2	32	0.2	2	0.4	0.9	0.3
3	24	0.3	3	0.7	2	0.5

Inclusions	Beam Size (µm)					
4	24	28	<3	<0.7	<2	<0.5
5	24	<0.3	<3	<0.7	<2	<0.5
6	32	<0.2	<2	<0.4	<0.9	<0.3
7	32	<0.2	<2	<0.4	<0.9	<0.3
9	24	13	<3	4.1	<2	<0.5
10	24	38	<3	<0.7	43	<0.5
11	44	3.5	<0.8	2.8	<0.5	<0.1
12	44	5.4	<0.8	<0.2	<0.5	<0.1
13	44	7.6	<0.8	<0.2	<0.5	<0.1
14	44	5.9	<0.8	<0.2	<0.5	<0.1
16	44	5.8	2.1	<0.2	<0.5	<0.1
18	24	<0.3	<3	<0.7	<2	<0.5
19	24	<0.3	<3	<0.7	<2	<0.5
20	44	<0.1	<0.8	<0.2	<0.5	<0.1
24	44	9	<0.8	<0.2	5	2.1
Calcite 5	32	<0.2	<2	<0.4	<0.9	<0.3
Feldspar 6	44	<0.1	<0.8	<0.2	<0.5	<0.1
Matrix 1	24	<0.3	<3	<0.7	<2	<0.5
Matrix 2	44	<0.1	<0.8	<0.2	<0.5	<0.1
Matrx 3	32	<0.2	<2	<0.4	<0.9	<0.3
Matrix 4	44	<0.1	<0.8	<0.2	<0.5	<0.1
Matrix 5	44	<0.1	<0.8	<0.2	<0.5	<0.1

Laser Raman

The sample was analyzed at the USGS Laser Ablation ICP-MS and Laser Raman

Laboratory in Denver for multielemental composition. This s the same sample used for

LA-ICP-MS analysis.

Table A-5: Laser Raman Calculations for Salinity of Fluid Inclusions

	Relative Raman signal at 3270cm-1	Relative Raman signal at 3410cm-1	I(3270)/ I(3410)	% salinity
incl1	11.812	14.2835	0.82696818	4.8
incl3	11.73	14.3163	0.819345781	5.3
incl11	12.1312	13.8576	0.875418543	1.7
incl20	12.13	13.8	0.878985507	1.5
incl22	11.2197	14.4475	0.776584184	8

Average	4.3

Na estimate	1.7%